Ultrastructure of emulsions - a comparative electron microscopy study

Jensen, Louise Helene Søgaard; Horsewell, Andy

Publication date:
2013

Document Version
Publisher's PDF, also known as Version of record

TECHNICAL UNIVERSITY OF DENMARK

Ultrastructure of emulsions

- a comparative electron microscopy study

Louise Helene Søgaard Jensen

May 2013

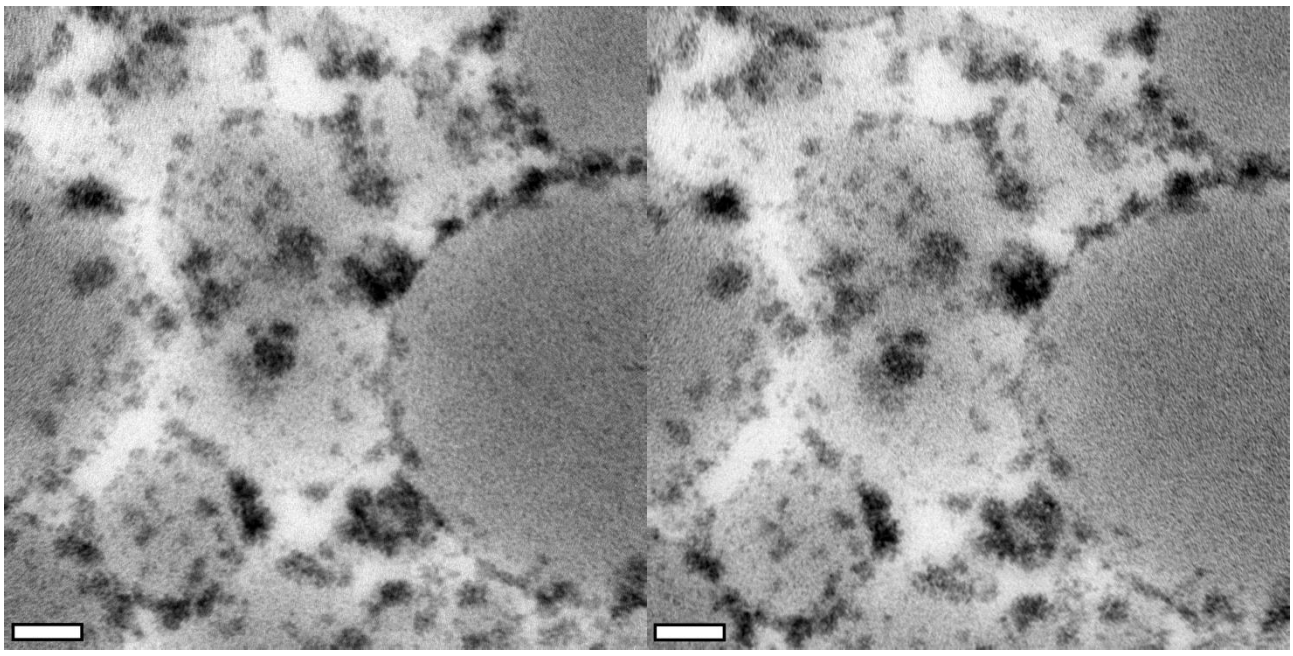

Ultrastructure of emulsions

- a comparative electron microscopy study

PhD Thesis

Louise Helene Søgaard Jensen

Center for Electron Nanoscopy and Department of Mechanical Engineering
Technical University of Denmark

Supervised by Dr. Andy Horsewell
Department of Mechanical Engineering
Technical University of Denmark

Front page illustration: Stereo micrograph from a chemically fixed emulsion displaying protein aggregates on the surfaces of oil droplets. Scale bar 50 nm.To see the 3D image, cross the eyes and focus on both images at once.

Preface

This project was supported by the Danish Food Industry Agency under the Ministry of Food, Agriculture and Fisheries and carried out under the research project “Omega-3 food emulsions: Control and Investigation of molecular structure in relation to lipid oxidation” a collaboration between the Department of Mechanical Engineering, the National Food Institute and Center for Electron Nanoscopy; all at the Technical University of Denmark.
The AP Møller and Chastine Mc-Kinney Møller Foundation are gratefully acknowledged for their contribution of the Center for Electron Nanoscopy.

I owe great thanks and am very grateful to:

Dr. Andy Horsewell (DTU MEK, Denmark) for your supervision, support, encouragement and your never ending trust in me. Most of all for being such a positive and optimistic person.

Dr. Bruno Humbel (EMF UNIL, Switzerland) for opening your lab to me and supervising me during my research stay. Thank you for sharing your extensive knowledge and for sharing also from your experiences as a scientist. It has been truly inspiring!

Dr. Celine Loussert (EMF UNIL, Switzerland). You have been an enthusiastic and patient supervisor during my research stay at the EMF. You have introduced me to so many new techniques and ideas, and answered a myriad of questions. Most importantly; thank you for your friendship! You are very special (in an excellent way!). Thank you for the long talks, for your support and for all the travels and good times we have shared. More will follow!

All at EMF UNIL. Caroline and Jean for all the discussions and fun lunch breaks; Antonio for the good vibes; Willie for helping me with the IT and Nathalie for your great help in dealing with the paperwork and authorities!

Our collaborators from the Lipid Oxidation Group (DTU FOOD, Denmark); Professor Charlotte Jacobsen, Anna Frisenfeldt Horn and Nina Skall-Nielsen. And thanks to Lis Berner, who have prepared the samples for me, sometimes on a very short notice. Thank you to Ulf Andersen and Betina Mikkelsen from Arla Strategic Innovation Center, who have welcomed me in their research lab in Brabrand.

Dr. Takeshi Kassama and Ryutaro Akiyoshi (DTU CEN, Denmark) for invaluable help with the STEM HAADF, EDS analysis, tomography and reconstruction and to Gunnel Karlsson (Kemicentrum Lunds Universitetet, Sweden) for help and suggestions with cryo-TEM and Adam Fuller for helping me with the cryo-FIBSEM work.

Dr. Roger Wepf (EMEZ, ETH, Switzerland) and Dr. Gerd Hause (Biocentrum, Martin Luther Universität Halle-Wittemberg, Germany) for welcoming me into their labs for short term research visits. And Dr. Andres Kaech (UZH, Switzerland), Dr. Kent MacDonald (Electron Microscope Lab UC Berkeley USA), Karen Thomsen (iNano Denmark) and Dr. Kristian Mølhave (DTU Nanotech) for fruitful discussions and constructive comments during the project.

My awesome colleagues at DTU CEN. You have provided a relaxed and cheerful, yet very ambitious atmosphere, and some quite extraordinary and special moments both in and out of the lab! And thank you to my colleagues at MEK for the fun we have shared.

Thank you, my wonderful family and friends for your love and great support - and patience.

And finally; Thank you Thomas. For your unlimited love and support. I will keep the echo of your encouraging voice with me forever..

Summary

Fish oil contains the two long chained omega-3 fatty acids eicosapentaenoic acid and docosahexaenoic acid. These are essential fatty acids and are not effectively converted from their precursor fatty acids in the human body. Hence it is advised to obtain these through the diet. Despite the recent debate about the effect of omega-3 supplements, the omega-3 fatty acids are subject to much interest from consumers, the food industry and several research fields. One route of fish oil administration is through fish oil enriched food products. It is possible to add fish oil to food products initially without off flavors. But the highly unsaturated nature of the fatty acids renders them especially subjective to oxidation; a process which creates undesired off flavors and deteriorates the nutritional value.

It is therefore of interest to protect the fish oil against oxidation. One method suggested to do so is the emulsification of the fish oil to oil in water emulsions. A number of studies have been carried out with the purpose of determining the effect of this strategy, but whether emulsification of the oil is advantageous or not seems to be dependent on the food matrix to which the emulsion is added. The Nanomega project, which is a cooperation between the National Food Institute, the Center for Electron Nanoscopy and the Department of Mechanical Engineering, all at the Technical University of Denmark, has dealt mainly with pure oil in water emulsions to describe the oxidation without the effect of an external food matrix. Two PhD projects were carried out in the Nanomega project. One investigated the effects of different features such as emulsifiers, oil content, pH values, droplet sizes and production methods on the oxidative stability of emulsions. The other, which is the work presented in this thesis, was concerned with the structures of the interfaces between oil droplets and water in these emulsions. The structure of the interfaces are interesting because it is generally acknowledged that the oxidation of the fish oil is initiated at the interface where the oil is in close vicinity to the water phase which might contain prooxidants such as trace metals and free radicals. It is thus speculated that the structure and composition of this interface can affect the oxidative stability of fish oil emulsions and perhaps provide protection against oxidation of the fish oil. The purpose of this thesis work was thus to identify and apply suitable methods for the characterization of these interfaces. In the Nanomega project the interfaces were stabilized by proteins and phospholipids from milk. They form interface layers which are expected to be very thin, i.e. between 2-10 nm. For this reason, electron microscopy was the method of choice. However, electron microscopy is inherently performed in vacuum and the emulsions presented a challenge by being liquid systems which are sensitive to changes in water vapor and temperature. Furthermore, to achieve resolution and contrast of structural differences in specimens, electron microscopy relies on the scattering of electrons and the emulsions contain only light elements with low mass contrast. The objective of this thesis was two-fold. One was to identify and further develop sample preparation methods to enable observation of the emulsions in the vacuum of the electron microscopes. Having developed the necessary experimental methods, the second objective was to characterize the structures of a number of emulsions that were found to be interesting for further analysis.

We have tested chemical fixations in different matrices and with different concentrations of fixative, employed high pressure freezing followed by either freeze-fracture cryo-SEM or freeze substitutions with different substitution media, and subjected some of the resulting samples to HAADF STEM tomography and EDS analysis.

We have analyzed the impact of glutaraldehyde on nano-emulsions by comparing shrinkage as a consequence of glutaraldehyde concentration. Furthermore we have compared the chemical fixation quality of larger oil droplets also as a consequence of glutaraldehyde concentration. We have characterized the structures of emulsions containing either 10% oil and oil droplets in the size range of ~130 nm or 70% oil emulsions with droplet sizes ~10-20 µm. We have characterized the structures of different emulsifiers, sodium caseinate, whey protein isolate and emulsifiers containing both proteins and phospholipids from milk, on the surfaces of oil droplets. Furthermore we have characterized a number of different emulsions with respect to the location and structural arrangement of excess emulsifiers in the water phase where they are expected to act as antioxidants. And finally we have observed that the structure of one of these emulsifiers, sodium caseinate, changes its structure as a consequence of whether the emulsion has been processed at high pressure or not. The results suggest a structural similarity with the native casein micelle and a similar response to high pressure conditions, but diverging slightly in the resulting structure. This deviation can probably be ascribed to missing calcium phosphate in the emulsifier.

Resumé

Fiskeolie indeholder de to lang-kædede omega-3 fedtsyrer eicosapentaensyre og docosahexaensyre. De er essentielle fedtsyrer og deres kort-kædede prækursorer konverteres ikke effektivt i kroppen. Derfor anbefales det at indtage disse gennem kosten. Trods den nylige debat om virkningerne af omega-3 kosttilskud er omega-3 fedtsyrer genstand for stor interesse fra forbrugerne, fødevareindustrien og flere forskellige forskningsområder. Én måde at indtage fiskeolie tilskud på, er gennem fiske olie berigede fødevarer. Det er muligt at tilføje fiskeolie til fødevarer uden ubehagelig bismag, men den flerumættede karakter af fedtsyrerne gør dem meget følsomme overfor oxidation. En proces, der skaber uønsket bismag og forringer den ernæringsmæssige værdi af fiskeolien.

Det er derfor af stor interesse at beskytte fiskeolie mod oxidation. Én metode at opnå dette er gennem emulgering af fiskeolier. En række undersøgelser er blevet udført med det formål at fastlægge effekten af denne strategi, men om emulgering af olien er fordelagtig synes at være afhængige af typen af fødevarer som olie er tilføjet. Nanomega-projektet, som var et samarbejde mellem Fødevareinstituttet, Center for Elektron Nanoscopy og Institut for Mekanisk Teknologi, alle fra Danmarks Tekniske Universitet, har beskæftiget sig primært med rene olie i vand emulsioner for at beskrive oxidation uden påvirkningen af en omkring-liggende fødevare. To Ph.d. projekter blev gennemført under Nanomega projektet. Én har undersøgt påvirkningerne fra forskellige variable såsom emulgator-type, olieindhold, pH værdier, dråbe størrelser og produktionsmetoder på den oxidative stabilitet af fiskeolie emulsioner. Den anden, som er fremlagt i denne afhandling, omhandlede strukturerne af grænsefladerne mellem olie dråberne og vand fasen i disse emulsioner. Strukturen af grænsefladerne er interessant, fordi det er almindeligt anerkendt at oxidation af fiskeolie bliver initieret på den grænseflade. Her er olien er i tæt kontakt med vand-fasen, der kan indeholde pro-oxidanter såsom spormetaller og frie radikaler. Det er derfor forventet at strukturen og sammensætningen af denne grænseflade kan påvirke fisk olie emulsioners oxidative stabilitet og måske yde beskyttelse mod oxidation af fiskeolien. Formålet med denne afhandling arbejde var derfor at identificere og anvende passende metoder til karakterisering af disse grænseflader. I Nanomega projektet var grænsefladerne stabiliseret af proteiner og fosfolipider fra mælk. De danner grænseflade lag, som forventes at være meget tynde, dvs. mellem 2-10 nm. Af denne grund var elektronmikroskopi et oplagt metode-valg. Elektronmikroskopi udføres normalt i vakuum. Emulsioner er flydende systemer, som er følsomme for ændringer i vanddamptryk og temperaturer og var derfor en udfordring for elektronmikroskopi. Desuden, er elektronmikroskopi afhængig spredning af elektroner for at opnå opløsning og kontrast af strukturelle forskelle i prøver, emulsioner indeholder kun lette elementer med lav masse-kontrast. Projektet havde derfor to formål. Et var at identificere og udvikle metoder til at præparere emulsionerne så de kunne karakteriseres i elektronmikroskoper under vacuum. Det andet var at implementere disse metoder til karakterisering af grænseflade-strukturer i en række emulsioner, der i projektet blev anset for at være interessante for strukturel analyse.

Vi har testet en række af kemiske fikseringer med forskellige koncentrationer af fiksativ og i forskellige matricer, benyttet højtryks-frysning efterfulgt af enten ”freeze-fracture” og cryo-SEM eller ”freeze-substitution” med forskellige substitutions medier. Desuden har vi analyseret nogle af disse prøver med HAADF STEM tomografi og EDS analyse.

Vi har analyseret virkningerne af glutaraldehyd på nano-emulsioner ved at sammenligne skrumpning som følge af glutaraldehyd koncentration. Desuden har vi sammenlignet kvaliteten af kemisk fiksering af større olie dråber som følge af glutaraldehyd koncentration. Vi har karakteriseret strukturerne af emulsioner, der indeholder enten 10% olie og olie dråber i størrelsesområdet ~ 130 nm eller 70% olie emulsioner med størrelser omkring ~ 8-20 µm. Vi har karakteriseret strukturerne af følgende emulgatorer på overflader af oliedråber i emulsioner: natrium kaseinat, valle protein isolat og emulgatorer som indeholder både proteiner og fosfolipider fra mælk. Desuden har vi karakteriseret en række forskellige emulsioner med hensyn til lokalisering og struktur af overskydende emulgatorer i vand-fasen, hvor de forventes at fungere som antioxidanter. Og endelig har vi karakterisetet strukturen af en af disse emulgatorer, natrium kaseinat, i emulsioner er blevet behandlet på under højt eller normalt tryk. Resultaterne tyder på en vis strukturel lighed med de miceller, kasein naturligt danner i mælk og et lignende respons på højt tryk. Den resulterende struktur afviger let fra de strukturer, naturlige kasein miceller danner efter at have været udsat for lignende tryk. Denne afvigelse kan formentlig tilskrives fraværet af calciumphosphat i emulgatoren.

List of publications and communications related to this thesis work

Articles

Horn, AF; Nielsen, NS ; Andersen, U; Jensen, LHS ; Horsewell, A; Jacobsen, C
Oxidative stability of 70% fish oil-in-water emulsions: Impact of emulsifiers and pH
European Journal of Lipid Science and Technology **113** (10) 1243-1257 (2011)

Dudkiewicz, A; Tiede, K; Löschner, K; Jensen, LHS; Jensen, E; Wierzbicki, R; Boxall, ABA; Mølhave, K
Characterization of nanomaterials in food by electron microscopy
Trends in Analytical Chemistry **30** (1) 28-43 (2011)

Horn, AF; Green-Petersen, D; Nielsen, NS; Andersen, U; Hyldig, G; Jensen, LHS; Horsewell, A; Jacobsen, C
Addition of Fish Oil to Cream Cheese Affects Lipid Oxidation, Sensory Stability and Microstructure
Agriculture **2** (4) 359-375 (2012)

Lu, HFS; Nielsen, NS; Baron, CP; Jensen, LHS, Jacobsen, C
Physico-chemical Properties of Marine Phospholipid Emulsions
J A O C S **89** (11) 2011-2024 (2012)

Horn, AF; Nielsen, NS; Jensen, LHS; Horsewell, A; Jacobsen, C
The choice of homogenisation equipment affects lipid oxidation in emulsions
Food Chemistry **134** (2) 803-810 (2012)

Articles in preparation

Pedersen, CL; Hansen, MJ; Jensen, LHS; Guldberg, LB; Feilberg, A; Nielsen, LP
Correlation between fungi and removal of hydrogen sulfide in air treating biofilter

Jensen, LHS; Loussert, C ;Humbel, BM; Horn, AF; Nielsen, NS; Jacobsen, C; Horsewell, A
The ultrastructure of casein in emulsions

Jensen, LHS; Loussert, C ;Humbel, BM; Horn, AF; Nielsen, NS; Jacobsen, C; Horsewell, A
The effect of preparation for electron microscopy on nanoemulsions

Posters and conference proceedings

Jensen, LHS; Horn, AF; Jacobsen, C; Nielsen, NS; Horsewell, A
Characterization of Emulsions of Fish Oil and Water by Cryo Scanning Electron Microscopy
Presented at: 17th International Microscopy Congress, Rio De Janeiro (2010)

Horn, AF; Nielsen, NS; Andersen, U; Jensen, LHS; Horsewell, A; Jacobsen, C
Lipid oxidation in omega-3 emulsions prepared with milk proteins
Presented at: 26th Nordic LipidFORUM Symposium, Ålesund, Norway (2011)

Horn, AF; Nielsen, NS; Jensen, LHS; Horsewell, A; Jacobsen, C
Emulsification technique affects oxidative stability of fish oil-in-water emulsion
Presented at: 102nd AOCS Annual Meeting & Expo, Cincinnati, Ohio, USA (2011)

Jensen, LHS; Horn, AF; Jacobsen, C; Nielsen, NS; Horsewell, A
Cryo-FIB SEM for Characterization of the Structure of Fish Oil Emulsions
MC 2011 Kiel, M7-P633, DGE – German Society for Electron Microscopy
Presented at: Microscopy Conference, Kiel, Germany (2011)

Jensen, LHS; Loussert, C ;Humbel, BM; Horn, AF; Jacobsen, C; Nielsen, NS; Horsewell, A
The structure of omega3 food emulsions
Presented at: 15th European Microscopy Congress 2012, Manchester (2012)

Pedersen, CL; Dezhao, L; Hansen, MJ; Feilberg, A;Jensen, LHS; Guldberg, LB; Schramm, A; Nielsen, LP
Sulfide oxidation in a biofilter
Presented at: 14th International Symposium on Microbial Ecology, Copenhagen (2012)

Horn, AF; Nielsen, NS; Jensen, LHS; Horsewell, A; Jacobsen, C
Emulsification technique affects oxidative stability of fish oil-in-water emulsions
Presented at: Science and Technology of Food Emulsions, London (2012)

Jensen, LHS; Loussert, C.; Humbel, BM; Horn, AF; Nielsen, NS; Jacobsen, C; Horsewell, A
Ultra structure of oil-in-water emulsions; a comparison of different microscopy- and preparation methods
To be presented at: Scandem 2013, Copenhagen (2013)

Jensen, LHS; Loussert, C.; Humbel, BM; Horn, AF; Jacobsen, C; Nielsen, NS; Horsewell, A
Ultra-structure of oil/water emulsions
To be presented at MC 2013, Regensburg, Germany (2013)

List of abbreviations

Omega-3 PUFA	Omega-3 polyunsaturated fatty acid
TEM	Transmission Electron Microscopy
SEM	Scanning Electron Microscopy
STEM	Scanning Transmission Electron Microscopy
EDS	Energy Dispersive X-ray Spectroscopy
FIB	Focused Ion Beam
CLSM	Confocal Laser Scanning Microscopy
HPF	High Pressure Freezing
I_h	Hexagonal Ice
I_c	Cubic Ice
LDA	low density amorphous ice
HAD	high density amorphous ice
VHDA	very high density amorphous ice
T_m	melting temperature
T_h	homogenous nucleation temperature
T_g	glass transition temperature
CEMOVIS	Cryo Electron Microscopy Of Vitreous Sections
GA	Glutaraldehyde
PFA	Paraformaldehyde
kV	Kilo Volt

List of figures

Chapter 1

Figure 1 18
Number of nanoemulsion publications the last 8 years

Chapter 2

Figure 2.1 21
Steps in the auto-oxidation
Figure 2.2 22
The basic components of an (o/w) emulsion
Figure 2.3 24
The native casein micelle
Figure 2.4 25
β-lactoglobulin
Figure 2.5 29
Hydration shells of protein molecules in aqueous solution
Figure 2.6 32
The aggregation of molecules as an effect of dehydration and fixation
Figure 2.7 35
Ice crystal damage in freeze-fractured emulsions
Figure 2.8 38
Pressure/temperature phase diagram for water
Figure 2.9 42
A schematic sketch of the HPF machine
Figure 2.10 45
Sublimation rate as a function of time and temperature
Figure 2.11 46
Freeze-fractures (cryo-SEM and replica TEM)

Chapter 3

Figure 3.1 54
Dehydration of suspensions of emulsions
Figure 3.2 55
Negative staining

Chapter 4

Figure 4.1 59
Overview of the experiments in this project

Chapter 5

Figure 5.1 62
Sample 2 mixed with low melting agar and fixed in

0.05%, 1%, 2%, 3% and 6% glutaraldehyde
Figure 5.2 64
Sample 6 mixed with low melting agar and fixed in 0.05%, 1%, 2%, 3% and 6% glutaraldehyde
Figure 5.3 66
Median and average droplet diameters of sample 6 in different chemical fixations and a boxplot of the data
Figure 5.4 67
Thickness of visible lines of low melting agar in 1:1 mixes
Figure 5.5 68
Black aggregates in chemically fixed samples
Figure 5.6 69
HAADF STEM and EDX results for two droplets from sample 2
Figure 5.7 71
Chemical fixations in agar pockets
Figure 5.8 72
Chemical fixations in capillary dialysis tubes
Figure 5.9 74
Freeze substituted samples with artifacts
Figure 5.10 76
Freeze substituted samples
Figure 5.11 78
Density plot of the droplet diameter of freeze substituted sample 6 and comparison to chemically fixed sample
Figure 5.12 79
STEM tomogram (HAADF and bright field) of freeze substituted sample 6
Figure 5.13 81
High pressure frozen freeze fractured sample 2 and 6 (cryo-SEM)
Figure 5.14 82
Sample 6, high pressure frozen and freeze substituted vs. high pressure frozen, freeze fractured sample (cryo-SEM)

Chapter 6

Figure 6.1 85
The structure of 70% emulsion with 2.8% NaCas
Figure 6.2 86
The structure of 70% emulsion with 2.8% WPI
Figure 6.3 88
The structure of 70% emulsion with 2.8% MPL20
Figure 6.4 89
MPL75, freeze-fracture cryo-SEM and cryo-FIBSEM
Figure 6.5 91
NaCas1.4 vs NaCas2.8 in CLSM and cryo-SEM
Figure 6.6 92
NaCas1.4 vs NaCas2.8 high pressure frozen and freeze-substituted, imaged at different angles
Figure 6.7 94
High pressure frozen freeze substituted samples 2 and 6
Figure 6.8 96
Cryo-TEM, samples 6 -9

Figure 6.9 98
The effect of production method on the structure of emulsions
Figure 6.10 99
Chemically fixed, oxidized 70% emulsions
Figure 6.11 100
Chemically fixed, oxidized 10% oil emulsion
Figure 6.12 101
Line scan EDX analysis, oxidized sample 2

Chapter 8

Figure 8.1 114
Casting agar pockets

Appendices

Figure A I 131
Screen shot from segmentation with e-cognition
Figure A II.1 132
Cryo-SEM holder for freeze fracture, hybrid system
Figure A II.2 133
Specimen carrier after fracture

List of tables

Chapter 2

Table 2.1 39
Relative cooling efficiencies of a selection of commonly used cryogens compared to propane

Chapter 3

Table 3.1 52
70% oil emulsions in this study

53
Table 3.2
10% oil emulsions in this study

Chapter 4

Table 4.1 56
Concentrations of fixatives for initial chemical fixation trial
Table 4.2 58
Emulsions in this study

Chapter 5

Table 5.1 65
The result of the post hoc test between samples fixed in different concentrations of glutaraldehyde

Table of Contents

Preface 2
Summary 3
Resumé 5
List of publications and communications related to this thesis work 7
List of abbreviations 9
List of figures 10
List of tables 13
1. Introduction 17
1.1 The Nanomega project 17
1.2 Food structure and microscopy 18
2. Theory 20
2.1 Oxidation processes in fish oil 20
2.2 Emulsions 21
2.3 Emulsifiers in this study and their theoretical effect on oxidation and interface layers 23
2.4 Characterization methods for emulsions 27
2.5 Fixations and other methods to image water-containing samples in the electron microscope 28
2.6 Chemical fixation 30
2.6.1 Glutaraldehyde 30
2.6.2 Osmium tetroxide 31
2.7 Fixation artifacts 31
2.8 Staining 33
2.9 Physical fixation 34
2.9.1 Liquid and solid water 34
2.9.2 Immersion freezing 39
2.9.3 High Pressure Freezing, HPF 41
2.10 Devitrification 43
2.11 Storing, processing and imaging of frozen specimens 43
2.11.1 Cryo-microscopy (SEM and TEM) 44
2.11.2 Freeze fracture and etching 44
2.11.3 Freeze substitutions 46
2.12 Electron microscopy 48
3. Research background 51

3.1 70% emulsions 51
3.2 10% emulsions 52
3.3 Experimental background 53
4. Project outline 56
4.1 Project aim 56
4.2 Project strategy 58
5. Results - Methods development 60
5.1 Chemical fixations 60
5.1.1 Samples mixed with agar 60
5.1.2 The artifacts of fixation in agar 66
5.1.3 About contrast in the samples 68
5.1.4 Fixation in agar pockets 70
5.1.5 Fixation in capillary tubes 71
5.2 Freeze substitution 73
5.3 High pressure freezing, freeze fracture and cryo-SEM 79
6. The micro- and nano-structure of fish oil emulsions 84
6.1 The effect of emulsifiers on structure 84
6.1.1 NaCas 84
6.1.2 WPI 86
6.1.3 MPL20 87
6.2 The effect of the amount of added emulsifier on the structure 90
6.3 The effect of emulsion type on structure 93
6.4 The effect of production method on structure 94
6.5 The effect of oxidation on structure 99
7. Conclusion and outlook 102
7.1 Conclusions 102
7.2 Outlook and future experiments 104
8. Materials and methods 106
8.1 Chemicals, consumables, equipment and microscopes 106
8.1.1 Chemicals 106
8.1.2 Consumables 108
8.1.3 Equipment 109
8.1.4 Microscopes 111

8.2 Preparation of emulsions 112
8.3 Protocols 113
8.3.1 Room temperature fixation and embedding in agar mix 113
8.3.2 Fixation in capillary tubes 113
8.3.3 Imaging in the confocal laser scanning microscope 113
8.3.4 Fixation in agar pockets 114
8.3.5 Freeze substitution 115
8.3.6 Sectioning and post staining 115
9. References 116
A. Appendix I 131
B. Appendix II 132

1. Introduction

1.1 The Nanomega project

The Nanomega project was conceived in 2008 as collaboration between the National Food Institute, the Department of Mechanical Engineering and the Center for Electron Nanoscopy, all located at the Technical University of Denmark. The idea was to apply a synergistic approach and combine experiences from different fields of science to explore oxidation in fish oil emulsions. The Lipids and oxidation group at the National Food Institute have a long-term experience in researching the possibilities of adding fish oil to food products. Addition of fish oil to industrial food products is of interest to both the food industry and consumers for reasons such as perceived health benefits and added commercial value. Fish oil is rich in the essential long chain omega-3 PUFAs eicosapentaenoic acid, C20:5n-3 (EPA) and docosahexaenoic acid, C22:6n-3 (DHA) which are not effectively converted from their precursor fatty acids in the human body (Brenna, Salem et al. 2009). Dietary supplementation with long chain omega-3 poly unsaturated fatty acids (omega-3 PUFAs) has been shown to improve cardio-metabolic health-parameters (de Leiris, de Lorgeril et al. 2009, Kris-Etherton, Harris et al. 2002) such as lower blood pressure (Appel, Milleri et al. 1993). It has other effects e.g. preservation of cognitive capabilities in the elderly population (Sonia Gonzalez, Huerta et al. 2010). Lately, other trials have found no effect by omega-3 supplements, e.g. in patients with cardiovascular risk factors or metabolic syndrome (Roncaglioni, Tombesi et al. 2013, Lana Lai, Petrone et al. 2013). There seems to be a need for standardization of experiments and further research in the epidemiology studies in the field (Poudyal, Brown 2013). The complexity of setting up such trials is exemplified by the fact that the effect of fish oil seems to depend on the foods eaten *with* the fish oil supplements as well (Ma, Liaset et al. 2011). However, effects can be shown at the cellular level, such as a dose-dependent inhibition of breast-cancer cells via pathways that introduce cellular stress and apoptosis (Wu, Harvey et al. 2005) and DHA is shown to modulate cell membrane structures by formation of lipid rafts (Stillwell, Shaikh et al. 2005). Omega-3 rich oil is an area of research not limited to medical or food science. Since the demand for fish oil is increasing research efforts are carried out to ensure that future demands for fish oil can be met in an eco-friendly way by e.g. metabolic engineering in transgenic plants (Ruiz-Lopez, Sayanova et al. 2012). Omega3-PUFAs like EPA and DHA contain a large number of double bonds which causes the omega-3 fatty acids to be highly susceptible to oxidation. This is a feature that limits the shelf-life of fish-oil enriched food products to a degree where it limits the accessibility to the market. Strategies for limiting oxidation and increasing the shelf-life of potential products are thus necessary for commercial production. One strategy for addition of fish oil to food products is to add the oil as an emulsion rather than as neat fish-oil. Studies so far have indicated that emulsification of the fish oil changes the oxidative stability of the product but it seems to depend partly on the food matrix to which the emulsion is added whether emulsification is an advantage (Nielsen, Jacobsen 2009) or not (Let, Jacobsen et al. 2007). It is therefore of interest to look at the pure emulsions to assess what determines the oxidation. It has been proposed that oxidation is, to some extent, dependent on the structure of the emulsion; including oil droplet size distributions and the thickness of the interface between oil and water (Waraho, McClements et al. 2011). This interface can be stabilized e.g. by food grade emulsifiers such as proteins and phospholipids from milk. The main objective of the Nanomega project was to study the oxidation stability of fish oil emulsions prior to addition to food products and finally to assess their use in model food systems.

And also to characterize the micro- and nano-structure of the emulsions, some of which had very small oil droplets.

Nano-emulsions are strictly defined as emulsions with droplets formed by shear-induced rupturing and droplet sizes below 100 nm (Mason, Wilking et al. 2006) but the term is used more broadly. Characterization of nano-emulsions is an area of growing interest as the nano-emulsions have applications not only in foods but also for drug delivery etc. Figure 1.1 displays the amount of hits according to publication year in the Thompson Reuters' WebOfKnowledge database of scientific publications and it is clear that research in the field is increasing. Because of the size of some of the oil droplets and the expected size of the interface layers, of e.g. 10 nm for sodium caseinate (Fang, Dalgleish 1993), electron microscopy appeared to be the appropriate choice of technique.

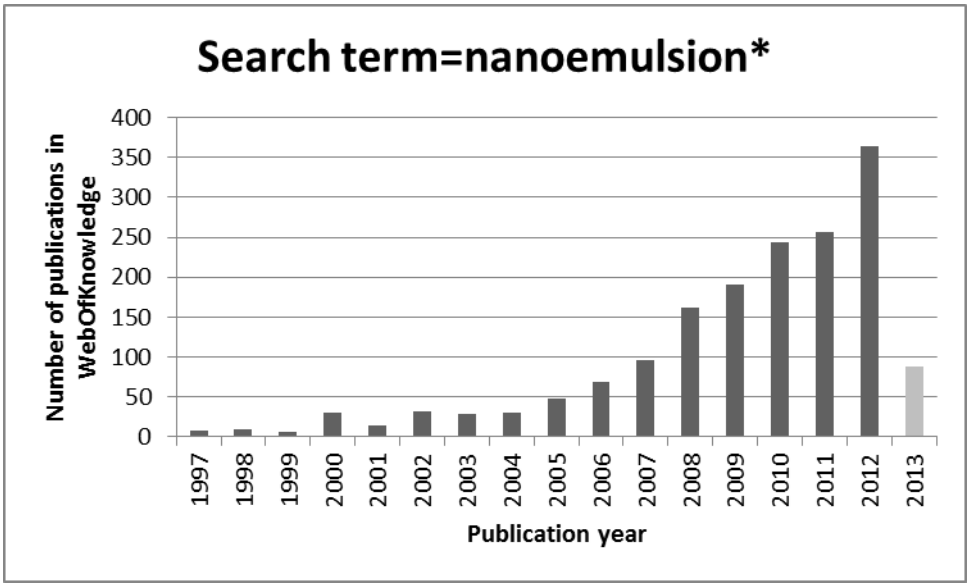

Figure 1. Number of nanoemulsion publications within the last 8 years (Thompson Reuters 2013)

1.2 Food structure and microscopy

The structure of foods is an important attribute in foods just as taste and smell. It affects the way we perceive food products, e.g. texture, but it also has a huge impact on other attributes such as taste, shelf life, water content etc. Variations in fat or protein content can have a big influence in how the food is perceived, e.g. in stirred yoghurt (Tomaschunas, Hinrichs et al. 2012) and studies are emerging in which electron microscopy data are combined with chemometrics and sensory analysis via principle component analysis (Varela, Chen et al. 2006, Allan-Wojtas, Sanford et al. 2003). Food microscopy is a sub field of material microscopy for soft matter and is just as versatile. Food samples are special in the sense that they often have a biological origin without exactly being biological samples. In biology, cells and tissues are highly ordered structures that diverge in sizes and types. Some are very small and liquid like suspensions of viruses; some are solid such as bone and cartilage while other samples like nerve cells are very large (in

microscopy terms), delicate and require careful and elaborate sample preparation to accurately preserve the fine structures within. Even though one can argue e.g. that meat is muscle cells; food scientists are rarely interested in the organelles within a single cell. Food samples rarely display highly ordered structures in the same sense as cells; rather they are composed of homogeneous materials in bulk samples e.g. casein micelles and fat globules in milk or starch granules in flour. What characterizes food samples are the repeating structures and the effect they have on the properties on a large scale. But the texture and size of interest can be just as diverse between different samples. It is necessary to identify the right method of characterization for food samples on behalf of their extent, their texture, water content and the order of structure of interest. And even for the same type of sample there may be need for several methods depending on the question to be answered with the specific analysis. An exhaustive description of all applicable techniques, alone or in combination, would be as impossible to produce as it is impossible to classify every single type of food sample and the structural or compositional question that researchers might come up with. Furthermore some samples might display several stages during aging or through a production line, extensively changing both structure and composition.

Liquid samples such as solutions and suspensions are a special case since the water content requires specific preparation methods for electron microscopy which is normally carried out under vacuum. Their liquid nature renders them especially susceptible to alterations of their structure as a result of the water content which is easily by manipulated by water vapor pressure (high or low), ice crystal formation, and perhaps the samples are prone to flocculation or creaming. The particles themselves might also react to the solution they are in, e.g. hydrophilic proteins which are stabilized by a hydration shell of tighter bound water molecules (Kellenberger 1987).

The work in this thesis has been a search for different methods in mainly electron microscopy for the characterization of the model emulsions in the Nanomega project. The emphasis has been to find and further develop these methods. And second to characterize the samples of interest by using a combination of these approaches. The solutions we found were not all applicable in Denmark at the time of the thesis work, which is why a great deal of the work presented in this thesis has been done at the Electron Microscopy Facility, Université de Lausanne. The group led by Dr. Bruno Humbel specializes in correlative microscopy and cell ultra-structure but it is also a core facility that faces the challenge of a number of diverse, incoming samples. Lucky for us they were brave enough to welcome me in the group for electron microscopy of our fish oil emulsions. Their expertise of sample preparation and wide selection of equipment greatly improved the nature of our results, of which many would not otherwise have been possible at the time of the experiments.

2. Theory

The Nanomega project is concerned with a delivery system for fish oil to food products; the oil in water emulsion, which is the best described delivery-system for lipidic materials to aqueous food products (Sagalowicz, Leser 2010). A very brief introduction to emulsions, the emulsifiers in this study and fish oil oxidation will be given. Imaging of emulsions by electron microscopy requires specialized preparation since electron microscopy in most cases is performed in vacuum. Thus the preparation methods for electron microscopy are very important for the outcome of the analysis and will form a large part of this chapter and also of the results section. Finally, this chapter includes a description of the imaging methods. Physical phenomena differ between simpler chemical systems of few components and complex biological systems by many orders of magnitude in complexity. Calculations of even simple systems require heavy computation and a lot of assumptions. Hence, empirical observations and a thorough understanding of the phenomena that lie behind the observations has been the leading motivation for the development in biological microscopy and sample preparation. Trial and error is still a large part of method development in biological microscopy and will continue to be so. Emphasis in this section has thus been given to explain the basic concepts and mechanisms, rather than to quote a large number of formulas that will not be used in calculations later. Furthermore, the project is cross disciplinary and finds itself between food science and soft matter microscopy. It is my hope that it will appeal to both groups.

2.1 Oxidation processes in fish oil

Lipid oxidation of omega 3-PUFAs in food products causes undesirable changes in appearance, texture, odour and flavour, e.g. fishy and rancid off-flavours (Jacobsen 1999). Two oxidation processes are important in such systems; autooxidation and photoinduced oxidation. Photooxidation is initiation of oxidation by light in the presence of photosensitizers whereas autooxidation results from the reaction of free radicals with oxygen after initiation by e.g. protein radicals, heat or metal ions (Jacobsen, Nielsen 2007). The emulsions in the present work have been subjected to autooxidation only. The autooxidation proceeds via a number of steps that are illustrated in figure 2.1. After initiation, the formation of alkyl radicals (R•) from unsaturated fatty acids (RH) occurs and the oxidation process proceeds as a chain reaction in the presence of oxygen to form peroxyl radicals (ROO•) which can react with unsaturated fatty acids to form hydroperoxides (ROOH) and new radicals (R•). Moreover, hydroperoxides can be decomposed by trace metals or heat to form new peroxyl radicals and alkoxyl radicals (RO•) which can accelerate the process by the formation of new hydroperoxides. In fish oil, with its very complex mixture of different fatty acids this results in a wealth of hydroperoxides with different chain lengths, HOO groups and structure of double bonds (Jacobsen, Nielsen 2007). Autooxidation results in primary and secondary oxidation products, and the hydroperoxides are the primary products. They are essentially taste- and odourless and are normally detected by chemical analysis. The secondary products of oxidation arise from

the alkoxyl radicals which can decompose further into non-volatile and volatile species. Due to the intricate nature of the lipid hydroperoxides, the complexity of the composition of the secondary oxidation products is even larger. In contrast to the lipid hydroperoxide, the volatile secondary oxidation products are responsible for the changes in aroma and flavour (Frankel 1991).

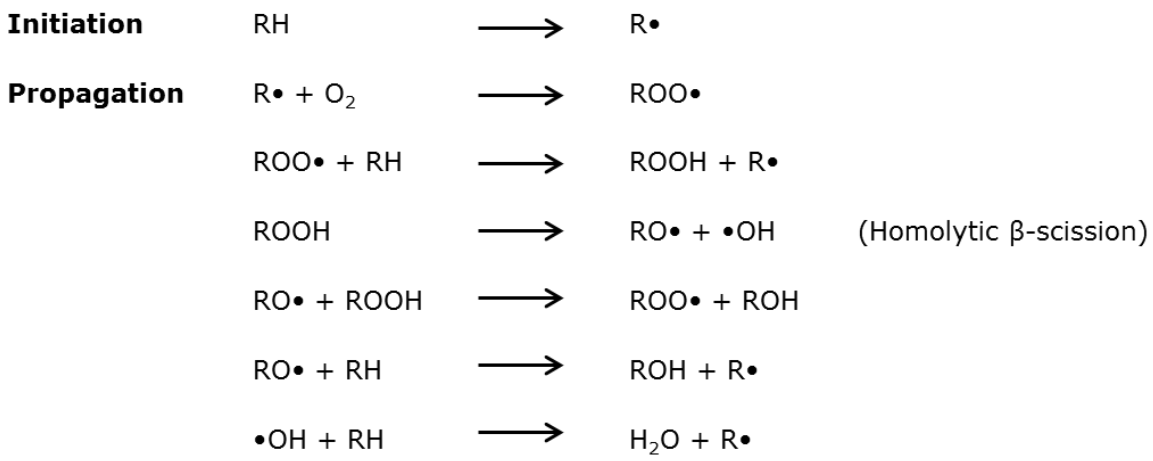

Figure 2.1. Steps in the auto-oxidation. Partly re-drawn from (Jacobsen, Nielsen 2007).

2.2 Emulsions

An emulsion is a system of two immiscible liquids which in the presence of a surfactant can form a colloid with one liquid being dispersed in the other (Bibette, Calderon et al. 1999). Hence the expressions dispersed and continuous phase. When oil is dispersed in water, it is referred to as an oil-in-water (o/w) emulsion and when the oil is the continuous phase in which water is dispersed, the emulsion is a water-in-oil (w/o) emulsion. Other configurations such as double emulsions, e.g. water-in-oil-in-water also exist. This work deals exclusively with (o/w) emulsions. A simplified schematic representation of an (o/w) emulsion is given in figure 2.2 below, represented by the water phase (continuous phase) in blue, the oil phase (dispersed phase) in yellow and an emulsifier (interface region) in orange. In reality, the systems are not so simple. Often, the emulsifiers are not just present at the interface region but are partly soluble in one of the phases. In general, but not always, the emulsifiers are soluble in the continuous phase, not the dispersed phase (Mason, Wilking et al. 2006) where they might form structures by self-interaction.

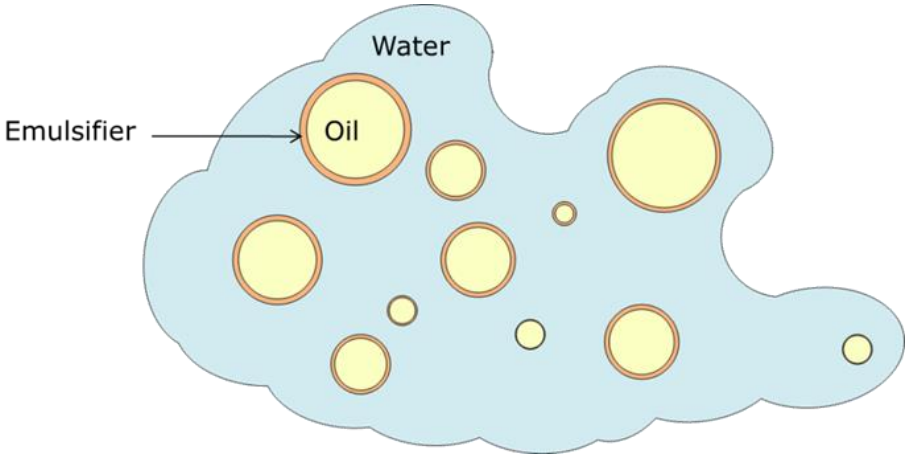

Figure 2.2. The basic components of an (o/w) emulsion; the water phase, the interface region with a stabilizing emulsifier and the lipid droplets.

Since there is interfacial tension between immiscible liquids the interface will tend to be as small as possible. The surface tension can be reduced by the addition of amphiphilic surfactants which will then occupy the interface region. Emulsifiers such as amphiphilic proteins or lipids, and hydrocolloids are used in foods. Emulsifiers can stabilize emulsions from coalescence, both by the formation of a mechanical barrier but also in some cases by production of an electrostatic barrier (Benita, Levy 1993). Emulsions can be destabilized by either coalescence in which two droplets fuse to a larger droplet due to the breaking of the film that separates them or, in case of nanoemulsions, by Ostwald ripening which is happening when the molecules in the dispersed phase are partly soluble in the continuous phase and large particles grow at the expense of small particles. In this mechanism, loss of molecules and subsequent diffusion through the continuous phase is more rapid from small particles. Both mechanisms can be largely eliminated by the appropriate composition of the emulsifier and the two phases (Mason, Wilking et al. 2006).

Emulsions are important in many fields such as the oil industry, as cutting fluids, in the pharmaceutical industry and in the food industry. The (o/w) food emulsion is well-known, e.g. mayonnaise and milk.

In general, emulsification makes oils more vulnerable to oxidation (Frankel, Satue-Gracia et al. 2002). The process is much more complicated than outlined above for pure oil and is acknowledged to include oxidation in all areas of the emulsion, i.e. water phase, interface layer and oil droplets (Jacobsen, Nielsen 2007). But it is also speculated that the oxidation in emulsions is largely initiated at the interface region where the oil is in close vicinity of prooxidants and oxygen. For this reason the droplet size and hence the area of this surface is expected to have great impact on the oxidation with smaller droplets oxidizing more easily because of a relatively larger surface area (McClements, Decker 2000). This has been confirmed in some studies (Jacobsen, Hartvigsen et al. 2000, Let, Jacobsen et al. 2007) while in other studies it seems that other factors are more influential (Let, Jacobsen et al. 2007, Sorensen, Baron et al. 2007).

By selecting carefully the ingredients of the emulsion, the oxidation process can be affected, e.g. it is important to ensure low oxidation level of the initial ingredients to delay the steps in the chain reaction. But the *type* of ingredients such as emulsifiers also has a large impact on the oxidative stability since some of them can act as antioxidants and a so-called “interfacial engineering strategy” can thus be applied to protect the omega-3 PUFAs against oxidation (Jacobsen, Nielsen 2007).

Keeping in mind that the emulsifiers are also present in the water phase and thus might exert certain antioxidative effects there as well.

Below is a description of the emulsifiers presented in this thesis. The milk proteins were selected on the basis of their common use in the food industry and on their possible antioxidative effect whereas phospholipids (lechitin) have been shown to change the interface layer and improve stability (Fang, Dalgleish 1993).

2.3 Emulsifiers in this study and their theoretical effect on oxidation and interface layers

Casein is a phosphoprotein from milk. In bovine milk it makes up roughly 80% of the protein and forms colloidal micelles of 30 nm to 600 nm which prevents precipitation of calcium phosphate (Donelly, Mcneill et al. 1984) to ensure delivery of these entities to suckling calves. The micelles are considered colloidal particles formed by casein (α and β types) wrapped up in water-soluble κ-casein molecules in micelles (Kralova, Sjoblom 2009). Caseins have four different components; αS1 (199 amino acid residues (aa), ~23.6 kg/mol), αS2 (207 aa, ~25.2 kg/mol) , β (209 aa, ~24 kg/mol) and κ (169 aa, ~19 kg/mol). These subtypes comprise ~38, 10, 40 and 12 % of the total casein in milk, respectively and the molecular weights vary slightly between genetic variants (Farrell, Jimenez-Flores et al. 2004).

The caseins do not have well defined secondary or tertiary structures (Gaspar, Appavou et al. 2008). Apart from the regions around the centers of phosphorylation, the caseins are essentially of the β-strands type but restricted in the formation of β-sheets due to conserved features of the primary structure; a feature that renders the proteins open, mobile and flexible (Holt, Sawyer 1993).

The structure of the native casein micelle is the subject of much debate. The latest model, which will form the basis of the following outline, describes the structure as nanoclusters ~2 nm of calcium phosphate attached to phosphorylation centers formed by 3-5 phosphorylated amino acid residues residing in a network formed by the tails of the casein molecules; with only small variations in protein density over the network. These tails are self-associated by weak interactions such as hydrophobic interactions, hydrogen- and ion bonding, weak electrostatic– and Van der Waal attractions (de Kruif, Huppertz et al. 2012). The casein micelle is suggested to contain water channels inside and have a sponge-like structure (McMahon, Oommen 2008). The Nanocluster model is shown in figure 2.3 (A) (Dalgleish, Corredig 2012). The cryo-electron tomography study presented in figure 2.3 (B) supports this structural model very well (Trejo, Dokland et al. 2011).

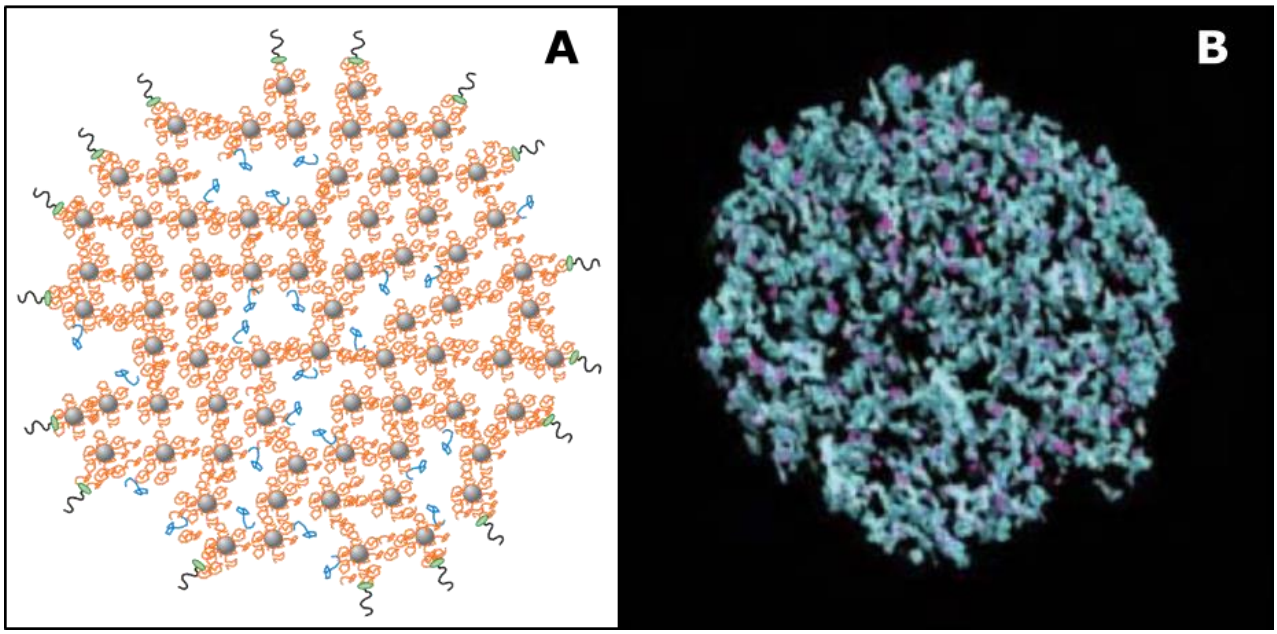

Figure 2.3. (A) The nanocluster model of the casein micelle and (B) Image from cryo-electron tomogram of the casein micelle (Dalgleish, Corredig 2012, Trejo, Dokland et al. 2011)

The caseins are not evenly distributed in the casein micelles. K-caseins lack phosphate centers to interact with the nanoclusters and are predominately located at the surface of the casein where they, being more water soluble than the other caseins, limit the growth of the micelles to extents larger than 150-200 nm by the limitation of available κ-casein to stabilize the micelle. Furthermore, a portion of the molecule is extended from the surface of the molecule in a 'hairy layer' of 5-10 nm which provides steric stabilization against close approach of the casein micelles. The αs1 and αs2 caseins are highly phosphorylated and are found throughout the structure where they interact with the nanoclusters. β-caseins are predominately found in the interior of the micelle where they are suggested to interact with the hydrophobic nanoclusters via their hydrophobic C-terminal and to stabilize the water channels with their hydrophilic N-terminal tails. (Dalgleish, Corredig 2012).

Sodium caseinate is basically the casein fractions from milk after removal of calcium phosphate, which is necessary for the formation of the native casein micelle. Caseins behave differently when they adsorb onto surfaces, i.e. oil droplets or solid, apolar surfaces such as latex particles. They do not penetrate significantly into the oil, as shown by the similar coverage of solid and liquid particles (Dalgleish 1998) but position themselves with their hydrophobic domains at the interface and the hydrophilic tails projecting into the aqueous solution. β-casein is expected to absorb via the hydrophobic domains in the C-terminal, with the hydrophilic tail protruding into the water phase, whereas the αs_1 is expected to adsorb more evenly over the molecule because of the position of hydrophobic domains closer to the middle of its sequence. This corresponds well to differences in thickness of pure layers with αs_1 creating thinner layers (Dalgleish 1996). K-casein tends to self-aggregate, and these aggregates are present in caseinate (Dalgleish, Corredig 2012).

Adsorbed proteins are not uniform but can occupy a range of different conformations with similar energy along a surface (Euston 2004). The flexible nature of the casein molecules especially enables them to

stretch or fold and apply coverage of oil droplets from by 1 mg/ m^2 which is the thinnest layer possible to a maximum of 3 mg/ m^2 where the layer is compact and the hydrophilic tails protrude further into the water phase. These layers corresponded to approximately 5-10 nm, respectively (Fang, Dalgleish 1993). By calculations (applying the mean value of 23000 g/mol) these minimum and maximum coverage correspond to 13 nm^2/molecule and 40 nm^2/molecule, respectively (Dalgleish 1998).

Because of the different adsorption behavior and the flexibility of the molecules it is difficult to predict the surface layer thickness of caseinate.

Whey proteins make up approximately 20% of milk proteins and consists to a large degree of β-lactoglobulin (168 aa, ~18.4 kg/mol) and α-lactalbumin (123 aa, ~14 kg/mol) (Farrell, Jimenez-Flores et al. 2004, Kontopidis, Holt et al. 2004). These are globular proteins and exhibit both 2' and 3' structure. α-lactalbumin is involved in the synthesis of lactose. The function of β-lactoglobulin is more diffuse and it is probably overexpressed in the mammary gland of lactating animals as a source of nutrition. It is found as a dimer above pH 3. The major part of the protein folds into an eight-stranded β-barrel structure with a ninth external β-strand and a three-turn α-helix. It has a central cavity that can accommodate linear molecules like fatty acids (Kontopidis, Holt et al. 2004). The structure (as bound to cholesterol) is shown in figure 2.4.

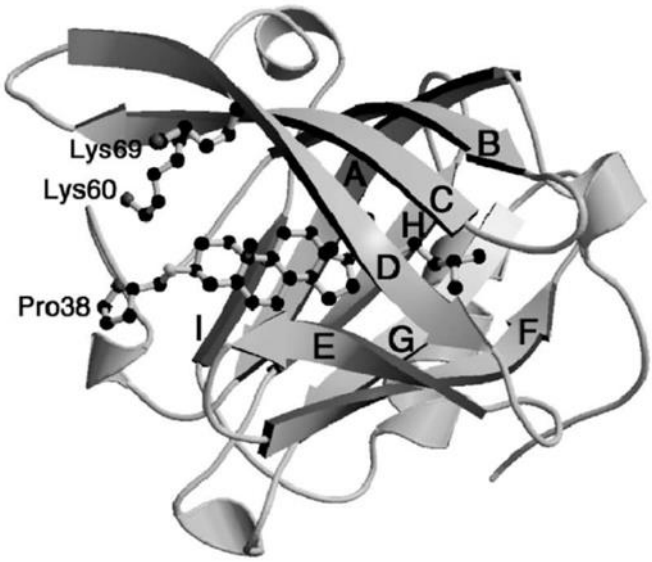

Figure 2.4. β-lactoglobulin (as bound to cholesterol) (Kontopidis, Holt et al. 2004)

The whey protein isolate (WPI) in this study consists mainly of β-lactoglobulin, which is thought to change conformation by unfolding at the interface when adsorbed (Dalgleish 1996) but only slightly, with conservation of the α-helix and alterations but not destruction of the β-structures at pH7. The external β-strand absorbs first and a slow unfolding of the protein follows (Fang, Dalgleish 1997). Nevertheless β-lactoglobulin is not expected to be able to stretch to a similar degree as that of casein as shown by higher requirements of WPI for minimum surface coverage (Hunt, Dalgleish 1994).

Phospholipids are amphiphilic molecules consisting of a polar head group and a hydrophobic tail. They are derived from either glycerol (phosphoglycerides) which consists of a glycerol backbone, a phosphorylated alcohol and two fatty acids, or from sphingosine resulting in sphingomyelin which consists of the

sphingosine backbone, phosphoryl choline and a single fatty acid chain. Their size (lengthwise) is in the range of a few nm. On the surface of an oil droplet they will extend their lipophilic tail into the oil droplet thereby stabilizing the emulsion and creating a monolayer. Excess phospholipids will not be soluble in the continuous phase but will form structures to limit the surface tension. Most phospholipids do not form micelles because their two fatty acyl chains are too bulky to fit into a micelle. The favored state of phospholipids in aqueous media is a bimolecular sheet called a lipid bilayer with the polar heads facing water and the hydrocarbon chains facing each other (Stryer 1999). Bilayers are self-annealing and will tend to form water containing vesicles, i.e. liposomes.

The milk phospolipids in this study are a mixture of many different phospholipids (Horn, Nielsen et al. 2011).

There are numerous ways that these emulsifiers can be speculated to affect the oxidation process.

It is generally found that transition metals are the major prooxidants in emulsions (Waraho, McClements et al. 2011) where they can decompose lipid hydroperoxides located at the droplet surfaces (Nuchi, McClements et al. 2001). Transition metals strongly catalyse oxidation in lipids and prevention of contact between them and the oil can increase the stability towards oxidation (Sagalowicz, Leser 2010). Emulsions have large surface areas where the lipids can come into close vicinity of prooxidants from the water phase. For an 'interfacial engineering strategy' the surface properties have therefore received much interest.

Furthermore, proteins are modified prior to lipid oxidation and only the adsorbed proteins are degraded during oxidation (Berton, Ropers et al. 2012) pointing further to the importance of the droplet surface.

This has led to examinations of the oxidation as an effect of the droplets sizes as smaller droplets lead to relatively larger surface areas. Studies have found an increase in oxidation by smaller oil droplets (Lethuaut, Metro et al. 2002) and oxidation appears to onset earlier in emulsions with smaller droplets, (Jacobsen, Hartvigsen et al. 2000) but levels out. Other results show the reverse (Let, Jacobsen et al. 2007, Ries, Ye et al. 2010). It seems that other factors than the size of the surface controls the oxidation and it is suggested that since a large surface area is a general attribute of all emulsions despite varying droplet sizes, that the rate of oxidation is simply not limited by the size of the surface area (Waraho, McClements et al. 2011).

It can be speculated that the thickness of the interface can form a thicker layer and thereby hinder contact of prooxidant trace metals and lipids. Different emulsifiers can be used to obtain differential layer thickness. For instance, casein in excess can form a thick interfacial layer around dispersed oil droplets of up to 10 nm compared to 1−2 nm for whey proteins (Dalgleish, Srinivasan et al. 1995). However, a cohesive, cross-linked surface layer of β-casein did not provide such protection indicating that prooxidants can diffuse readily through the barriers of interface layers and react with the lipids (Kellerby, Gu et al. 2006).

Protein layers might provide protection by electrostatic hindrance of prooxidant-lipid interaction (Kellerby, McClements et al. 2006). The surface charge depends on the emulsifier type and is affected by pH. The so-called isoelectric point (IEP or pI) is the pH value at which the negative and positive charges on the molecule are equal. So conversely, when the pH is higher than the pI of the protein, the negatively charged droplets oxidize faster and this might be mediated by attraction of cationic transition metals (Waraho, McClements et al. 2011).

Chelation, i.e. the formation or presence of bonds (or other attractive interactions) between two or more separate binding sites within the same ligand and a single central atom (McNaught, Wilkinson 1997), might provide protection against oxidation by the sequestering of transition metals. Casein chelates and sequesters divalent cations such as iron because of its clusters of phosphoserine residues (Sugiarto, Ye et al. 2009) and it has been suggested that oxidation of the oil droplets is increased by having more casein at the interface because metal ions will be positioned closer to the interface (Villiere, Viau et al. 2005). WPI protein can also chelate iron (Tong, Sasaki et al. 2000), but not to the same extent as sodium caseinate, probably because of a lower amount of phosphoserine residues (Sugiarto, Ye et al. 2009). WPI is a free radical scavenger via its sulfhydryl groups (Tong, Sasaki et al. 2000, Elias, McClements et al. 2005).

But there is also protein in the water phase. Unadsorbed proteins in the water phase have antioxidative capabilities (Berton, Ropers et al. 2011). And the antioxidative effect of protein content (in the water phase) has been shown to offset the effect of attributes such as droplet size and protein type (Ries, Ye et al. 2010). Casein or WPI in the continuous phase seems to protect the emulsions against oxidation and oxidation is accelerated when the excess protein is removed from the continuous phase (Ries, Ye et al. 2010)(Faraji, McClements et al. 2004).

Phospholipids (lecithin) with casein can change the interface layer and improve stability (Fang, Dalgleish 1993) but it has recently been published that especially the presence of a phospholipid at the interphase led to increased oxidation of an emulsion made with β-casein. This was related to a larger degree of heterogeneity of the interface as imaged by atomic force microscopy (Berton-Carabin, Genot et al. 2013).

In contrast to the figure 2.2, it should now be obvious that emulsions are quite complex systems and they represent a challenge in structure characterization, especially by electron microscopy. This is not only because of the complexity of the structure nor the minute sizes, i.e. below 10 nm interface layers. For electron microscopy, which is inherently performed with the specimen in vacuum, the real challenges presented by emulsions are that they are liquid, self-organizing systems which are very subjective to changes in temperature and vapor pressure. Furthermore, electron microscopy relies on the scattering of electrons and all components of these systems contain only light materials such as carbon, oxygen and nitrogen which have low mass contrast.

2.4 Characterization methods for emulsions

Since the emulsions are liquid and with a relative high water content it is strictly necessary to preserve the structure before placing it in the vacuum of the electron microscope.

Electron microscopy of soft and liquid samples often requires extensive preparation and it is thus a good idea to have an initial idea of how to proceed, e.g. by use of light microscopy to gain an idea about the size and location of the structure of interest. The choice of preparation prior to electron microscopy depends on the type of microscopy needed to image the structure of interest. Very generally, transmission electron microscopy (TEM) is used for smaller features and requires thin films though which an electron beam can be transmitted and scanning electron microscopy (SEM) is used for larger structures and bulk samples by

scanning an electron beam across the surface. The dual beam microscope can assist by specific removal of material by the focused ion beam either creating thin lamella of a bulk sample for TEM inspection, or gaining access to specific areas inside the bulk structure for SEM imaging directly and the method is also applied sequentially in creating 3D reconstructions of the microstructure, i.e. 'slice and view'. 3D reconstructions can also be achieved by serial sectioning of block faces inside the microscope, serial section by ultramicrotomy for TEM, and tomography techniques. The boundaries between the types of microscopy are not rigid and preparation methods can further bridge the gap between the methods which make it possible to use different types of microscopy for characterization of different aspects of samples. Most notably by 'correlative microscopy' than integrates fluorescence optical microscopy, including confocal microscopy, and electron microscopy (both TEM and SEM). And finally there is more information than just images to be collected in the microscopes, e.g. spectroscopic techniques, including x-ray generation during electron imaging, which provide information of the elements in the sample. The possibilities seem inexhaustible and new developments are often driven by specific research questions.

A prerequisite for imaging is the successful preparation of the samples. This is a crucial step. No matter how good a collection of microscopes – if the initial preparation is insufficient and causes artifacts, the result will be a collection of very good images of artifacts. Cryo methods and chemical fixations alone or in combination make up a large part of this preparation for biological samples and is the scope of this thesis.

2.5 Fixations and other methods to image water-containing samples in the electron microscope

Water is the basis of life; it is abundant in nature, and present in almost all biological samples. It cannot be regarded as passive solvent but takes active part in the stabilization and confers movements and functionality in proteins which normally require a hydration shell of water molecules of approximately n=2 for normal function. This is illustrated in figure 2.5 in the classic figure by Kellenberger (Kellenberger 1987) (left) and a modern model of myoglobin shown with its hydration shell of n=1.911 water molecules (Frauenfelder, Chen et al. 2009). In the case of biological membranes which expose polar head groups to the water, the water is expected to interact to an even larger extent and it is hypothesized that the hydration layer of structured water might in fact interfere with the access of certain molecules to the membranes. The extent of structure of hydration layer in these cases is affected by the actual composition of the membranes (Higgins, Polcik et al. 2006). Hydration shells and the bulk water are also referred to as perturbed or unpertubed water, respectively. The term 'bound water' is sometimes used to describe the perturbed water but it is quite misleading since there is no binding kinetically or thermodynamically but a fast exchange between perturbed and unperturbed water, with interaction strengths like that of water-water (Halle 2004). In a cell, almost all of the water can be interpreted as being bulk water (Dubochet 2009). But nevertheless, the presence of water affects proteins in solutions, e.g. proteins in the cytoskeleton are slaved directly to fluctuations in the intracellular water (Lenormand, Millet et al. 2011). Large scale protein motions are affected by fluctuations in bulk water while the internal protein motions are controlled by the hydration shell water (Frauenfelder, Chen et al. 2009).

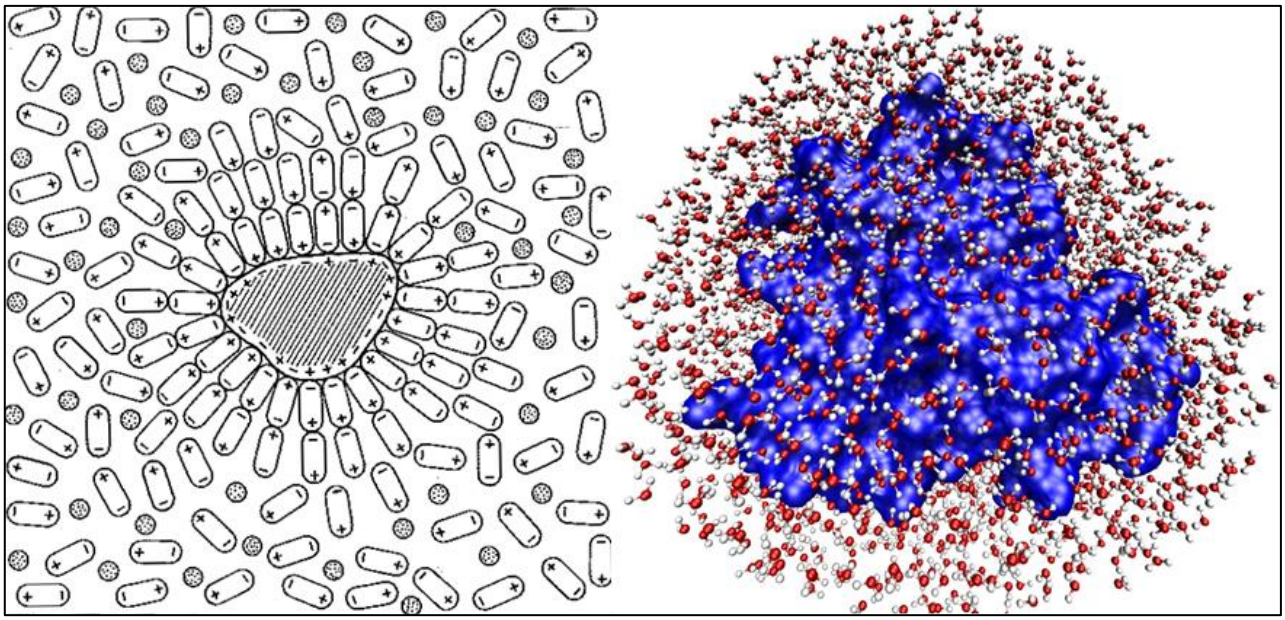

Figure 2.5. Hydration shells of protein molecules in aqueous solution. Adapted from (Kellenberger 1987) and (Frauenfelder, Chen et al. 2009)

Removal of the hydration shell will affect proteins since their function and folding, i.e. position of side chains and active sites, depends on the balance between hydrophilicity and hydrophobicity and hence the presence of the water. When the hydration shell is removed, the hydrophilic molecules will collapse, adhering either to each other or the support matrix. And yet, dehydration is an important part of all preparation methods that does not involve imaging of the native, hydrated samples. To avoid dehydration of samples, there are several methods. One is cryo-electron microscopy where the samples are imaged while frozen, but also methods of imaging samples in their hydrated state at room temperature exist, such as environmental scanning electron microscopy (ESEM) or imaging through an electron transparent membrane in a closed holder, a so-called wet cell. The methods have relatively low resolution, e.g. 100 nm for imaging low contrast materials in a wet cell (Thiberge, Nechushtan et al. 2004). Also ESEM has a rather low signal-noise ratio because electrons are scattering in the chamber because of the gaseous water molecules. Especially in cases with liquid samples which require rather high vapor pressure of water even at temperatures close to 0 °C to stay hydrated (Stokes 2008). Another problem is that in scanning electron microscopy the imaging is from the surface and the surface of a liquid, like our emulsions, is rather dull and featureless to look at. To see the different constituents in the emulsions we would have to charge the samples and utilize the fact that electrons behave differently in the water phase and the oil phase. This is a consequence of the pi orbitals of the alternating double bonds in the unsaturated fats. This phenomenon gives rise to a secondary electron charge contrast that can be used to distinguish unsaturated fatty acids from water (Stokes, Thiel et al. 2000). But again the low resolution offered by the method was insufficient for the work in this thesis. It should be mentioned that the methods have other advantages such as the possibility to perform dynamic experiments under the electron beam; i.e. with pressure and temperature for the ESEM or even some manipulation in the chamber with the right tools, but it has not been relevant in this project.

It seems therefore, that the interesting methods are limited to chemical fixation, cryo microscopy and a combination of these.

2.6 Chemical fixation

Chemical fixation is used not only in electron microscopy but in microscopy in general. The basis of chemical fixation at room temperature is a crosslinking of the protein molecules within the sample to facilitate the subsequent removal of water. Without stabilization, the samples would aggregate and collapse to a large degree during dehydration. In this project we have worked with a combination of two aldehyde fixatives, glutaraldehyde and formaldehyde. Furthermore we have performed post-fixation of lipids with osmium tetroxide.

2.6.1 Glutaraldehyde

Glutaraldehyde is a dialdehyde with two active groups. It is extensively used in preparation for electron microscopy due to its ability to preserve fine structures. It crosslinks fast and irreversibly. Fixation with glutaraldehyde requires a buffer to counteract a lowering of pH during fixation which could potentially affect the efficiency of glutaraldehyde (Hayat 1986). The fixation process is complicated and is dependent on duration, pH, temperature, protein structure and concentration. Glutaraldehyde is soluble in both water and organic solvents and it works by crosslinking of proteins in an array of complex processes that proceed though many steps and through several routes. For a thorough outline of these reactions, the reader is referred to (Hayat 2000). Glutaraldehyde forms both inter and intra molecular crosslinks. It preserves the tertiary structure of proteins, probably because the amino groups which are the primary target for glutaraldehyde crosslinking are predominantly located at the surface of the proteins due to their hydrophilic nature. It can as well form bridges in the presence of lysine, which is present in all the protein emulsifiers in this study (protein sequences can be found at (Farrell, Jimenez-Flores et al. 2004). Glutaraldehyde does not really react with lipids except certain phospholipids containing free amino groups, including phosphatidylethanolamine and phosphatidylserine (Gigg, Payne 1969, Wood 1973) which are present in the milk phospholipid fraction used in this study at 25.2% and 8.6% of the total phospholipid fraction, respectively (Horn, Nielsen et al. 2011). It is important to find a good concentration of glutaraldehyde since it causes excessive shrinkage of cells in high concentrations while too low concentration results in extraction of cell material, and even changes within a reasonable limit might affect the volume of the sample e. g. contraction of extracellular space in nervous tissue. Concentrations of 1.5 - 4% apply to most animal and plant tissues and fixation at low temperature should reduce shrinkage.

Glutaraldehyde diffuses slowly because of its relatively large molecular size and is often used in combination with formaldehyde – (or paraformaldehyde as is the polymeric form of formaldehyde). In solution, it is basically formaldehyde. Formaldehyde is a relatively small molecule and diffuses very fast, also into dense tissues. It is a reversible fixative, creating methylene bridges at the peptide chains that can be removed by washing with water. Often, a combination of glutaraldehyde and formaldehyde fixation is

applied to fix the samples fast with formaldehyde and then crosslink irreversibly with glutaraldehyde. The two aldehydes enhance the effect of each other, a mixture that is stronger than if used sequentially.

The double fixation is normally followed by postfixation with osmium tetroxide, OsO_4, and glutaraldehyde fixation without postfixation is considered unsatisfactory for most applications (Hayat 2000)

2.6.2 Osmium tetroxide

OsO_4 is non-polar and readily diffuses through lipid bilayers. It is volatile at room temperature and highly toxic. OsO_4 fixates unsaturated lipids by oxidation of their double bonds with one OsO_4 for every double bond and also acts as a non-coagulant fixative for some proteins. It might be able to fix the relative position of amphiphilic proteins in membranes and other structures by building bridges between aliphatic side chains of lipids and the peptide bonds of certain proteins (Hayat 2000). OsO_4 becomes consumed by fatty tissues fast and its penetration into samples is superficial (Bahr 1955) which is why small sample sizes are advisable. OsO_4 is not only a fixative but also acts as a stain because different species of reduced osmium are present in the samples after fixation (White, Andrews et al. 1976) supposedly deposited at the polar end of the lipid molecules, where they add high contrast to osmophilic structures such as lipid bilayer membrane structures and lipoproteins. Furthermore reduced osmium species enhance post staining with lead (Hayat 2000).

2.7 Fixation artifacts

All fixations are inevitably causing artifacts. Macromolecules in an aqueous environment will not stay in their position when water is removed unless they are stabilized in some way. Hence, unavoidable and well-understood artifacts have to be accepted, but it is important to be able to recognize these artifacts, and to understand what causes them in order to interpret micrographs correctly. In addition to the shrinking mentioned above, glutaraldehyde also causes aggregation of molecules through the crosslinking. Figure 2.6 is an often used figure (Kellenberger 1987) that exemplifies some of the structural changes that can take place during crosslinking and during dehydration of chemically fixed samples with the top row displaying the native structure and the bottom row exemplifying potential fixation and dehydration artifacts. Globular particles can form networks or larger aggregate networks. In the presence of fibrillar structures the globular particles sediment on these structures rather than forming networks on their own. And fibrils can aggregate to complex networks with greater or lesser branching. One example is aggregation or clumping of chromatin suspensions where chromatin is fixed into an artificial and complex network as compared to the non-aggregated structures that are observed by cryo-microscopy of vitrified sections (Dubochet, Blanc 2001).

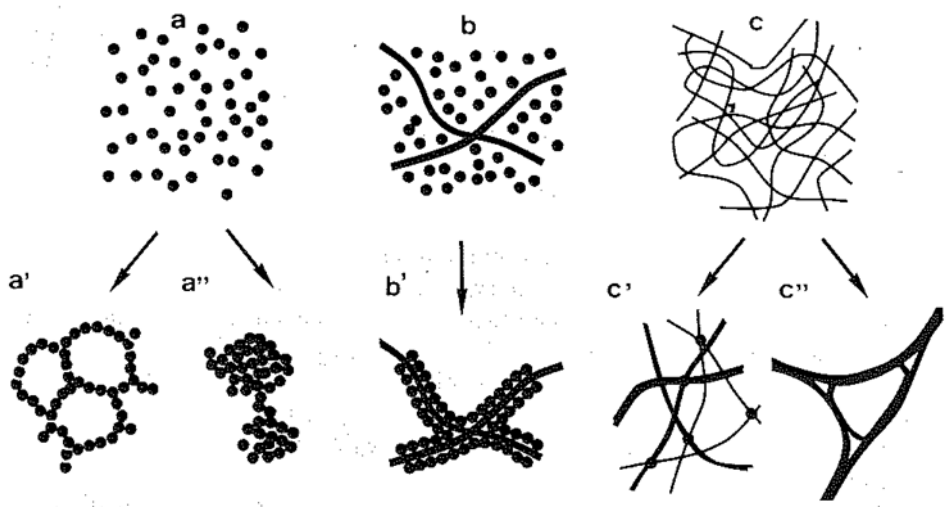

Figure 2.6. The aggregation of molecules as an effect of dehydration and fixation.

Upon long fixation times, complex lipids might be mobilized by glutaraldehyde, reorganize inside the sample and become stained in the subsequent OsO_4 post fixation to appear as artificial myelin bodies (Hayat 2000). If traces of glutaraldehyde are remaining in the sample due to inefficient washing after the fixation, it might react with OsO_4 to produce fine, electron dense granules of reduced osmium in an unknown process. This is not a poststaining artifact but can be an inherent defect from the fixation procedure. Longer rinsing times should minimize the phenomenon, but prolonged washing can cause uneven fixation, aggregation, shrinkage or swelling. Granules can also be attempted to be removed from already made sections by periodic acid or H_2O_2 (Hayat 2000). Washing with water can dissolve and disintegrate unfixed cellular materials, why a buffer is preferred in the washing step.

OsO_4 causes protein structural changes, especially when prefixed with glutaraldehyde (Lenard, Singer 1968). But without glutaraldehyde fixation, proteins will leak out and membranes become freely permeable to small ions and molecules. And despite fixation by glutaraldehyde followed by OsO_4, a considerable amount of lipid is lost in the subsequent dehydration step (Hayat 2000) predominantly in the high concentrations of solvents. Fixation, rinsing and dehydration at colder temperatures, i.e. 0-4 °C can limit the dehydration. According to (Sjostrand 1989) OsO_4 binds to hydrophilic sites in the proteins, causes unfolding and thus exposes even more binding sites which then leads to improved binding of other heavy metals. The unfolding of the polypeptide chain should also make the proteins more hydrophilic. Apparently this is affecting more polar proteins because they have more binding sites for OsO_4 at their surface. By dehydration they could aggregate, or be extracted. Prolonged treatment with OsO_4 thus causes degradation and extractability of cell constituents (Bahr 1955), a fact that was earlier utilized by some researchers to carefully extract the cytosol from cells by dilute OsO_4 for SEM 3D visualization (by stereo pairs) of intracellular structures (Lea, Hollenberg et al. 1992). Today this technique is by far superseded by slice and view in the dual beam or 3D view microscopes.

2.8 Staining

The stains that are used in this thesis are shortly outlined below. Numerous other stains exist, with a wealth of applications, but the combination of uranyl acetate and lead citrate used in this study is versatile and often used (Hayat 2000).

There are negative and positive staining methods. The negative staining implies coating the sample with a thin layer of metal salts, which can be cationic or anionic, and penetrates also to hydrophilic surface cavities and thus utilizing the negative contrast originating from the heavy metals' stronger scattering than the light material to outline the sample. This effect also implies that hydrophobic sites are not optimally stained but they will be surrounded by the stain. The method was successfully demonstrated by (Brenner, Horne 1959) for phosphotungstic acid negative staining of tobacco mosaic virus and turnips yellow mosaic virus. In addition to the improved contrast negative staining also confers higher electron dose tolerance and some negative stains can act as fixatives. In principle, there is no reaction between the negative stain and the sample, but some positive staining is almost always a part of negative staining (Hayat 2000). Uranyl acetate stain (van Bruggen, Wiebenga et al. 1960) is a commonly utilized negative stain. The cation UO_2^{2+} is approximately 0.4-0.5 nm in size. Charged proteins below their isoelectric point at pH 4.5 should repel this ion and the staining should be negative. But the uranyl acetate cations have strong affinity for phosphate and carboxyl groups in e.g. lipids and some proteins and the staining is not just negative. Uranyl acetate can stabilize lipids and promote good adherence to support films, the staining protocols are fast and negative stained samples are normally stable and can be stored or longer time (Hayat 2000). It has additional fixative capabilities and is able to fix proteins very fast, i.e. millisecond time-scale (Zhao, Craig 2003) making it very efficient for negative staining. Even though negative staining confers some stability to the structures, the negative staining across holes in the support film, if possible, is preferred as drying can cause flattening due to surface tension (Harris 2008).

In positive staining the actual microstructure is stained directly. There is an attraction of heavy metal salts to specific sites and staining of sections with heavy metals salts (Watson 1958) is used to enhance contrast in sections. Uranyl acetate as a positive stain works by binding of not just UO_2^{2+} but a variety of cations, anions and neutral species of the general type $UO_2(OUO_2)_{n+1}^{2+}$ (Hayat 2000) to both positively and negatively charged groups in the biological tissues of TEM sections, preferably phosphate and carboxyl groups. Its staining abilities are better than other heavy metal compounds, e.g. phosphotungstic acid and potassium permanganate (Hayat 2000). Uranyl acetate should be protected to light as it forms precipitates and should be filtered prior to use.

Lead citrate binds to organophosphate and other anionic sites, but also glucogen (Reynolds 1963). Uranyl acetate and lead citrate are often used together to target and contrast different structures in sections which might react with different stains. Lead citrate binds to negatively charged components such as hydroxyl groups and sites that react with osmium (Ellis 2007). CO_2 from the air forms precipitates with lead citrate and CO_2 free environments or short staining times should be applied. Lead citrate is bound by reduced osmium and defects in the fixation procedure can cause a fine, dark precipitate which may be set throughout the whole section. It is believed to be a consequence of insufficient removal of glutaraldehyde prior to osmification.

Prolonged washing steps can reduce staining intensities of uranyl acetate and lead citrate, with the largest effect on lead citrate and should be avoided.

Recently substitutions are being sought after due to the toxicity and limited availability of uranyl acetate such as samarium triacetate and gadolinium triacetate who stains effectively both in positive and negative staining but do not possess the same fixative powers (Nakakoshi, Nishioka et al. 2011) or hafnium chloride in methanol which gives good contrast in a variety of specimens with lead citrate (Ikeda, Inoue et al. 2011). In both cases OsO_4 fixation was still applied and was found to be essential not only as fixative but also for pretreatment to staining for enhanced contrast (Nakakoshi, Nishioka et al. 2011). Even Oolong tea extract has been shown to substitute uranyl acetate (Sato, Adachi et al. 2008) and the search for substitutions for substitutions for uranyl acetate is likely to continue since its restrictions of obtainability are likely to increase.

2.9 Physical fixation

As mentioned, chemical fixation techniques causes some artifacts and it is at least essential to know them for correct interpretation of micrographs. But it would be even better to preserve the true ultrastructure of the sample and avoid alteration by crosslinking. A way to achieve just that is by cryofixation which is a physical fixation where the samples ideally are in their native, hydrated state. Furthermore, cryofixation is fast and almost simultaneously fixes all components of a given sample.

This type of fixation can then be followed by cryo microscopy i.e. imaging of frozen samples or by processing the samples in various ways so they can be imaged at room temperature. This makes cryo fixation a very crucial step in the imaging of many liquid and semi-liquid samples and the nature of water and freezing is outlined below.

2.9.1 Liquid and solid water

Water has some very unusual properties compared to other liquids. They originate mainly from the structure of the water molecules and the H-bonding. Some of these properties are very important for cryo microscopy and sample preparation of cryo-fixed samples. One important aspect is that ice is less dense than liquid water. Actually, the thermal expansivity for water has its minimum at 4 °C below which it is increasing again (Rasmusse, Mackenzi 1973). The volume of ice is 9% larger than water at ambient pressure and approximately 17% larger at 2 kbar (Marion, Jakubowski 2004). It should be obvious that the formation of ice crystals can severely damage the structure of water containing samples.

On the nano scale the formation of ice crystals changes the structure of the sample quite dramatically. This is because only water molecules are incorporated into ice crystals and by their growth they are effectively extracting water from the remaining solution and creating a phase separation between the water and the solutes which will finally be pushed at the front of the growing ice crystals into ridges between the formed ice crystals. These structures are often referred to as eutectic ridges. As a result everything that was before in solution will be confined there. These ridges can be visualized by freeze-fracture and deep etching of the

water (see later section for details about the technique) and the eutectic ridges are then seen as an artificial network in the sample, somewhat resembling a honeycomb structure. The holes left after the deep etching are the spaces previously occupied by crystalline ice. Figure 2.7 (A) illustrates such a "network" of ridges, from a fractured surface of a freeze-fractured sample imaged by cryo-SEM. In the upper left corner of the micrograph (A) is the edge of the original surface of the sample. That side has been closest to the cryogen during freezing and here there are no visible holes. It can be seen that the size of the holes between the ridges appear with distance from the surface and grow in sizes towards the lower right corner of the image, illustrating another important point, which is that the growth of ice crystals is dependent on cooling rate, a subject that will be discussed in detail below. The size of the holes between the ridges cannot be directly linked to the size of ice crystals (Dubochet 2007). 2.7 (B) is an example of what can happen if the sample of interest is so small, that it can become trapped inside the eutectic ridges.

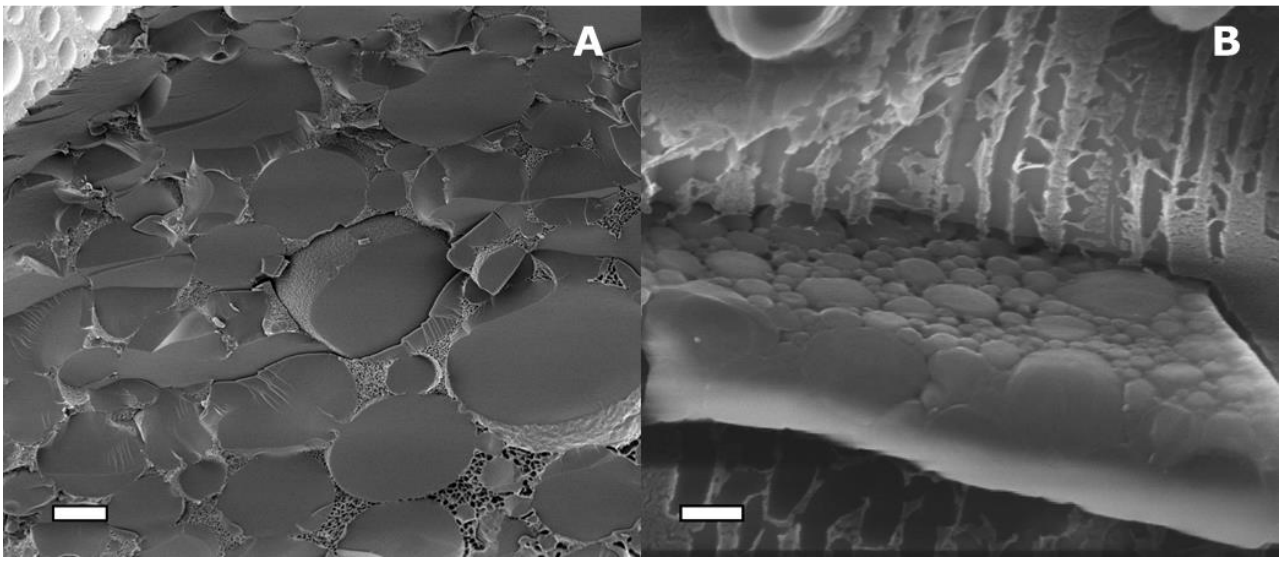

Figure 2.7. Freeze-fractured emulsions. The micrograph depicts oil droplets and eutectic ridges to exemplify ice crystal damage in cryo preparation of emulsions. (A) Scale bar 2 µm. The oil droplets are relatively large and have not been effectively moved by the ice crystal formation, it is only the proteins that occupy the water phase of that emulsion that have been subjected to effective translational movements. Instead the droplet surfaces are slightly deformed with imprints from the ice crystals. If the droplets had been smaller, they too could have been trapped inside the ridges as shown in (B) Scale bar 300nm. Oil droplets in the nano range have effectively been pushed at the front of a growing ice crystal. [NB. Bad freezing is not the only artifact in the image; the sample has been very deeply etched and partly melted with the electron beam to illustrate the droplets; in addition the sample is charging, drifting and vibrating].

According to the example above, the key to good physical fixation is to preferentially avoid ice crystal formation during the cryo-fixation, or to at least to limit the size of the ice crystals to an extent where they do not alter the structures of interest.

Three temperatures are important for the understanding of the freezing behavior of water. The melting temperature (T_m), the homogenous nucleation temperature (T_h), and the glass transition temperature (T_g). T_m is the temperature at which the liquid state becomes more stable than the solid phase. Within one

crystal, all energy will be absorbed and then the water becomes liquid. At ambient pressure this is happening at 0 °C. The term freezing point for this temperature is somewhat misleading since water does not necessarily freeze below its T_m. When water is cooled below T_m, the nucleation and growth of ice crystals requires an increase in Gibb's free energy for the creation of a surface between the new crystalline phase and the liquid before the energy falls to the stable solid state. This requirement can only be fulfilled by the energy released by the crystallization and the process is thus proportional to the volume of the nucleating ice crystal. Close to T_m, the free energy of crystallization is small and a large particle is needed to overcome the energy barrier. In pure water, such large particles are highly unlikely. But if there is a foreign surface that can help reduce the surface of the ice crystal and effectively serve as a nucleation point, then the new crystal might overcome the energy barrier by forming on this surface. This process is called heterogeneous nucleation. At lowering temperatures the energy associated with crystallization is larger and thus smaller and smaller particles are required for homogenous crystallization and it becomes an increasingly probable event even in pure water. The estimated critical particle size at -5 °C is ~45.000 water molecules whereas it is only ~70 water molecules at -40 °C (Zachariassen, Kristiansen 2000). In the absence of foreign particles, e.g. in pure water, super cooling can take place down to about -41 °C in very small droplets with a diameter of 5 µm (Chaplin 2013). Small volumes reduce the risk of heterogeneous nucleation. A theoretical maximum of crystallization rate has recently been calculated to be at -48 °C (Moore, Molinero 2011). T_g is the temperature at which the water turns into a glass, i.e. a material with the structural properties of water but the mechanical properties of a solid. Below this temperature there is not enough energy in the system for crystallization. For water, this temperature is ~137 °C (Chaplin 2013).

The mechanism of the nucleation and crystallization process is extremely complicated and to a large degree still unknown. The growth of an ice crystal is, in a simplified explanation, taking place at the rate at which there is equilibrium between the heat generated by the crystallization and the heat removed by cooling. Slow freezing causes a few large nucleation sites and ramified crystals due to excluded solutes on the surface of the growing crystal. The excluded solutes form a concentration gradient on the crystallization front which limits the crystallization rate. Differential concentrations in lateral directions cause the crystal to branch out to sequester more water molecules in a ramified structure. Fast freezing produces multiple nucleation sites and finer crystals.

Ice without crystals is referred to as amorphous or vitreous ice, according to the way it is produced.

Depending on temperature and pressure there are many forms of solid water, including 12 (Salzmann, Radaelli et al. 2006) stabile crystal forms of ice, one metastable crystal form and several polyamorphous forms. Even metal structure of water is predicted to occur at very high pressures (Militzer, Wilson 2010). There is a wealth of descriptions of non-crystalline ice, produced by different methods and all belonging to 3 energy mega basins in the energy landscape (Loerting, Winkel et al. 2011); low density amorphous ice with 0.94 g/cm^3 (LDA), high density amorphous ice with 1.17g/cm^3 (HDA (Heide 1984)) and very high density amorphous ice with 1.25 g/cm^3 (VHDA). (Densities are all given for ambient pressure). Amorphous ice with the same density derived by very different routes might have similar properties, but according to (Chaplin 2013) they are likely to be structurally different i.e. some being simply collapsed crystalline ice and others being structurally closer related to water. Amorphous ice and vitreous ice are both LDA forms, but produced by different pathways. Amorphous ice can be e.g. formed by condensing water vapor on a surface below 110 K (Burton, Oliver 1935). Vitreous ice is formed by rapid cooling of small quantities of

water. Vitrification of water was proven almost simultaneous by x-ray and electron diffraction, respectively (Bruggeller, Mayer 1980, Dobochet, Mcdowall 1981). The differences between amorphous and vitrified ice are of minimal importance in microscopy and analysis, so the terms are often used interchangeably (Echlin 1992).

For microscopy the interesting ice forms are hexagonal ice (I_h), cubic ice (I_c) and vitreous ice. They all have lower densities than water. At very low temperature, i.e. microscopy cooled by liquid helium, the HDA form can be produced from these by electron radiation, which can cause problems since its viscosity is lower than the LDA form and it flows under the electron beam (Heide, Zeitler 1985).

I_h is the most favorable structure of ice energetically and thus the most common in nature, e.g. the six-fold symmetry of ice crystals formed from liquid water. Slow freezing at normal pressure is a first order phase transition and produces crystalline hexagonal ice in which the water molecules are a tetrahedral structure cross-linked to hexagonal crystals. Four oxygen atoms are set on a rhombic base, each in the center of a tetrahedron formed by four oxygen atoms and each water molecule is hydrogen bonded to the four nearest neighbors.

I_c is a metastable form of ice that exists between -150 °C and -80 °C. In nature it is normally only found in the outer atmosphere (Murray, Knopf et al. 2005). In the lab I_c can be created by condensing water vapor onto a clean surface below 143 K or heating vitreous ice above ~135 °C or even by fast freezing of liquid water (Dobochet, Mcdowall 1981). I_c does not just form from I_h by further cooling and if I_c is seen in the sample, it is a warning that something is wrong with the preparation or it is a sign that there is water vapor contamination inside the microscope (Echlin 1992).

Since I_h is less dense than water the melting point, T_m, of water is decreasing with increasing pressure. This is favored up to 2050 bar where the high density morphologies Ice II and Ice III become more favorable. At 2050 bar, T_m of water is -22 °C. As opposed to I_h, Ice II and ice III have increasing melting points with increasing pressure and the T_m at 2050 bar is thus at its minimum. T_h is depressed to -92 °C at 2 kbar (Kanno, Speedy et al. 1975). Solutes in the water also increase the capability of super cooling which is dependent on both the nature of the solute and their concentration. Like with pressure, for solute concentration the relation between T_m and T_h is linear (Kanno, Miyata et al. 2004). This is useful for most biological samples as will be explained later. A phase diagram depicting the T_h and T_m as a function of pressure is shown below.

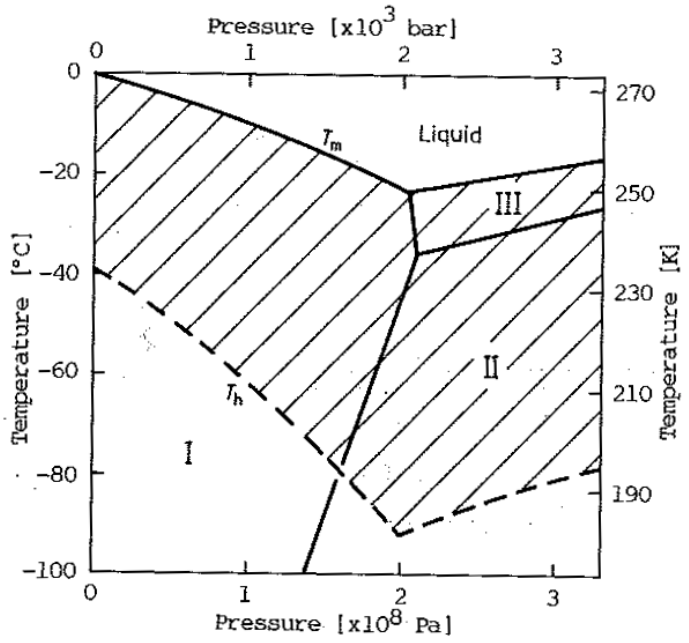

Figure 2.8. Pressure/temperature phase diagram for water, with temperature as a function of pressure. I, II, and III are the stable ice polymorphs and the marked area is the region in which super cooled water exist. Figure by (Bachmann, Mayer 1987).

The growth of ice crystals is related to the cooling rate. So what is the cooling rate required to obtain vitreous ice? It is not known exactly (Dubochet 2009), but estimates are in the range of $>5*10^5$ K/s (Vanhecke, Graber et al. 2008) in biological samples and up to $\sim3*10^6$ K/s for pure water or aqueous solutions (Hayat 2000) at ambient pressure and $>10^4$ K/s for adequate freezing of biological samples (Kaech 2009). The freezing rate required to vitrify a sample is complex and depends on the nature of sample and its solutes, its thickness, and the pressure. For instance, ice nucleation is normally initiated outside cells in tissues because of the high concentration of solutes inside, and only when all the heat is absorbed from the outside of a cell, the nucleation will take place inside (Dubochet 2007). And as can be seen from the phase diagram above, high pressure lowers the level of T_h, effectively acting as a cryoprotectant, which is utilized for high pressure freezing, a method that will be outlined later.

Previously the quality of the freezing has been evaluated by the researcher by the subjective expression ”adequately frozen” but whereas vitrified samples are always judged adequately frozen, the reverse is not true and the morphology of a sample is not completely indicative of the state of the water after cryo-fixation (Studer, Michel et al. 1995). For thin, vitrified films imaged directly in cryo-TEM, vitrification can be assessed from the diffraction pattern. Vitreous water lacks any crystallinity and therefore does not show diffraction spots in TEM. Whether water is actually vitreous or containing microcrystallites comes down to the resolution in the diffraction pattern (Echlin 1992). For bulk samples the only reliable methods to indicate vitrification is to use a cryo ultramicrotome to cut thin sections to be viewed in cryo-TEM, keeping the sample always under the devitrification temperature. The technique is called Cryo Electron Microscopy Of Vitreous Sections (CEMOVIS). Moreover, on the contrary to what was previously believed, one visible ice crystal “void” in a sample after processing does not correspond to one ice crystal. Hexagonal ice crystals are large and ramified 3D structures and once they form, the process is fast. CEMOVIS has revealed that in most cases all the small crystalline domains inside a cell have the same crystal orientation, thus belonging to the same crystal (Dubochet 2007).

A number of freezing techniques have been developed to avoid the formation of ice crystals by either fast cooling rates or by lowering the required cooling rate. These range from simple immersion of a sample in a cryogenic gas to methods involving thousands of bars of pressure and sophisticated and relatively costly equipment. All these methods involve the transfer of heat through the surface of the sample via a medium which can be a cryogenic gas or a metal surface. Cooling is a diffusion process of heat and the rate depends on the square of the sample thickness. At room temperature the thickness of a sample that can be vitrified is in the range of 10 µm. According to the calculations of (Studer, Michel et al. 1995), internal cooling rate is then in the order of $>10^5$ K/s (Studer, Michel et al. 1995). Below is a summary of the most common methods used for vitrification.

2.9.2 Immersion freezing

Immersion freezing, or plunge freezing, is the plunging of a sample into a cryogenic gas at high velocity. It can be both thin films on TEM grids and bulk samples.

The table below lists a few of the cryogens listed by (Sitte, Edelmann et al. 1987) which are still commonly used, their efficiency being related to that of propane:

Table 2.1

Cryogen	*Freezing point (°C)*	*Cooling efficiency compared to propane*
Ethane	*-171*	*1.3*
Propane	*-190*	*1.0*
Boiling nitrogen	*-196*	*0.1*
Nitrogen at freezing point	*-210*	*0.2*

Ethane is a very efficient cryogenic gas. It is the cryogen of choice for the plunge freezing of thin films of suspensions for cryo-TEM. The bare grid method is a rather simple preparation method in which a suspension is put on a grid, which is then blotted and plunged into a cryogen (Adrian, Dubochet et al. 1984). The method has the advantage to negative staining that the 3D structure of the sample is preserved much better because the sample is not dehydrated. The two methods can be used in combination by cryo negative staining (Adrian, Dubochet et al. 1998) thus utilizing the good contrast from the negative stain and the preservation of the structure without drying artifacts. Numerous plunging systems exist, including homemade plungers, but also fully automated options are available (Frederik, De Haas et al. 2009), offering higher reproducibility and demanding less experience from the user. Before plunging the grid into the cryogen, it is important that the liquid film is thin enough for imaging in the TEM. Cryo-TEM is performed on grids with holey or lacey carbon, with the liquid film spanning the holes. The carbon layer is normally hydrophobic and it is necessary to make the carbon hydrophilic get a good spreading across the carbon film (De Carlo 2009). After applying the suspension to a hydrophilic grid, it is necessary to blot the grid to make

the sample thin enough. That can be done by automation or it can be done by hand which requires experience. It is possible to assume a thickness of the remaining film by observing the film. Different methods have been devised such as the appearance of a purple-orange reflection (Jaffe, Glaeser 1984) or to observe the grid under the light microscope and estimate when half of the squares are seen filled with liquid (Adrian, Dubochet et al. 1984). It can also be a mere assessment of the time point when the film is beginning to break down. All these methods are subjective and meant to ensure a thickness of around 100-300 nm which is thin enough for sufficient freezing with plunging into liquid ethane and imaging in cryo-TEM. After blotting it is important to avoid drying out the now very thin liquid film before it is plunged into the cryogen. This is done by performing the blotting and plunging the grid inside a humidity controlled chamber (Bellare, Davis et al. 1988). Also the temperature is sometimes controlled, depending on the equipment. By carefully maintaining the humidity at 100 % and plunging fast, liquid films are maintained during the short times between blotting and plunging. Excessive blotting procedures can also be necessary for samples which are viscous or in other ways differ from dilute suspensions. Normally the grids are plunged into liquid ethane of high purity. Plunging by hand-held tweezers is not fast enough to generate the necessary cooling speed in most cases (Sitte, Edelmann et al. 1987). After plunging, the grid is kept shortly in the gaseous nitrogen just over the liquid nitrogen to drain ethane, after which it is submerged into the liquid nitrogen. Here the remaining ethane will solidify and create a thin protective layer over the vitrified sample. The grid is transferred to a cryo transfer holder under cooling by liquid nitrogen. The ethane which is left on the surface of a sample will quickly evaporate in the microscope. It is noteworthy that the blotting step causes a number of artifacts to the samples imaged with this method. First of all, the filter paper does not remove the same amount of sample and solute, causing the blotted sample to have a different concentration. Secondly, the vitrified film is not of equal thickness but a meniscus which is thinnest in the middle of the holes in the holey or lacey carbon. Hence the samples will be organized according to their size inside this meniscus. Third, there will be an exclusion of samples which are too thick compared to the carbon layer in the holey and lacey grids and fourth, structures that are liquid might shear, e.g. oil droplets that form lipid layers on the surface of the liquid film, formerly known as unidentified fatty objects (UFOs) (Almgren, Edwards et al. 2000).

As opposed to ethane, propane tends to stick to the sample. But propane has the advantage of being cheap and easy to obtain and is mostly used when the sample does not come into direct contact with the sample. Propane is an effective cryogenic gas and is used for instance in the propane jet freezer. Instead of plunging the sample into the propane, a jet of liquid propane is shot at very high speed from both sides onto a sandwich of thin metal plates containing the sample (Moor, Kistler et al. 1976) and the method is providing very high cooling rates at the surface ($> 3*10^4$ K/s). Samples of up to 20 µm can be frozen satisfactory by using this method and recently the fast fixation was used to demonstrate the self-assembly of liposomes (Jahn, Lucas et al. 2013). Also single jets exists and homemade systems can be built. The operation of the Balzer's propane jet freezer by is very well suited for freezing a large amount of samples and the machine is relatively small.

In table 2.1, nitrogen, both boiling and at its freezing point are being deemed poor cryogens. The reason for the low efficiency of nitrogen is two-fold. Since the boiling point of nitrogen is so low, the freezing will be disturbed by calefaction. Also known as the Leidenfrost phenomenon, the large temperature difference between the sample and the nitrogen causes the nitrogen to evaporate at a fast speed and envelope the sample with a pocket of insulating gas. By depressurizing the nitrogen and solidifying it, this effect is

delayed because nitrogen will have to pass through two phase transitions before forming the envelope. And high freezing rates can be achieved by the use of liquid nitrogen at its freezing point, but only for very small samples. A second problem with nitrogen is its very low heat capacity. Together these properties makes liquid nitrogen unfit for direct cryo-fixation. Instead liquid nitrogen is used to cool other cryogens such as the aforementioned ethane and propane.

Indirect freezing by the contact between a metal surface which has been cooled by a cryogen is another possibility to achieve higher cooling rates than by immersion the sample directly in the cryogen gas. Samples are introduced to a polished, cold metal block at high speed (Vanharreweld, Crowell 1964) in the metal mirror freezing also called slam freezing. The slam freezing systems are small, simple and can be home-made. During freezing it is required that the mirror is kept very clean to confer optimal cooling and this requires some work during the freezing of multiple samples. Very high freezing rates in the order of 2.5-5*10^4 °C/s can be obtained (Hayat 2000) if vibrations and bouncing is limited.

2.9.3 High Pressure Freezing, HPF

As mentioned, the best vitrification methods at ambient pressure have a limit of approximately 10 µm of vitrified sample (Kaech 2009, Studer, Michel et al. 1995). To circumvent this limit, one must alter the physical properties of water to lower the cooling rate needed for vitrification. This can be done by the addition of cryoprotectants. Or it can be done by changing the pressure. As depicted in figure 2.8 the nucleation point and melting point of water changes according to pressure. The diagram also depicts that the smallest distance between the vitreous state and the liquid state is around 2000 bar. At this temperature, water nucleates at ~92 °C. See phase diagram for water in figure xx. Furthermore, the freezing rate to create vitreous water is lowered by approximately 100 fold at this pressure (Studer, Michel et al. 1995) which corresponds very well to the fact that the thickness of vitrified sample increase by a magnitude of 10 by the application of high pressure (SARTORI, RICHTER et al. 1993).

Cooling is a heat transfer process and the rate depends on the square of the sample thickness. According to calculations by (Studer, Michel et al. 1995), there is a maximum thickness after which the external cooling rate no longer influences the internal cooling rate. E.g. the thickness dependence eliminates the effect of external cooling rate at a thickness of about 80 µm for a 600 µm thick sample. The center of a 200 µm thick sample is affected by an increase in cooling rate up to 10^5 K/s after which the effect decreases. For even thinner samples, the limit for the effect inside would be up to 40-50*10^5 K/s (Studer, Michel et al. 1995). The calculations state that most samples thicker than 200 µm can probably not be vitrified, still depending on the exact required rate for vitrification in the sample.

There are currently two principles used in high pressure freezing. Either the sample is pressurized inside a small container via a pressure transmission fluid in the Empact machine which uses methylcyclohexane for pressurization and subsequently cools the specimen with a jet of liquid nitrogen. This causes the use of liquid nitrogen to be much smaller than the HPM machines and the machine itself is also much smaller. But the sample size diameter is limited to 1.5 mm compared to currently 6 mm diameter in the HPM machines.

Or in the high pressure freezing machines (HPM10 and HPM100) where liquid nitrogen is both the hydraulic liquid and the cooling agent. The HPM10 machine has been used in the majority of published results until now (Kaech 2009) and it is also the machine used in this study. It is described below.

Figure 2.9 depicts the system. For the build-up of pressure, the HPM10 uses a bladder-type pressure accumulator (2) under the pressure of 300 bar. When released, the pressure moves a piston (6) into liquid nitrogen in a high pressure chamber, thereby raising the pressure to approximately 2100 bar. The liquid nitrogen will move towards the specimen pressure chamber (13) where the sample sandwich is being held by a special sample holder that can withstand the pressure and the same time allows access of the nitrogen to the sandwich surface. The specimen chamber is initially filled with alcohol which will be decompressed and displaced by the nitrogen. The sequential process causes a delay in the order of 20 ms between the pressurization and the cooling. After vitrification, the sample is moved very quickly from the specimen pressure chamber to a bath of liquid nitrogen, under which the sandwich can be removed from the holder in a specific unloading device. In the HPM100, this step is happening automatically, with the vitrified sample being delivered in a small nitrogen Dewar.

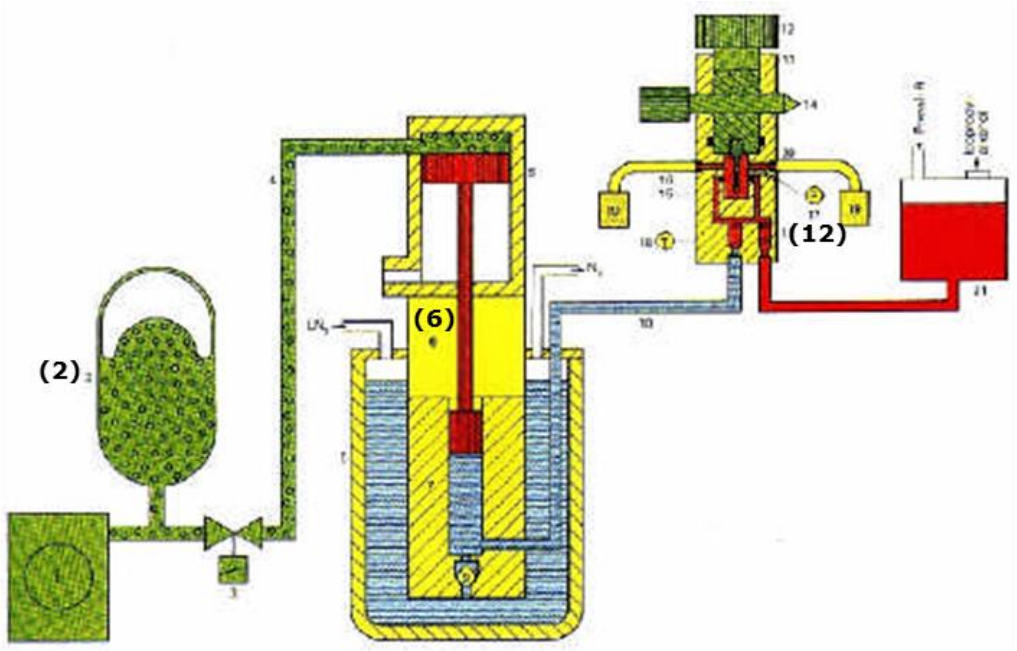

Figure 2.9.
A schematic sketch of the HPF machine (Abra-Fluid AG 2007).

Due to the high pressure it is important to prevent air bubbles which will collapse under the pressure. This can be done by a range of different agents. In some cases, it has been shown to introduce structural changes in very delicate structures, possibly by the delay between pressurization and cooling (Leforestier, Richter et al. 1996). Samples frozen in the high pressure freezer contains vitreous ice that is estimated to be about 10% more dense compared to water that is vitrified at ambient pressure and samples can as well contain crystalline ice of the high-density morphologies (Richter 1994).

The HPM10 and HPM100 are relatively costly options and they use a lot of liquid nitrogen, compared to other freezing equipment types. There is a recent publication about self-pressurized freezing. The method is utilizing the fact that water expands when it freezes. Clamping copper tubes containing liquid samples and plunge freezing them in a vertical orientation will create a large pressure inside the small tubes. While Ih is forming and expanding in the end which will first be in contact with the cryogen, the other end will be pressurized to an extent where vitreous ice will be formed (Leunissen, Yi 2009). There are arguments against this method, such that the build-up of ice crystals in one area of the sample can drain water from other parts of the sample effectively dehydrating these areas. By drainage of water the sample will not be in its native hydrated state even though it appears well frozen. There is thus no such thing as partly well frozen samples because of this effect (Dubochet 2007). Nevertheless, the degree of damage by dehydration depends on the sample and equipment for this technique is now being produced, using U-formed tubes supposed to be plunged with the legs first, creating a pressure that allows the U part to be frozen under high pressure (Leica Microsystems 2013).

2.10 Devitrification

Crystalline ice in the sample can occur not only during the freezing but also after devitrification, a phase transition to cubic ice where small, compact ice crystals in the range of 0.1 µm are formed. Pure water is devitrified to form cubic ice at -135 °C and at slightly higher temperatures in the case of solutes though still well below 100 °C (Dubochet 2009). The rate of devitrification and also the further transition to hexagonal ice are temperature dependent. The transformation to hexagonal ice is taking place around -80 °C but such an event cannot be imaged in the electron microscope because the ice would simply sublimate too fast at this temperature (Dubochet, Adrian et al. 1988). The devitrification process is further accelerated by electron beam irradiation (Dubochet 2009). The devitrification, and possibly also the transition from cubic to hexagonal ice, is happening in a solid matrix and is most probably happening by rotation of the water molecules. Hence, only minimal translational movement should take place and the diffusion coefficient of macromolecules is almost zero, suggesting that the samples will be embedded in small ice crystals instead of vitrified water (Dubochet 2007). Accordingly, this type of ice crystal formation does not disturb the samples to the same degree as the crystal formation during freezing of liquid water. This is very beneficial since the devitrification temperature means that many of the low temperature procedures performed on cryo-fixed samples, e.g. freeze substitution are in fact not performed on vitreous samples but on devitrified samples (Humbel 2009, Dubochet 2007).

2.11 Storing, processing and imaging of frozen specimens

Even though the devitrification itself might impose only minor reorganization of the sample microstructures, the samples can also be subjected to migratory recrystallization, i.e. the migration of water molecules from smaller unstable ice crystals to larger and more stable crystals, during longer storage times at too warm temperatures. Contrary to the smaller rearrangements in devitrification, recrystallization

can severely damage a sample. The rate is dependent on the temperature and the presence of solutes and it is near impossible to calculate an appropriate temperature limit for biological systems which is why they are normally stored under liquid nitrogen (Echlin 1992). Samples can be kept almost forever like this (Bachmann, Mayer 1987)

2.11.1 Cryo-microscopy (SEM and TEM)

When a sample is frozen, or hopefully vitrified, there are a number of routes to proceed. The methods used in this work are outlined below. If the sample is a suspension that is plunge frozen on a grid, it can be transferred to the TEM and viewed directly by the means of a cryo-transfer holder. If a bulk sample should be viewed in cryo-TEM, it will have to be sectioned and then transferred to the TEM while frozen, i.e. the CEMOVIS technique mentioned earlier. Or, a bulk sample can be fractured and viewed directly in cryo-TEM (Belkoura, Stubenrauch et al. 2004), a technique that could possibly alleviate some of the artifacts originating from the blotting procedure mentioned previously. When the sample is in the TEM, it is important to not damage the sample with the electron beam. Dedicated low-dose software exists to control the electron dose and in general, low magnification is used for sample location, the beam is blanked when not imaging and deflected to adjacent areas for focusing. A certain amount of underfocus is necessary to obtain any contrast in the images as the only contrast obtainable is phase contrast.

Another way to image the frozen sample is by cryo-SEM. Cryo-SEM is excellent for producing images of the surface of frozen samples and by the technique of freeze-fracture and deep etching, one can get a good idea of the bulk structure of the sample.

2.11.2 Freeze fracture and etching

In cases where it is necessary to gain access to the inside of a bulk sample, e.g. suspensions like emulsion samples, the frozen sample can be fractured. Freeze fracture techniques are applied either to samples that are imaged directly in cryo-SEM or they can be replicated for the replicas to be subsequently cleaned and imaged at room temperature in the TEM. The fracturing takes place under vacuum to avoid any contamination of the fresh fracture surface by condensation of water vapor on the sample. Samples break in a relatively uncontrolled fashion, but always along the planes of weakness such as lipid bilayers or interfaces between different phases (Echlin 1992). The fractures are made with a cooled instrument to avoid heat transfer, either a knife or a blunt instrument. The fracture from a blunt instrument introduces tensile stress and a single fracture plane; a knife introduces shear forces just ahead of the knife and thus a series of conchoidal (like glass and flint) fractures (Echlin 1992). Each fracture method has their advantage according to the sample. It is important not to touch the fresh sample surface by the instrument to avoid contamination, mechanical damage and partial melting; debris from the fracture process can also be problematic since large debris can cover features of interest and smaller debris tends to be attracted to the electron beam and interfere with imaging. Furthermore, debris that is relocated to areas that are not efficiently cooled might sublimate and redeposit on the sample surface as ice contamination. For this reason, the sample should always be surrounded by colder surfaces that can act as a sink for water vapor (Umrath 1977). Microscopes that are used for cryo-microscopy are equipped with cold-fingers directly over the sample and it is also advisable to not have the sample too cold during transfer steps.

Following freezing and potentially a freeze-fracture, the temperature can be raised to etch ice from the surface by sublimation. Water molecules can change phase directly from solid to gas at low temperature and pressures. The degree of etching can be controlled by temperature and sublimation time. The figure below (2.10) displays the sublimation rate in nm/s depending on pressure and temperature.

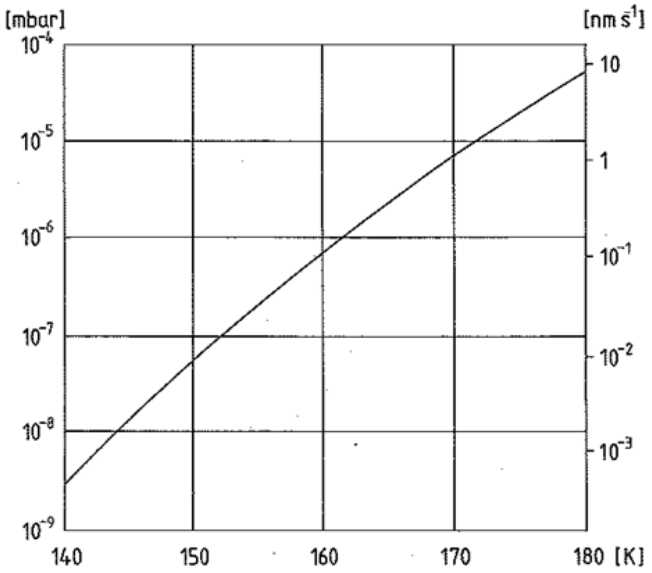

Figure 2.10. Sublimation rate as a function of time and temperature (Bachmann, Mayer 1987)

The sample can even be subjected to deep etching to reveal up to 10 µm which can expose entire monolayers of cells (Heuser 2011). The sublimation rate decreases eventually because of an increased concentration of solutes on the surface of the fracture. And low molecular weight solutes are mobile on the ice surface at the etching temperature and can relocate laterally. Small proteins can clump after longer etching times (Bachmann 1987). It is advised to find the optimum time and temperature by trial and error and sublimation can be performed in the chamber in the presence of a cold trap while imaging for such purposes. After sublimation it is possible to deposit a layer of conducting material on the surface. Or to image the uncoated sample by the application of very low kV. If the deposition of electrons from the primary beam is on balance with the emission of electrons from the surface, negative charging of the sample can be eliminated (Goldstein, Newbury et al. 2003). The sample is viewed at temperatures where the sublimation from the sample surface is not problematic, i.e. -140 °C -130 °C. If the scope is to image a vitrified sample, the temperature must be kept under T_g. -But if microscopy occurs after a sublimation step, where the sample must necessarily have been devitrified, this is no longer an issue. The sample is held cold by means of a cryo-stage in the microscope chamber and is often imaged by low kV.

Even Environmental SEM of frozen samples has been demonstrated, using nitrogen gas as an imaging gas (Stokes, Mugnier et al. 2004). The sample can also be shadow coated with a heavy metal by an angle and either visualized directly under an in-lens detector or; a stabilizing carbon layer can be deposited on top of the shadow coating for the creation of freeze-fracture replicas. Either way, the shadow coating gives a clearer image of the sample topology. Figure 2.11 below exemplifies the two methods. (A) high pressure

frozen freeze-fractured, etched and shadow-coated (sputtered tungsten) emulsion imaged in cryo-SEM by an in-lens detector and (B) propane jet frozen, freeze fractured, etched, shadow coated (sputtered platinum) replica of an emulsion droplet imaged in TEM. The images also very well illustrate the contrast difference between the two microscopes. In SEM, the thicker regions of the coating appear bright because the Tungsten emits more electrons, whereas the shadows appear dark since they have not been coated because of the shadowing angle (usually 45°). In TEM, thicker regions of the coating are dark because the platinum scatters more electrons which make the shadowed region appear bright.

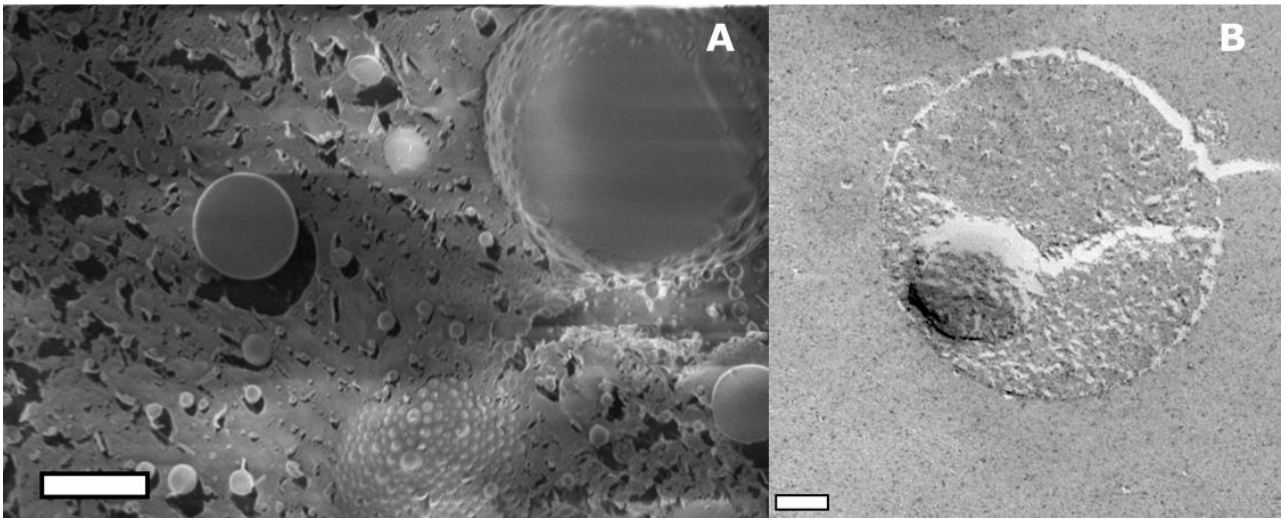

Figure 2.11. (A) high pressure frozen freeze-fractured, etched and shadow-coated (with tungsten) emulsion imaged in cryo-SEM by an in-lens detector, scale bar 1 µm. As in (Lu, Nielsen et al. 2012) but previously unpublished micrograph and (B) propane jet frozen, freeze fractured, etched, shadow coated (with platinum) replica of an emulsion droplet imaged in TEM, scale bar 50 nm (unpublished material). NB. The directions of the coating/shadows are not the same in the two images.

2.11.3 Freeze substitutions

Instead of imaging the frozen sample directly it is possible to preserve the structure for room temperature sectioning and microscopy. The technique by which frozen water is removed from the sample by an organic solvent is called freeze-substitution (Müller, Marti et al. 1980, Vanharreveld, Crowell 1964). It is possible to proceed with embedding without the addition of fixatives by embedding at low temperature, as demonstrated by Humbel *et al* (Humbel, Marti et al. 1983). For embedding at room temperature, the method requires additional addition of fixatives and the method is thus a hybrid between cryo- and chemical fixation. Different solvents are applicable depending on the sample e.g. methanol and acetone. The dehydration step where water is removed from the sample by diffusion will have to take place at a temperature where recrystallization is avoided, but above the melting temperature of the substituent. Since devitrification takes place already at 150K for pure water the success of this method is ascribed to solutes acting as cryoprotectants (Steinbrecht, Mueller 1987). The rate of dehydration depends on the temperature and what the water holding capacity of the solvent is at that temperature. The rate of substitution by some commonly used solvents at different temperatures and different concentrations of water are given by (Humbel, Marti et al. 1983). First, water is substituted with an organic solvent. This

happens while the sample is being held at -90 °C. When the water molecules diffuse out into the substitution medium, the sample will become exposed to the substitution medium. Once the water has been substituted this step usually takes at least 8 hours the temperature can be raised without the risk for recrystallization. As the temperature is slowly increased the sample is fixed by the different fixatives contained in the substitution cocktail. Uranyl acetate becomes active when there is access to the negative charges in the phosphate groups of the proteins (Humbel 2009) while OsO_4 will be active when the temperature is -70 °C (White, Andrews et al. 1976) and glutaraldehyde in the range of -40 - -30 °C. In acetone and low concentrations of glutaraldehyde, an additional incubation of 1 hour at 0 °C increases the contrast of biological membranes (Wild, Schraner et al. 2001). Finally the sample is embedded, and sectioned by ultramicrotomy. Methanol is a fast substituent at 183K and can substitute in the presence of water (Humbel, Marti et al. 1983). It melts at 179.1K and can contain 29% (V/V) of water at 183K (Steinbrecht, Mueller 1987). Addition of water can enhance biological membranes (Walther, Ziegler 2002) and seems to be helpful for polar substituents, including acetone (Buser, Walther 2008, McDonald, Webb 2011). It is active in the range between -60 and -40 °C and it has been suggested that it is due to stabilization of the hydration shell of proteins (Buser, Walther 2008) We chose methanol for the freeze substitution based on the work of (Smith, Goff et al. 2004) and their work with freeze substitution of ice cream. The substitution is normally done in freeze substitution machines to control the temperature, but was previously performed in Styrofoam boxes with dry ice. And these techniques are now reemerging as quick protocols for freeze substitution in just 90 minutes to three hours versus the several days it normally takes (McDonald, Webb 2011).

Low temperature does not prevent denaturation of proteins rather it causes the proteins to become less hydrophobic which should promote their unfolding and denaturation (Kellenberger 1987). Yet, low temperature does prevents denaturation during dehydration, but it is because of an increased viscosity of the, potentially denaturizing, media, during dehydration and embedding (Sjostrand 1990).

As mentioned in section earlier, pure water is devitrified at -135 °C and even by the cryoprotective action of solutes in the concentration found in most cells and tissues the devitrification stays below 100 °C. So it is inevitable that freeze-substitution at -90 °C is performed on cubic ice but this should not cause morphological changes in the range of resolution of biological samples (Humbel 2009). According to (Dubochet 2007) the water molecules do not move much during the devitrification process, which is probably happening by rotation with only minor translational movements and the rearrangement should thus not displace the biomolecules which cannot diffuse in the solid matrix they are in. Furthermore, again according to (Dubochet 2007) it could very well be that the second phase transition to hexagonal ice which takes place probably around -80 °C is also not accompanied of translational movements of macromolecules. Indeed, an attempt (Buser, Walther 2008) to create large ice crystal aggregation in a sample as a positive control by heating it up very fast during freeze substitution created only minor and diffuse aggregation patterns.

Methanol has been shown to extract more lipid than acetone; up to 45% vs 5% (Weibull, Villiger et al. 1984) but the addition of glutaraldehyde to the dehydration medium can counteract lipid extraction (Humbel, Mueller 1986).

Alternative substitution protocols using epoxy as fixative thus avoiding the use of OsO_4 which have protein degradative properties and can cause distortion of lipid bilayers have been proposed. Epoxy reacts mainly

with nucleophilic sites and is speculated to do so at -50 °C - -30 °C when the hydration shell surrounding the protein is gone (Matsko, Mueller 2005).

Since even freeze substitution and low temperature embedding is seen to cause aggregation the best option is to observe the frozen, hydrated sample in its native state. A comparison of meristem cells of *Zea Mays* prepared by chemical fixation and room temperature embedding; vitrified, freeze substituted and low temperature embedded; or vitrified cryo-sectioned samples showed large differences, especially in the structure of chromatin. Chemically fixed samples displayed aggregated material and a complex matrix whereas in the frozen hydrated cells, the appearance was described like a 'thick soup', with the freeze substituted samples displaying an intermediate appearance (Dubochet, Blanc 2001).

2.12 Electron microscopy

Three types of electron micrographs are presented in this thesis. These are scanning electron microscopy (SEM), transmission electron microscopy (TEM), and scanning transmission electron microscopy (STEM). In addition, analytical data obtained by energy dispersive X-ray spectroscopy (EDS) are presented. The basic image formation or signal of each method is briefly outlined below.

In electron microscopy a focused beam of electrons is utilized for imaging and analysis purposes. The resolution of most electron microscopy techniques is limited by the probe size of the incident beam, although somewhat degraded by the exit probe size as influenced by the interaction volume of the electrons in the sample.

When high energy electrons interact with a specimen it gives rise to a variety of different signal types. The signals that are transmitted through the sample are relevant for thin samples only and comprises two of the types of microscopy presented here, TEM and STEM. The difference being that TEM is performed with a collimated beam of parallel electrons and STEM is performed by scanning a focused electron beam in a raster across the sample. Either way, the electron beam is modified during its passage through the specimen. This can be by elastic and inelastic interactions, for thin specimens mainly elastic interactions.

Electrons interacting with the outer (valence and bonding) electrons undergo inelastic collisions. They are transmitted with changes in energy (and, correspondingly, wavelength) and they will transfer energy to the sample. The inelastically scattered electrons thus have lower energy. Inelastically scattered electrons predominate in biological samples; a process which creates a large amount of damage in the samples, causing heating, mass loss and changes in composition.

The elastically scattered electrons are high energy electrons that have interacted with the field of atomic nuclei in the sample. These electrons are transmitted with unchanged energy/wavelength but will have a change in direction and an associated phase shift. This elastic process can also produce selective interference effects in Bragg diffraction to form contrast in crystalline samples and to form diffraction patterns.

Inelastic scattering or high angle scattering might give rise to electron loss and this will confer a contrast in the amplitude, i.e. atomic number contrast. This contrast is largely unimportant with unstained biological specimens but contributes to an extent that is comparable with the phase contrast in samples that have been negatively stained. In bright-field TEM the scattered electrons are often absorbed by an objective lens aperture whereas the un-diffracted part of the beam passes through the aperture hole to form an image. Negatively stained samples can be imaged only slightly underfocused – just enough to produce good phase contrast for the very small structures in the sample. With negatively stained specimens underfocus values in the range 100 nm-1µm are sufficient.

With unstained specimens or very thin stained ones phase contrast is the dominant contrast mechanism. Phase contrast is the constructive or destructive interference between the elastically scattered waves and the unscattered, transmitted wave. The phase shift in the scattered waves produces phase contrast, which is strongest when the scattered wave has been brought exactly into or exactly out of phase with the unscattered wave and interferes with this wave. With small, unstained specimens, a larger extent of underfocus is needed and correction can be necessary.

In STEM, the electron beam is focused and scanned over the sample in a raster.

Dark-field imaging employed in (STEM) allows imaging of biological specimens also without staining with very high resolution. By detecting the electrons scattered at very high angles; high angle annular dark field (HAADF) imaging, it is possible to perform Z-contrast microscopy (Liu 2005).

In addition to these interactions, when electrons interact with the electrons of the sample atoms, these can be excited to a higher state and the surplus energy is released e.g. by characteristic X-rays. These X-rays carry specific information about the atomic number of the element and the transition that occurred during interaction and can be used for microanalysis of the sample. The resulting signal is sorted according to energy into a histogram of numbers of counts by X-ray energy which forms a spectrum with both qualitative and quantitative information about the elements in the sample. The position of the peaks in the spectrum identifies the elements and the area under the peaks is proportional to the number of atoms. The spectrums also have contributions from the total number of atoms in the irradiated area by the continuous X-ray spectrum originating from the slowing down of the electron beam by the electrostatic field of the sample. This forms a continuous background in the spectrum which can be used to assess the total mass of the sample. The ratio of counts between the peaks and the background can thus be used as the basis for quantification.

In a Scanning Electron Microscope (SEM) electrons are focused into a beam that is scanned across the surface of a bulk specimen in a raster and all signals are thus collected from the same surface that the electron beam is entering. The resulting electron signal is collected from each point in the raster in a serial manner and used to generate a scan image.

When the primary electrons enter the specimen they interact within a certain volume beneath the surface referred to as the interaction volume. The penetration depth and the shape of the volume are dependent not only on the sample atom number, but also the energy of the incoming electrons. The probability that a primary electron will interact with an atom in the sample (the cross section) is inversely proportional to the primary beam energy and proportional to the sample atom number which means that the cross-section is

larger for low energy electrons in a high mass sample. The distance an electron travels before encountering a collision is known as the mean free path. These values can be used to predict the interaction of the electrons in a given sample by applying a program which uses a Monte Carlo algorithm, e.g. Casino (monte CArlo SImulation of electroN trajectory in sOlids) (Hovongton, Drouin et al.)

As mentioned above, the electron signal used in SEM is electrons that have interacted with the specimen and re-exited through the surface. These electrons are divided into two classes by means of the energy they retain after interaction with the sample. The backscattered electrons; BSEs, are electrons with high energy that have interacted elastically with the nucleus of specimen atoms and have not lost energy. They are detected above the specimen for this reason by a back scattered electron detector; BSED, which is placed directly above the specimen. The signal is dependent on the atomic number of the sample since the elastic mean free path is shorter for heavy elements and the chance of interacting elastically with heavier elements is larger. This gives an element contrast where heavier elements appear brighter (i.e. back scatter more electrons) than lighter elements. The second signal is the secondary electrons; SEs, that result from inelastic interaction with the electrons of the specimen atoms. These electrons have lower energy which means that their direction can be affected when they exit the sample. Under vacuum conditions they can be accelerated towards a secondary electron detector consisting of a scintillation material where the signal is detected and amplified by a photomultiplier tube (Everhart, Thornley 1960). The detector applies a positive electrical bias to a metal mesh around it, hereby attracting and accelerated the electrons towards it. Other secondary electron detectors exist, such as in-lens systems or detectors used for e.g. low vacuum conditions.

Secondary electrons from the lower part of the interaction volume might not have energy enough to leave the sample again, and it is thus only from the top part of the interaction volume that secondary electron signal can be collected. The contrast in secondary electrons does in fact depend on their ability to escape the surface and this gives rise to the edge effect. The edge effect is characterized by bright appearance of edges protruding the surface while depression edges appear dark. Furthermore, the SE detector is most commonly placed to the side of the specimen stage and not directly above the specimen. As a result surfaces facing the detector appear brighter than the opposite since electrons escaping surfaces that faces away from the detector might get re-absorbed into these surfaces. Such images normally give information about the topography of the sample surface. The low energy secondary electrons that escape the surface and contribute to the SE image typically have energies below 50 eV (Stokes 2008).

3. Research background

As outlined in chapter 2, oxidation of fish oil emulsions is a complex area and the oxidation depends heavily on many factors that are often defined by the food matrix to which the oil is added. In order to simplify the system, this project dealt with pure (o/w) emulsions. The emulsions which are presented in this thesis represent two potential delivery systems to food products.

3.1 70% emulsions

One was a system where the oil content is very high; 70%. This emulsion is also very viscous, with a texture like thick mayonnaise and relatively large oil droplet sizes of ~8-20 µm. This is a delivery system for fish oil that has not been studied in great detail but would be suitable in formulations where the large oil droplets could be dispersed. In this conformation, several emulsifiers were tested. Sodium caseinate, NaCas at two different concentrations, NaCas1.4 (1.4%) and NaCas2.8 (2.8%), respectively; whey protein isolate, WPI (2.8%), mixtures of milk phospholipids and proteins at 20% and 75% phospholipids of the total emulsifier content, MPL20 (2.8%) and MPL75 (2.8%), respectively and lecithin (2.8%). These emulsions were made at two pH values, pH7 and pH4.5.

The oxidative stability of the emulsions was monitored by determination of peroxide values and volatile oxidation products during storage at 19 °C in the dark for 42 days and this was compared to the values for neat oil (Horn, Nielsen et al. 2011).

Only emulsions with protein-based emulsifiers at pH7 oxidized equal or less than neat oil. NaCas emulsions oxidized less than WPI emulsions and a high concentration of NaCas provided better protection against oxidation than did NaCas1.4. And this was despite the fact that droplet sizes in NaCas 2.8 were ~half the size, and therefore had a much larger surface area, of NaCas1.4 droplets. This could be indicative of the metal chelating effect of NaCas in the water phase as has been shown previously (Faraji, McClements et al. 2004)

At pH4.5 all of the emulsions oxidized more than neat oil. At this pH, the PI of the proteins is positive and should repel prooxidants. However, the oxidation rate was increased. One of the milk phospholipids-based emulsions, MPL20 oxidized the least at both pH values and at pH4.5 equal to NaCas1.4.

Based on these findings, we chose to characterize the structure of a selection of the emulsions. NaCas2.8 was oxidatively more stable than neat oil at pH7 and was chosen for this reason. NaCas1.4 was chosen to see, if we could observe any effect at the interface from the difference in concentration of the emulsifier. WPI was chosen for comparison of the two types of protein base emulsifiers and MPL20 was chosen for assessing the phospholipid impact on the structure and because it was the most promising emulsifier of the ones tested. For comparison, pH7 was chosen for this emulsion as well. The 70% emulsions are listed in table 3.1.

Table 3.1. 70% oil emulsions in this study

Sample number	*Oil content*	*Emulsifier*	*Droplet size (D3,2)**
1	*70%*	*NaCas 1.4%*	*18.4±0.11 µm*
2	*70%*	*NaCas 2.8%*	*7.5±0.02 µm*
3	*70%*	*WPI 2.8%*	*21.5±0.07 µm*
4	*70%*	*MPL20 2.8%*	*10.2±0.06 µm*

**Droplet sizes measured by laser diffraction and given by the Sauter diameter which is the diameter of a sphere that has the same volume/surface area ratio as a particle of interest (Sauter 1926).*

3.2 10% emulsions

The other type of emulsions were 10 % emulsions, representing smaller oil droplets of ~120-135 nm (Horn, Nielsen et al. 2012) which would be suitable for highly liquid food products. To prepare these small droplet sizes, larger oil droplets in a pre-formed emulsion are disrupted in a secondary emulsification step and two types of equipment are widely used in the industry for this process. One is the microfluidizer, in which the emulsion is passed through an interaction chamber that ends in a small passage. The other system is a two-valve homogenizer. In the two-valve homogenizer, in which the pre-emulsion is passed through two valves, one for creating small oil droplets and one for disruption of flocks (Schultz, Wagner et al. 2004). Oil disruption is thought to happen when the flow changes from laminar to turbulent before the passages. It has previously been shown that milk was affected very differently after passing through either of these two systems, with different conformation of protein and fat droplets after homogenization. The microfluidizer seemed to disrupt native casein micelles and create small, i.e. 30-50 nm, fat droplets surrounded by protein compared to the two-valve homogenizer (Dalgleish, Tosh et al. 1996).

For this reason it was hypothesized that the two types of equipment could create different protein conformation in fish oil emulsions, both on the surface and in the water phase and that this could affect oxidation. The oxidation was accelerated with iron and it was expected that casein would be more stable compared to whey protein, since NaCas is an efficient metal chelator. The emulsions were prepared at pH7. Slightly different pressures were required for the formation of similar droplet sizes, which were desired for similarity in the surface areas. The applied pressures can be seen in table 3.2.

Table 3.2. 10% oil emulsions in this study

Sample number	*Oil content*	*Emulsifier*	*Production method*	*Droplet size (D3,2)**
6	*10%*	*NaCas 1%*	*Microfluidizer*	*135±0.6 nm*
7	*10%*	*WPI 1%*	*Microfluidizer*	*129±1.2 nm*
8	*10%*	*NaCas 1%*	*Two-valve homogenizer*	*119±1.2 nm*
9	*10%*	*WPI 1%*	*Two-valve homogenizer*	*135±0.6 nm*

**Droplet sizes measured by laser diffraction and given by the Sauter diameter which is the diameter of a sphere that has the same volume/surface area ratio as a particle of interest (Sauter 1926).*

The four emulsions were stored at 19-20 °C for 14 days and oxidation was monitored by peroxide values and secondary volatile oxidation products. After the storage period, the peroxide values were higher in the NaCas emulsions than the WPI emulsions, but this was explained by a larger content of secondary volatile oxidation products in the WPI emulsions, indicating that the primary oxidation products had been decomposed to secondary oxidation products in the WPI emulsions. In conclusion, NaCas showed higher oxidative stability compared to WPI as expected. Furthermore, the oxidative stability of NaCas emulsions was not affected by the equipment used. This was in contrast to the WPI emulsions where the emulsion prepared with the two valve homogenizer oxidized faster than the emulsion prepared on the microfluidizer (Horn, Nielsen et al. 2012).

All of these emulsions were subjected to structural analysis by electron microscopy. Only in our trial, we did not add iron for accelerated oxidation, so we could store the emulsions for 42 days for potential cross comparison to the 70% oil emulsions.

In those cases, where the emulsions (both 70% and 10%) were stored for imaging of the oxidized emulsions, they were stored at 4 °C instead of 19-20 °C to prevent significant degradation of the emulsions prior to microscopy.

3.3 Experimental background

For a brief outline to relate the sizes of the samples to known structures; the emulsion droplets from the 70 % oil emulsions ranged from ~8-20 µm, which corresponds roughly to human cells from skin cells down to the red blood cell. The 10 % oil droplets were in the range of ~120-135 nm which corresponds roughly to the common influenza virus. And the interface layers; ranging from 10 nm to just a few nm would correspond to the size of an antibody and down to the width (not length) of the human DNA. For further comparison, the water molecule is ~0.275 nm in diameter (Chaplin 2013).

Chemical fixation and dehydration of suspensions of oil droplets can pose some difficulties. If the droplets are the only object of interest, there are reports of simply mixing the emulsions with solutions of OsO_4

followed by glutaraldehyde fixation and embedding (Jeppsson, Schoefl 1974) which gave impressive results. But to be able to observe the entire sample it was necessary to fix the sample while inside a container that is permeable to the fixatives and alcohol, but not the components of the emulsion. Secondly, since the method implies removing water, which is a large component of the system and stabilizes the proteins and oil droplets, they will collapse since the oil droplets are not distributed in alcohol in the same way. The situation is exemplified in figure 3.1 in which milk is encapsulated in capsules made from agar. The capsules were designed with an air bubble to enable that they could float in the fixative, and as can be clearly seen after osmification, the sample has completely collapsed in the lower part of the capsule.

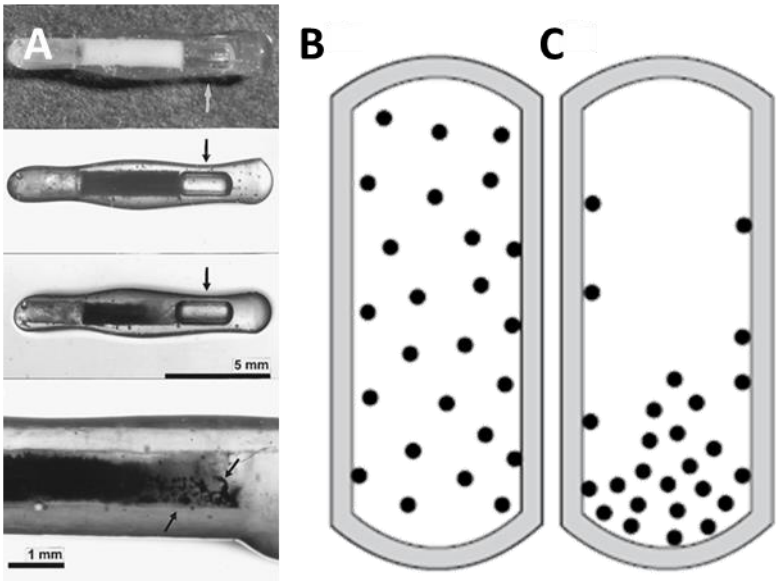

Figure 3.1. Dehydration of suspensions of emulsions. Re-composed from larger figure (Kalab, Larocque 1996).

Nevertheless, such capsules have been used for fixation and smaller capsules have yielded results with a lower degree of aggregation (Du Plessis, Tiedt et al. 1986). The formation of such capsules is quite difficult due to their delicate nature, especially when they are very small. Furthermore, it is important to work fast in order to avoid gelation at the wrong time. In the present work we created pockets instead of capsules and we also utilized low-melting agar in another way; by mixing the sample itself with low-melting agar. It is a technique that is used in biological microscopy using either agar or gelatin (Wood, Klomparens 1993) (Bozzola 2007). We attempted both, but the gelatin mixtures did not solidify satisfactory for further processing. Also, gelatin reacts with osmium hence the agar was the best choice since it was expected that we would need osmium to fix the lipids. In biological electron microscopy, capillary tubes are also frequently used for holding small samples like suspensions of bacteria of nematodes during high pressure freezing (Hohenberg, Mannweiler et al. 1994). This method could also be used to hold the suspensions of oil droplets during chemical fixation. Chemical fixation with glutaraldehyde does impose artifacts on samples (Hayat 1986) and cryofixation, especially cryo-TEM has been used extensively to image self-assembled systems (Vinson, Bellare et al. 1991, Almgren, Edwards et al. 2000). The method is superior to negative staining because the samples are hydrated and do not aggregate as a consequence of drying, which made it a natural choice for the emulsions containing 10% oil and small oil droplets. Drying can be a

large problem as shown in figure 3.2 which is a negative staining with uranyl acetate for one of the samples, presented as number 6 in the following result section. For this reason we did not use negative staining further. Another issue with cryo-TEM however is, that the thin layers of emulsifier on the surface of oil droplets are not visible by this method as that would require a difference in the atomic mass.

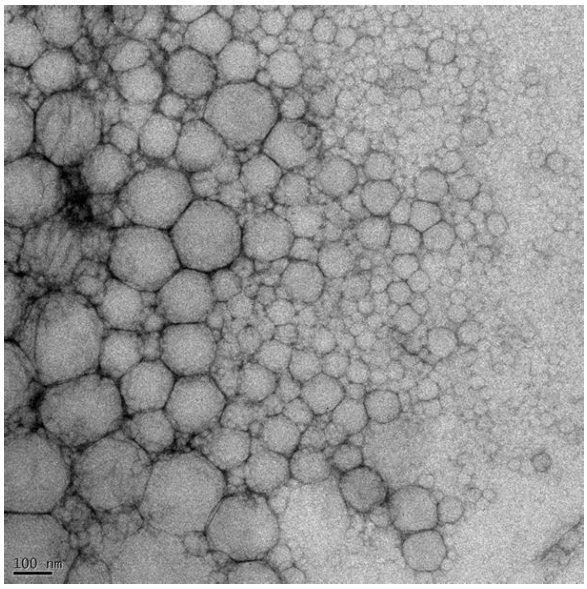

Figure 3.2. Negative staining by uranyl acetate of a 10% oil emulsion made with NaCas. The sample is displaying drying artifacts such as aggregation and deformation of droplets. Scale bar 100 nm.

The large oil droplets in the 70% emulsion were far too big for imaging by cryo-TEM which operates with films of a few hundred nm. Methods such as fixation followed by either embedding and etching away part of the resin (Brooker, Wells 1984) or critical point drying for SEM (Hatziantoniou, Deli et al. 2007) can be used to image larger oil droplets, but the droplets seem distorted and the methods do not reveal any detail of the protein structure. Freeze-fracture cryo-SEM of high pressure frozen samples was expected to give much fewer artifacts. One problem with this method can be that only water is etched by sublimation and cross-fractures of the protein layer on the surface of the droplets might not be exposed. Freeze-fracture replication is the equivalent method for smaller oil droplets. We attempted this method with the 10% oil droplets (see figure 2.11 B) but had the same problem and the method was not applied further. For these reasons, we also prepared freeze-substituted samples of both the 10% samples and the 70% samples as this would combine a gentler fixation with the possibility for heavy metal staining and cross sections of the large oil droplets. The method has been used with some success (Smith, Goff et al. 2004) for lower magnifications of dairy products.

However, chemical fixations are faster and cheaper with respect to the use of the specialized equipment needed. If the results were almost identical, it might be that chemical fixations could be sufficient in some cases, especially if we could optimize the method by exploring different matrices for holding the liquid samples. We thus wanted to compare the results from freeze substitution with chemical fixations.

4. Project outline

We set up a series of experiments to find the best methods for imaging the delicate structures of the emulsions and to characterize of the oil/water interface (thickness and organization). It has been shown that there is a difference in the oxidative stability of the emulsifiers and it is unclear whether this difference arises as a consequence of structural attributes of excess protein in the water phase. It has also been established that the production equipment affects the stability of emulsions containing WPI but not NaCas. Based on the knowledge we gained from the chemical analyses of the emulsions, there were a number of questions about the structures that we wanted to answer by these methods.

4.1 Project aim

The aims of the experiments presented here were to:

A Identify the methods most suitable for imaging the emulsions and their interfaces by electron microscopy

There are numerous ways to visualize emulsion samples, depending on the structures of interest and also importantly the availability of equipment. Emphasis in this thesis was put on testing and comparing as many different methods as possible to identify relevant techniques and to choose the methods with the best rationale for specific questions about the samples. We selected two samples to test through most of the methods and from there select the appropriate methods to apply to a larger number of samples.

The selected samples were sample 2 and sample 6 from Table 4.1. A 70% oil emulsion emulsified with 2.8% NaCas and a 10% oil emulsion emulsified with 1% casein prepared in the microfluidizer. They were chosen to represent the variety in texture (thick mayonnaise-like texture *vs* milk-like texture), oil content (70 % *vs* 10%), droplet size (µm range *vs* nm range) and production methods (mixing *vs* high pressure methods) in the samples.

Table 4.1	*0.05%GA+2.5%PFA*	*1%GA+2.5%PFA*	*2%GA+2.5%PFA*	*3%GA+2.5%PFA*	*6%GA+2.5%PFA*
Sample2	*x*	*x*	*x*	*x*	*x*
Sample6	*x*	*x*	*x*	*x*	*x*

The methods we chose were:

- Chemical fixation of (1:1) sample and low melting agar mixtures in 5 different concentrations of glutaraldehyde (GA) mixed with 2.5% paraformaldehyde (PFA) as shown in table 4.1. This was performed for sample 2 and 6. Later, this type of fixation was made for all samples with 3% glutaraldehyde and 2.5% paraformaldehyde.
- Chemical fixation inside agar pockets in 3% glutaraldehyde and 2.5% paraformaldehyde. This was performed for all samples.
- Chemical fixation inside capillary dialysis tubes in 3% glutaraldehyde and 2.5% paraformaldehyde. This was performed for the 10% oil emulsions (6-9).
- High pressure freezing, freeze-substitution, deep etching and cryo-SEM. This was performed for samples 1, 2, 4 and 6.
- High pressure freezing, freeze substitution and room temperature embedding. This was performed for all samples with 2 different types of substitution media.
- Plunge freezing and cryo-TEM. This was performed for samples 6-9.
- Furthermore, some samples were analyzed with STEM EDS analysis (2 and 6) and we recorded a STEM HAADF and bright field tomogram of sample 6.
- We also made negative stained samples and freeze fracture replicas from samples 6-9. But these methods were given up early in the project.

B To apply these methods on a selection of emulsion samples for characterization

The questions we wished to answer about the samples were:

- What are the structures of the interfaces of different emulsifiers and can we identify differences between them?
- Are there any structural differences between emulsions with different concentrations of the same emulsifier?
- Are there any differences between 10 % emulsions produced by different methods?
- Are there any visual signs of oxidation in the emulsions?

The emulsions are summarized in table 4.2.

Table 4.2 Emulsions in this study

Sample number	*Oil content*	*Emulsifier*	*Production method*	*Droplet size (D3,2)**
1	*70%*	*NaCas 1.4%*	*Stephan mixer*	*18.4±0.11 µm*
2	*70%*	*NaCas 2.8%*	*Stephan mixer*	*7.5±0.02 µm*
3	*70%*	*WPI 2.8%*	*Stephan mixer*	*21.5±0.07 µm*
4	*70%*	*MPL20 2.8%*	*Stephan mixer*	*10.2±0.06 µm*
6	*10%*	*NaCas 1%*	*Microfluidizer*	*135±0.6 nm*
7	*10%*	*WPI 1%*	*Microfluidizer*	*129±1.2 nm*
8	*10%*	*NaCas 1%*	*Two valve Homogenizer*	*119±1.2 nm*
9	*10%*	*WPI 1%*	*Two valve Homogenizer*	*135±0.6 nm*

**Droplet sizes measured by laser diffraction and given by the Sauter diameter which is the diameter of a sphere that has the same volume/surface area ratio as a particle of interest (Sauter 1926).*

4.2 Project strategy

We chose well-established methods in electron microscopy as described previously; chemical fixation, cryo fixation followed by freeze substitution, cryo fixation followed by freeze fracture and cryo-SEM and cryofixation followed by cryo-TEM. Furthermore we tested a number of different matrices for the chemical fixation. The experiments reported in this thesis can be summarized by Figure 4.1:

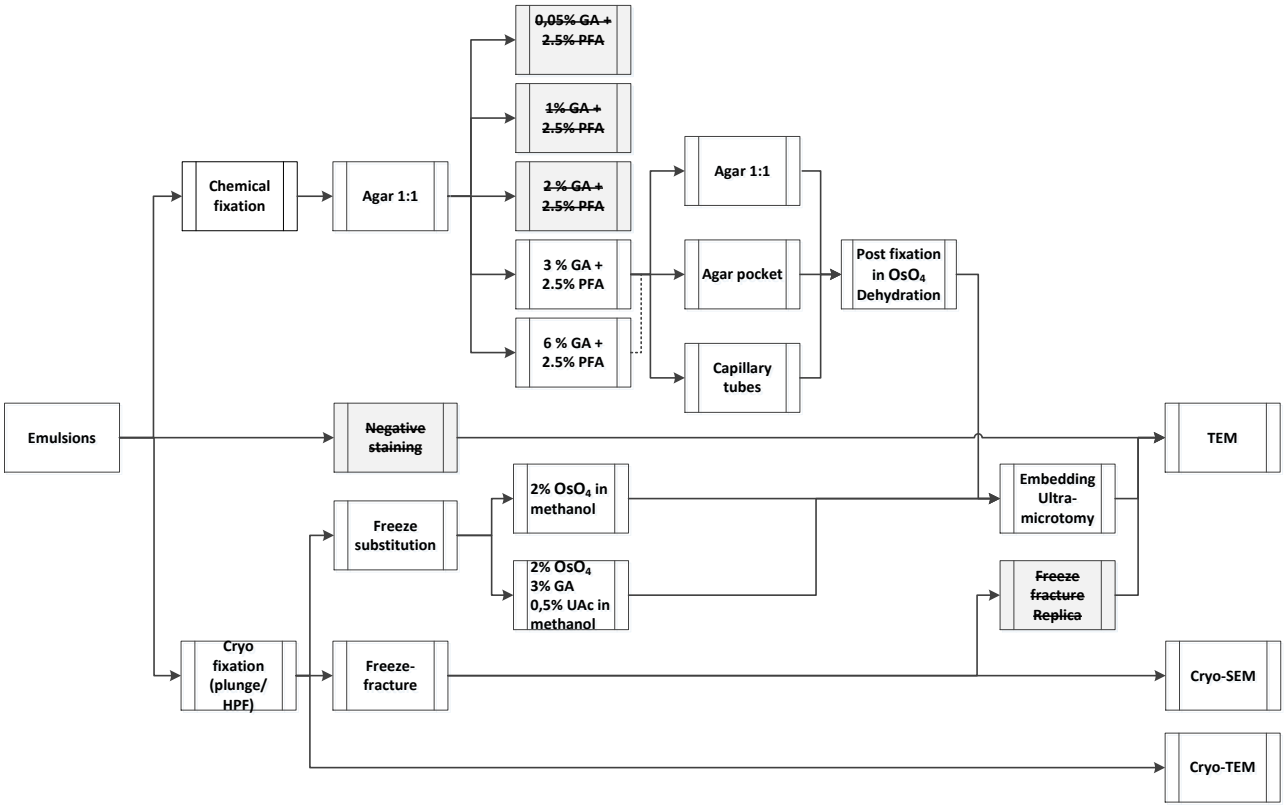

Figure 4.1 Overview of the experiments in this project .methods in grey boxes (strike through) were applied further after initial trials.

The results of the thesis work are divided into two Chapters. The first results chapter presents the results from the testing, development and comparison of different methods on the two model samples (2 and 6). These results are collected in Chapter 5: Methods development which will explore relevant methods to image the samples, the type of information these methods reveal and discuss the application of methods to the samples. Secondly there are the answers to questions about the actual samples. These results are collected in Chapter 6: The micro- and nanostructure of fish oil emulsions.

5. Results - Methods development

5.1 Chemical fixations

Chemical fixations were tested in a variety of different matrices as outlined in Chapter 4. The different results are described and visualized below.

5.1.1 Samples mixed with agar

The samples were mixed 1:1 with low melting agar and fixed as described in Chapter 8 (materials and methods). Glutaraldehyde is known to cause shrinkage and distortion of the samples (Hayat 2000). To find the optimum concentration of glutaraldehyde for chemical fixation we compared five different concentrations of glutaraldehyde; 0.05%, 1%, 2%, 3% and 6%; combined with 2.5% paraformaldehyde in all cases. Mixing the sample with agar dilutes the samples and makes the droplets appear distinct and thus easy to image for assessment of the effect of the fixatives on the droplet morphology. We prepared a series of both of the two model samples (sample 2 and 6). The droplets were not overlapping in most cases which facilitated the use of thresholding and segmentation to analyze larger amounts of droplets in cases where the droplets were small enough, i.e. samples 6-9. The samples with small oil droplets were thus analyzed by thresholding and segmentation, whereas the samples with large oil droplets were analyzed by visual inspection of the morphology of the samples.

The results for sample 2 are shown in figure 5.1. The images that would be expected would be round, smooth droplets with contrast from the OsO4 inside the oil droplets and stained protein layers on the smooth surfaces. The left column in figure 5.1 shows the interface layers and the right column shows overview images of the droplets. In all cases the droplets were mixed well into the agar and they were easy to find because they were dispersed over the entire sections. In all cases it was possible to see the protein surface layers as well as the droplets; or in the case of oil extraction, the place where the oil droplet had been. In some cases the droplets were cut close to the equator of the droplet, i.e. orthogonal to the surface layer and appeared to have thin well-defined surface layers. In other cases the droplets were cut above or below this point and appeared to have wide, less-well defined surfaces as the two overview images from 3% and 6% fixations in Figure 5.1 (H) and (J) exemplify. And in all cases the agar formed a network around the droplets seemingly interacting with the surface layers and proteins of the samples (this is especially clear in (J) and (H). We do not know whether the protein in the water phase was adhered to the agar or extracted. Also electron dense granules were visible; both in the agar and on the surface of the oil droplets. These granules will be discussed in detail later.

With the lowest concentration of glutaraldehyde, i.e. 0.05% the surface layers were very distorted. The appearance was wavy. The oil was extracted from the almost all of the droplets and in many droplets the surface layers had collapsed to create half-moon shaped “ghosts” where the oil droplets had been. Figure 5.1 (A) and (B) exemplifies this situation. In (A) the interface layer is the line in the middle of the micrograph. The (previous) inside of the droplet is to the right side and the outside is to the left. Outside the droplet, visible agar lines are seen. In (B) is an overview from an oil droplet where the oil is extracted

and the surface layer is collapsed to form a half moon shape. The wavy structure of the layer is also visible (arrow). Using higher concentrations i.e. 1-2 % there were almost no droplets where the oil was fully extracted. But there were droplets where part of the oil inside was extracted as shown in (D) and (F). The surfaces were in some cases still distorted and wavy (D) and (F), black arrows. In other cases the surfaces seemed smoother (C) and (E). According to (Hayat 2000) inefficient fixation of proteins in cells prior to osmication causes proteins to leak out and membranes to become permeable. Probably this effect is also responsible for the lipid extraction in the droplets fixed in low glutaraldehyde concentrations since these were subjected to the same OsO_4 postfixation. With 3% and 6% glutaraldehyde there were only very few distorted droplets, the majority had round appearances and no extraction of oil (H) and (J), thus suggesting appropriate fixation. The surfaces appeared much smoother than with the other concentrations of glutaraldehyde (G) and (I).

There was a thus large increase in the quality of fixation between 2% and 3% glutaraldehyde but no difference between 3% and 6% glutaraldehyde as assessed by visual inspection of the micrographs. To prevent the loss of extensive amounts of lipids during the dehydration steps, Hayat (Hayat 2000) recommends to fix, rinse and dehydrate in the cold, which we did, using an automatic tissue-processor (see Chapter 8). Additionally it is possible to only dehydrate samples partially because lipid extraction takes place predominately at high solute concentrations. We could thus have dehydrated the samples partly and used a hydrophilic resin. Hayat (Hayat 2000) also states an alternative protocol for partial dehydration using epon, that contain very brief dehydration steps in 95% ethanol at 0 °C followed by infiltration with epon and methanol, also at 0 °C. Both of these methods might have improved the retention of lipids in the samples. Another thing could be the washing step which we carried out with water and not buffer. Since this can cause removal of poorly fixed materials in cells, we might suspect that the same applies to the emulsions. But also the surface layers were poorly fixed with glutaraldehyde concentrations below 3%, so in conclusion it seemed to be the appropriate concentration for chemical fixation.

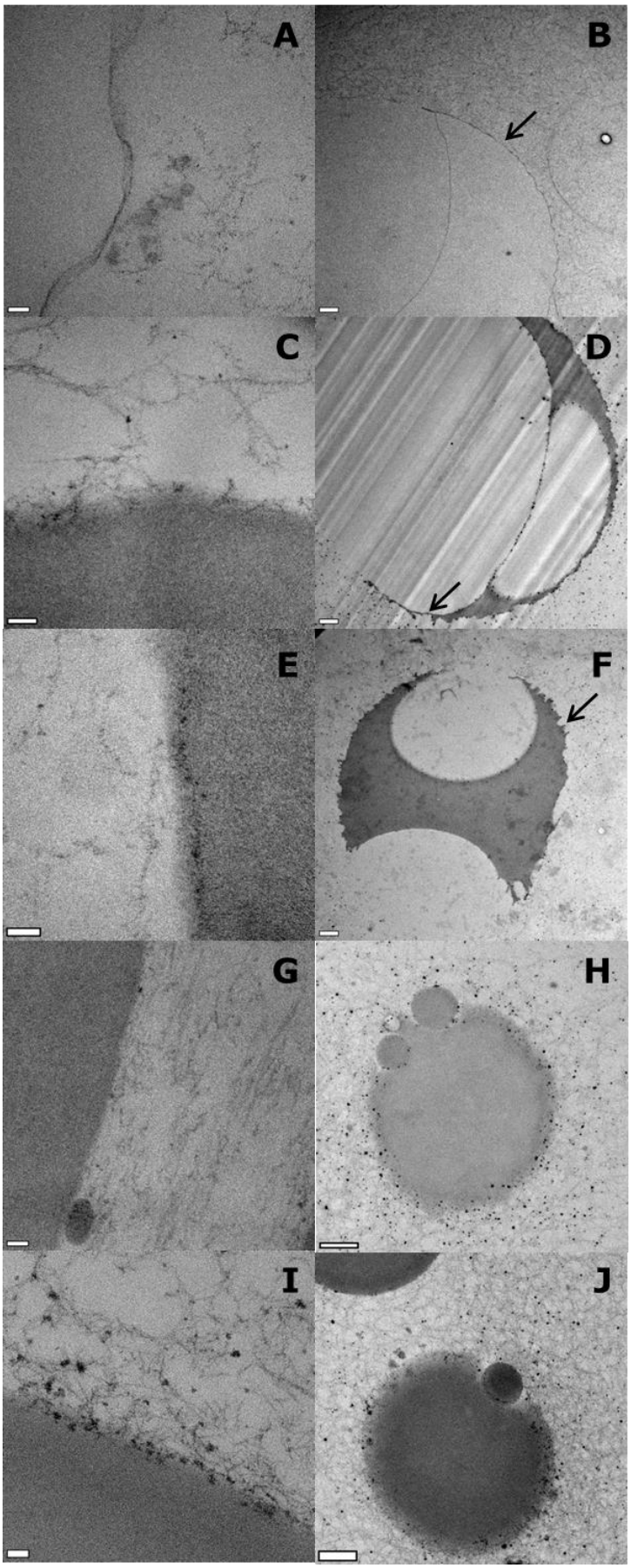

Figure 5.1. Chemical fixations of agar mixed sample 2 (70% oil). The rows are from top; 0.05% glutaraldehyde, 1% glutaraldehyde, 2% glutaraldehyde, 3% glutaraldehyde and 6% glutaraldehyde. Left column depicts the interface layers in association with lines from the agar. The right column depicts overview images. Scale bars of left column 50 nm; right column 500 nm.

Extraction of oil and wavy interface layers was seen mainly in glutaraldehyde concentrations of 2% and below (A-F) whereas the samples appeared well-fixed with 3% and above (G-J).

The micrographs of sample 6 fixed with the different concentrations of glutaraldehyde are shown in figure 5.2. In all concentrations of glutaraldehyde the oil droplets looked well preserved with round and smooth appearances. The interface layers was also visible in the droplets that had been actually sectioned, but the appearance was different from sample 2 due to the smaller size of the droplets leading to a large curvature inside the section which meant that the droplets were rarely cut at the equator. By visual inspection of the samples there was no obvious difference between the samples that had been fixed by different concentrations of glutaraldehyde.

To obtain knowledge about any possible difference between the fixations the images were subjected to thresholding and segmented for image analysis using ImageJ (Rasband 1997-2012). The areas of the droplets were measured and recalculated to diameter. We set a cut-off value in the segmentation of a= 1250nm^2 (d~40nm). This was done to avoid sampling the dark particles in the images which are not oil droplets and will be discussed in detail later. For comparison, we also did the analysis also with a cut-off value of 500 nm^2 (d~25nm). Below that level, the program would pick up too much noise. But with the cut off value of 500 nm^2 this would include not only the aggregates close to the sample surface but also many of the dark particles in the agar matrix and the result would thus depend more of how much of the agar matrix would take up of the image area and not so much on the sample itself why this analysis was discarded.

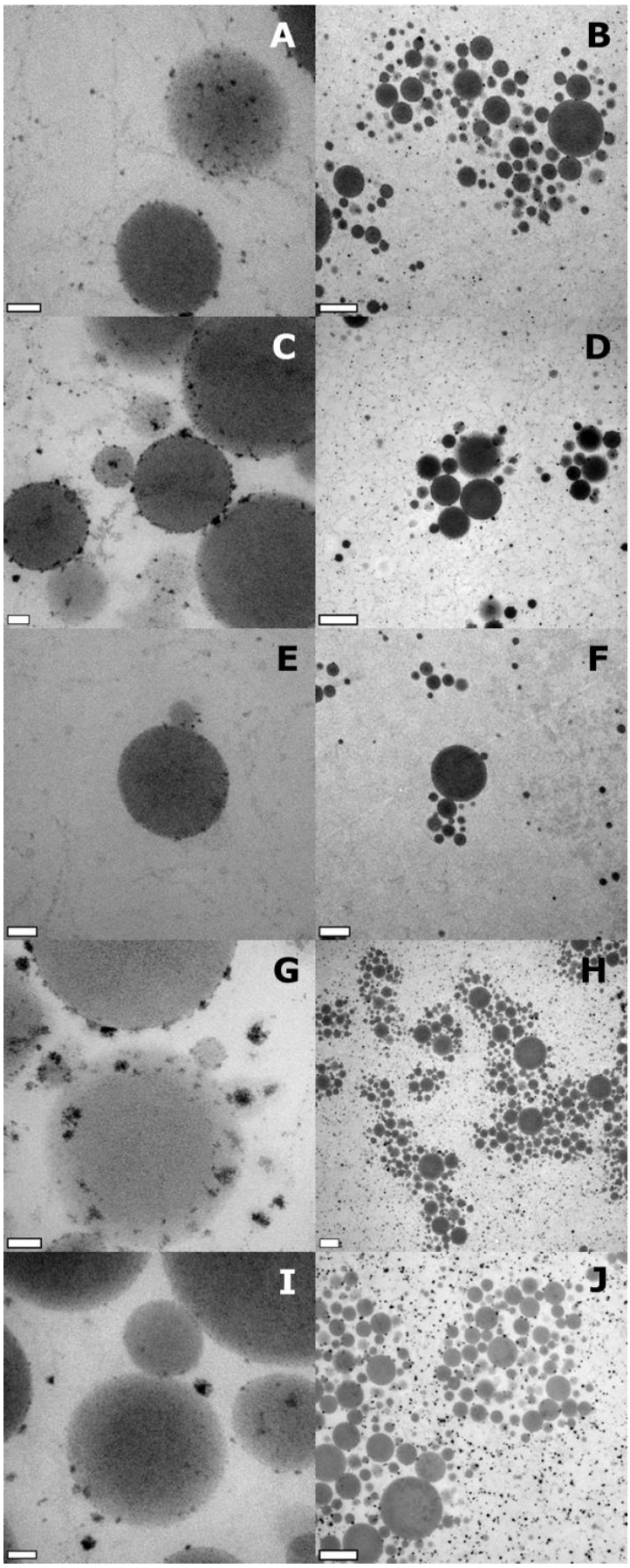

Figure 5.2. Chemical fixations in agar of sample 6 (10% oil) emulsions. The rows are from top; 0.05% glutaraldehyde, 1% glutaraldehyde, 2% glutaraldehyde, 3% glutaraldehyde and 6% glutaraldehyde. Scale bars of left column 50 nm; right column 500 nm. Just by visual inspection of the sections everything seemed well preserved and it was impossible to directly see any differences between the samples.

The datasets were processed for statistical analysis in R (R Development Core Team 2011). Due to the non-parametric data, the Kruskal-Wallis rank sum test was used to distinguish between the samples. The test returned a p-value lower than 2.2e-16 indicating a strong significant variation on droplet diameter with concentration of glutaraldehyde. The post hoc test was performed by a series of pairwise Mann-Whitney-Wilcoxon tests. To correct for the multiple pairwise tests we used Holm's sequential Bonferroni (Holm 1979).

The results from the post hoc test are depicted in table 5.1 below:

Table5.1	*0.05%*	*1%*	*6%*	*3%*
1%	*0.19*			
6%	*<2e-16*	*9.7e-11*		
3%	*<2e-16*	*2.5e-13*	*1.0*	
2%	*1.0*	*0.067*	*<2e-16*	*<2e-16*

With a confidence interval of 0.95 the results indicate significant differences such that the data is divided into two groups. Group 1 contains 0.05%, 1% and 2% which are all significantly different from both 3% and 6% but not from each other. And group 2 contains 3% and 6% which are also not significantly different from each other but from all of the samples in group 1. The result is reflecting the distributions of 3% and 6% being cut off but it is also strongly indicative of a shift in the droplet diameter between 2% and 3%. Figure 5.3 depicts the mean and median droplet diameter and a box plot of the data which clearly shows the difference between the groups. The median diameter of the droplets decreased from group 1 (111nm, 96 nm and 116 nm) to group 2 (60nm and 61nm). From the median diameter values it is indicated that there is no difference from 3% to 6%, but this could also be affected by the two distributions facing the same cut-off value.

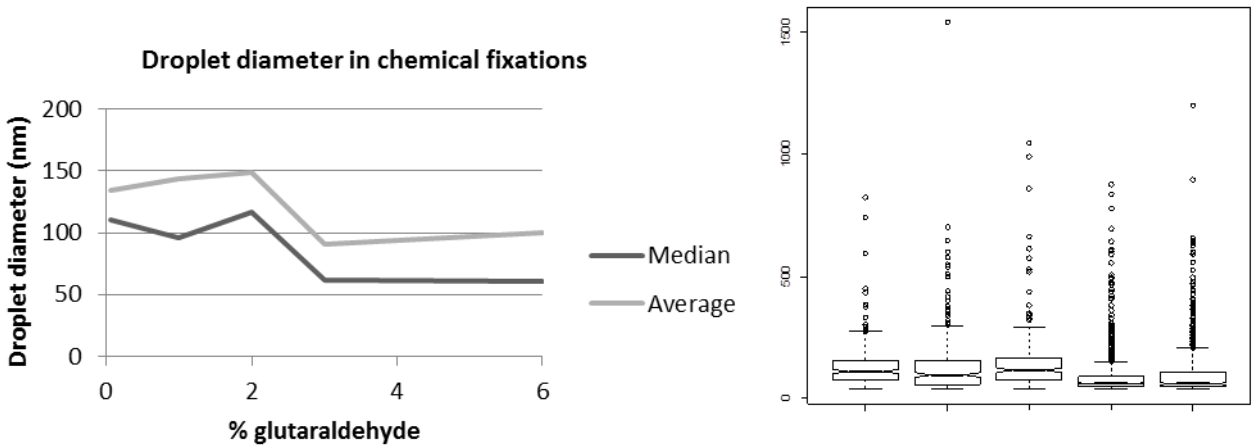

Figure 5.3. The results seemingly indicate that the diameter finds a minimum from 3% glutaraldehyde but caution needs to be taken to conclude this because of the cut off values applied.

It is a possibility that other emulsions containing other ingredients would react differently to chemical fixations with glutaraldehyde. To discover this, a good approach would be to repeat this experiment for a variety of emulsions and analyze the datasets together with variables about the chemistry of the emulsions by multivariate data analysis.

We prepared several of the samples in both 3% and 6% glutaraldehyde but have decided to use mainly the micrographs from the 3% glutaraldehyde fixations for further analysis to also be able to compare to the 70% emulsions at a later point.

5.1.2 The artifacts of fixation in agar

In all the samples there were visible lines from the agar. They were measured to be between 1-6 nm thick with median values around 2-4 nm ± 1 nm. Since there is excess protein in the water phase it could potentially be associated with the agar or it could be extracted. There did not appear to be any detectable difference in the thickness of these lines when comparing the different concentrations of glutaraldehyde in any of the two samples tested, see graph in figure 5.4 below. But the agar lines seemed to be more abundant in the samples that were fixed in higher concentration of glutaraldehyde as can be seen by inspecting the micrographs in figure 5.1 through increasing glutaraldehyde concentration.

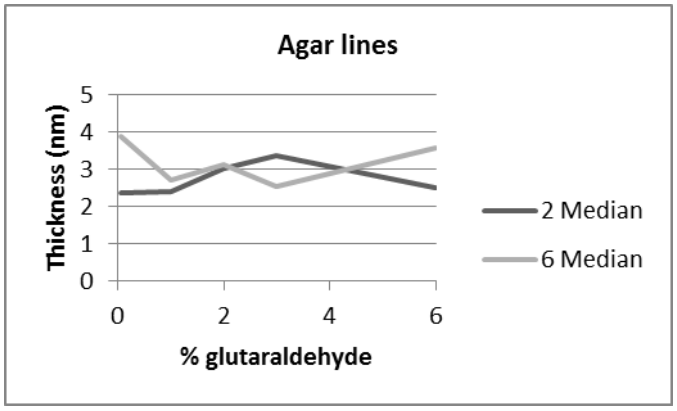

Figure 5.4. Thickness of the agar lines in the micrographs.

Another thing that was present in these samples were the previously mentioned dark, electron dense aggregates that were either associated with the agar lines or the surface of the droplets. To complicate things even more, it was unclear whether they were two species of condensed particles, one that was localized everywhere in the samples and one that was localized at the surface of oil droplets, or if they were the same. A particle in an agar matrix is shown in Figure 5.5 (A). The sample is from an agar pocket, far away from the sample. It contains the dark contrasted aggregates. STEM EDX analysis has confirmed it to contain both lead and osmium; 4.7 and 3.2 % (w/w) respectively. We suspect that there can be two explanations for the aggregates. Either they are the electron dense granules that might arise from traces of glutaraldehyde in the samples reacting to form reduced osmium species that later binds lead as well (Hayat 2000). It could be that the rinsing of these samples before the post fixation in OsO_4 was not sufficient, though thorough, and that the agar matrix retains traces of glutaraldehyde. Or, it could be excess protein from the water phase that had dispersed into the agar matrix during fixation or dehydration. In the emulsions that were not fixed inside agar, the particles had aggregated only on the surface of the droplets. These granular particles did not seem to be a precipitate from the staining, since the particles were never located at the surface the sections, i.e. we never saw them on the cut surface of droplets that would belong to the section surface. See figure 5.5 (C) which shows a stereo micrograph to display that the aggregates are, in fact inside the sections. The reader can attempt to cross the eyes and focus on both images to obtain a stereo image of the sample. It is an old technique but it still remains useful for visualization of samples in 3D without the creation of a tomogram or FIB stack. It is a quick method to obtain such knowledge in both TEM and SEM and is very useful also for samples that are too sensitive for tomography (Gramm, Müller et al. 2010). The sample in this stereo micrograph has been fixed inside a capillary tube, i.e. without the presence of agar and in a matrix where casein cannot be extracted. (More about this fixation method in section 5.1.4). Since we know that excess proteins are present in the water phase, it is likely to be not only unspecific reduced osmium but also excess protein from the water phase of the emulsions which have denatured and collapsed onto the surface of the droplets. This is indeed likely because the amounts of dark particles in this matrix, where the proteins cannot be extracted from, are much more abundant. Figure 5.5 (B) shows a close-up of such a particle from the surface of an oil droplet. It consists of many small granules of little more than half a nanometer. An additional argument against staining precipitates is that none of these granules were seen in freeze substituted material even in cases where the post staining was done in the same batch as the chemically fixed samples.

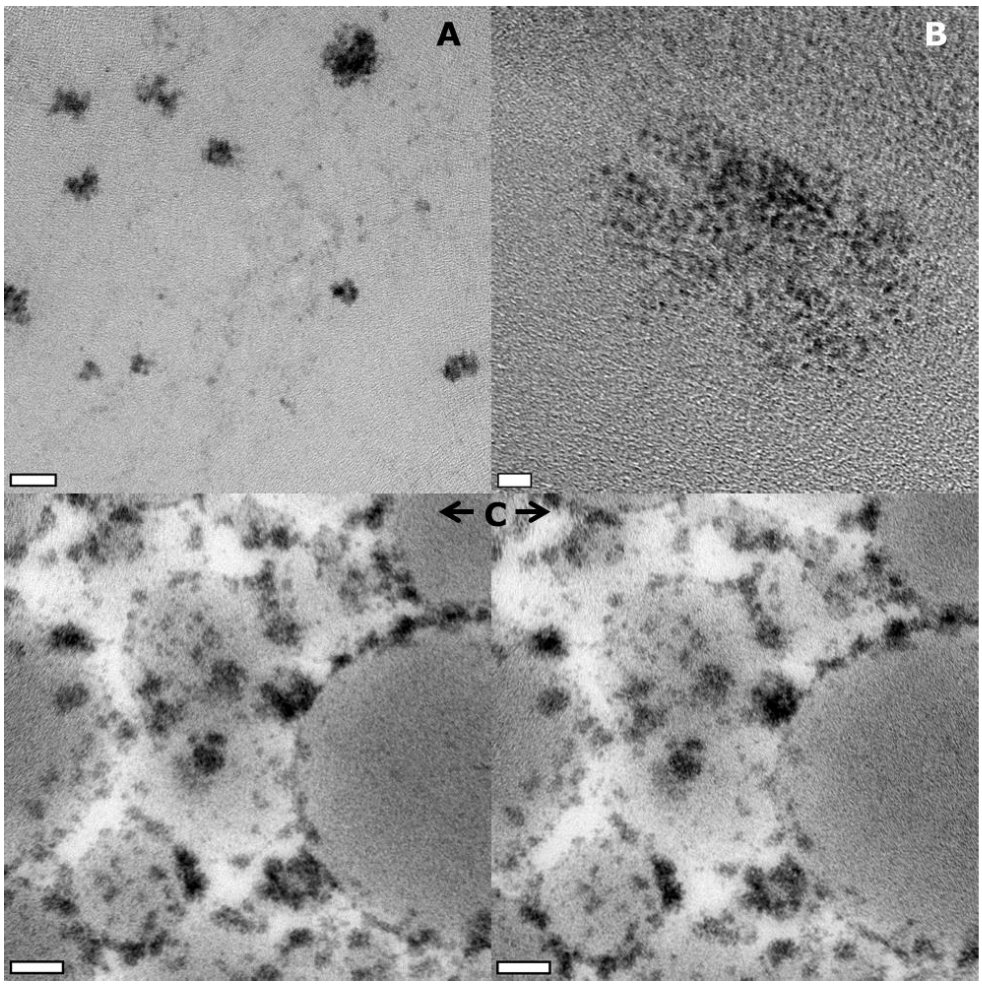

Figure 5.5. (A) Agar lines from a pure agar matrix, scale bar= 20nm, (B) Close up of a particle on the surface of an oil droplet, scale bar 5nm, (C) Black particles on the surface of oil droplets inside a capillary tube, stereo micrograph, scale bar 50nm

5.1.3 About contrast in the samples

The samples showed good contrast from the staining. To characterize it further we subjected oil droplets to line scans of EDX analysis and HAADF imaging in STEM. The figure 5.6 shows the bright field and HAADF micrographs with the line that was scanned. The light points below the line in (A) and across the large oil droplet in (B) are from beam damage. Below the micrographs is the STEM intensity profile and at the bottom is the result of the EDX analysis. The examples are shown below for two oil droplets. The STEM profile confirms the contrast difference we see in the image for the larger droplet that appears to have enhanced electron density at the edge (A). When analyzing what is causing this effect, we came to the conclusion that it was mainly due to variations in the OsO_4 content which seemed to increase closer to the surface. The effect was visible only in some of the droplets. In (B) the intensity is merely plateauing in the middle of the droplet; not decreasing. Whether the enhanced surface density of some of the fixed droplets

is a feature related to droplet size, the penetration of OsO_4 into the droplets or the synergistical staining by lead and osmium would require a large amount of samples to be analyzed.

In addition to Os and Pb, we found Si, Cl and Cu. Si and Cl might be from the glass containers that this sample has been in contact with (Takeshi Kassama, personal communication). Cu is from the grid mount.

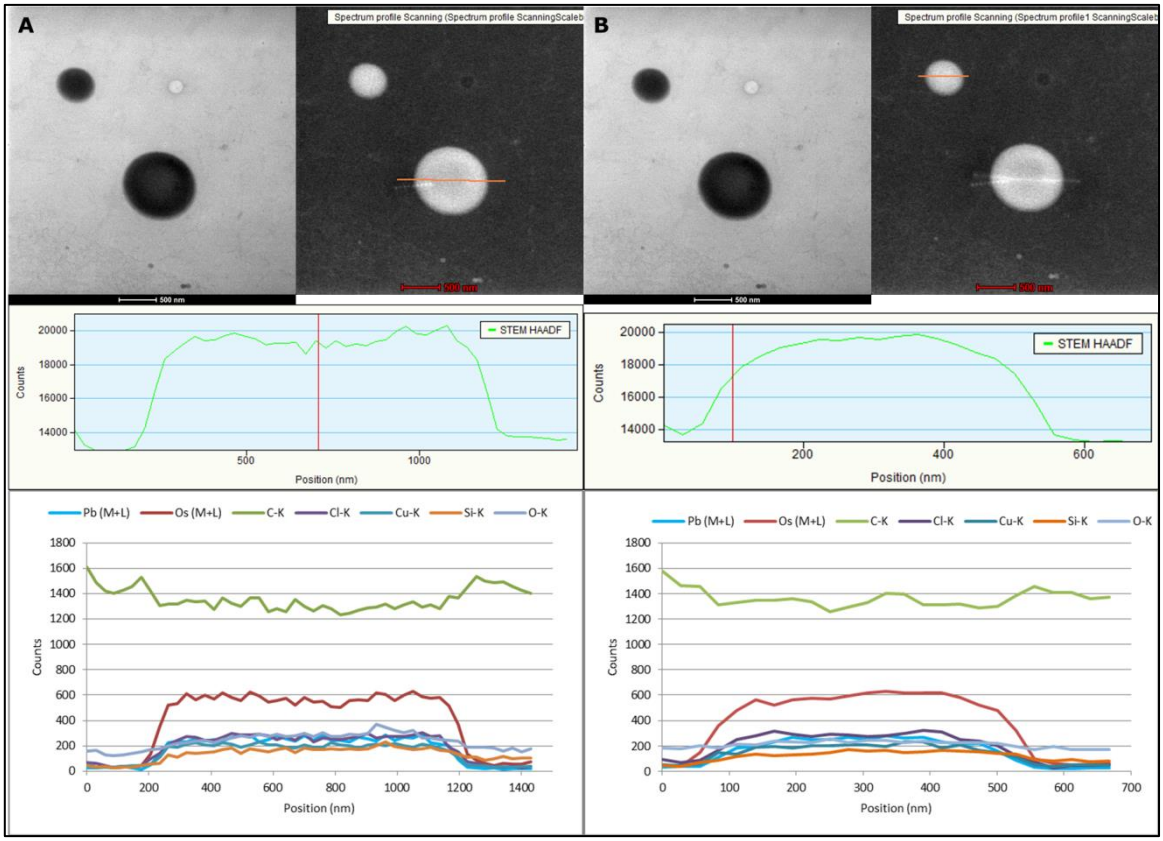

Figure 5.6. Line scan EDX analysis of two droplets from sample 2, (A) is the large droplet in the image and (B) is the small droplet.

To sum up the agar mixtures; the images from the agar mixes showed good preservation of the oil droplets and their surfaces. The protein between the droplets must be condensed along this agar matrix, extracted or be part of the black particles/aggregates in the images. The fact that the dark particles are much more abundant in a matrix where an extraction is not possible suggests that a lot of the extra protein is in fact extracted in the agar mixed samples but specific experiments would have to be carried out to confirm this. One problem by using this method to study the actual structure of the sample is that the samples are diluted 1:1 and do no longer represent the true structure.

In some droplets the layers seem very thick and fuzzy while they look thin and sharp in others. This is because of the curvature of the droplets which depends where a given droplet is sectioned. With a section thickness of approximately 70 nm this can give some very wide projections of the surface layers in large droplets. Furthermore, sectioning of large droplets also bears the risk of underestimating the droplet size if

the droplet is not sectioned near to the equator. The appearance of the surface layer can hint whether this is a problem, since the surface layer of droplets that are sectioned close to the equator will appear sharp and thin compared to the angled surface layers. In the 10 % emulsions, the effect is not so pronounced. Instead it is possible to see droplets that are so small that they are entirely contained in the section and thus it is possible to see their surface.

5.1.4 Fixation in agar pockets

To surpass the problem with diluting the samples we also developed agar pockets to encase the emulsions during chemical fixation. Instead of the large agar capsules developed by Kalab (Kalab, Larocque 1996) or the minute, but difficult-to-produce capsules (Du Plessis, Tiedt et al. 1986), we made small pockets from agar, see Chapter 8. The pockets were relatively easy to create and very easy to handle during fixation. But it proved to be slightly difficult to find the place to section the blocks because the agar blackened in the OsO_4. The large droplets in sample 2 were never completely free from the agar matrix as can be seen in figure 5.7 (A) below. It is very probable that the sample collapsed onto the agar pocket during dehydration, which is natural since the cross-linked protein-matrix that might have been between the oil droplets was probably not strong enough to stabilize such large droplets. We would have expected that this method was most suitable for the 70% emulsions. However, opposite of expectations, we had very good results with the sample 6, the 10% emulsion with the milk like structure. With sample 6, the only problem was how to prevent the thin emulsion from running out of the pocket prior to fixation but when that was achieved the method created very good samples. Even though the samples had been dehydrated, the droplets did not collapse on each other to an extent where they were distorted. (B) Sample 6 10% emulsion with a very preserved layer of emulsion between the layers of surrounding agar. It is possible to see the edge where the agar begins. In this case we can assume that there is no agar between the oil droplets of the sample and that the structures we see there (C) are true sample. There are no agar lines inside the sample but there seem to be the same form of aggregates on the droplet surface as there is in the agar matrix, as discussed earlier. (D) is a STEM HAADF image which shows high Z contrast and the aggregates are clearly seen. We saw no sedimentation of the oil droplets to the surface of the agar pocket and this is potentially a promising way to perform chemical fixations for preserving the structure of the small droplets. They must still adhere to something, i.e. each other, but they did not look compressed in any way even though it seemed that the pockets had collapsed to give a very thin layer of sample, either during the application of the top layer of agar or during the dehydration. This can be seen in 5.7(B) where the layer is in fact only approximately 8 µm thick. Compared to the capillary tubes shown in figure 5.8 there were very little extra protein or aggregates, and it could be that extra protein was extracted.

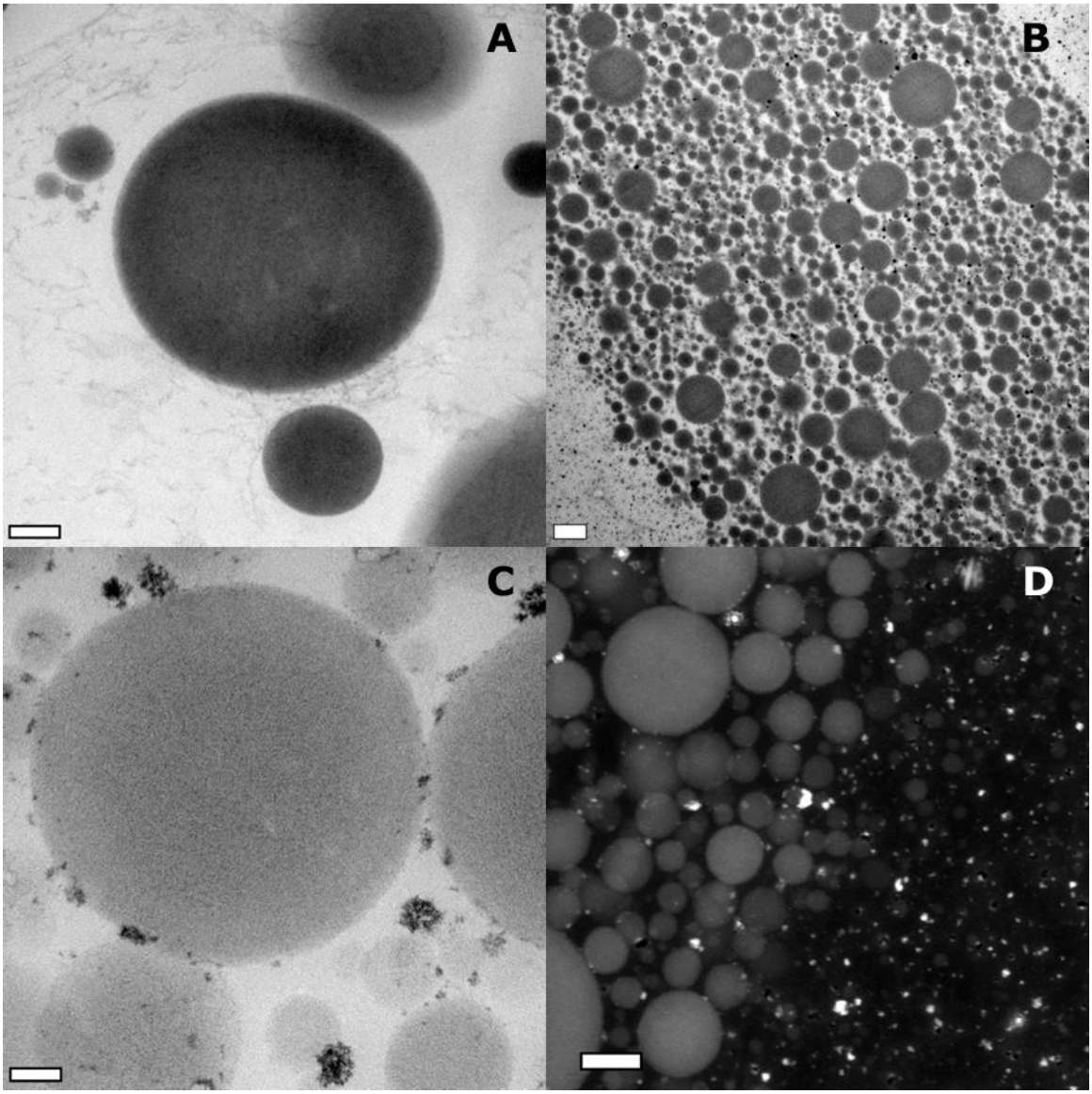

Figure 5.7. (A) Sample 2; Oil droplets in 70% emulsion fixed inside agar pocket with visible agar lines, scale bar 200 nm (B) Overview of 10% emulsion matrix sample 6, scale bar 500nm (C) Oil droplets of 10% emulsion fixed inside agar pockets, scale bar 50 nm, (D) STEM HAADF image of sample 6 and surrounding agar pocket, scale bar 200nm.

5.1.5 Fixation in capillary tubes

For the 10% oil droplets we also tried to hold them in capillary dialysis tubes during fixation. In this case there is no agar in the sample. The micrographs below are from samples fixed in 3% glutaraldehyde with 2.5% PFA. For practical reasons we did not attempt this method with the 70% emulsions since they were too viscous to go inside the capillary tubes. Figure 5.8 (A) shows a cross section of a capillary tube containing the sample. It can already be seen from this image that the sample has collapsed on the side of the tube and in some areas inside. This implies that deductions about overall structure of the sample should be made with caution. Results from both 3% and 6 % glutaraldehyde showed good fixation except for the act that the samples seemed to be condensed to a degree where the droplet shape was slightly distorted in some areas. This is probably no surprise when inspecting the first image (A). But we can also

clearly see the protein between the droplets and this time it has nothing to do with the possibility of traces of glutaraldehyde causing unspecific osmium residues in the agar. Furthermore the protein could not be extracted during dehydration, because the cutoff value for the dialysis tubes was 5000 kDa. The protein seems to be condensed or aggregated in some areas while only sparsely distributed in other areas (5.8 (B and C)). In many areas there were cracks in the structure, as if the fixed sample has broken into pieces in the processing which is likely since they become slightly brittle and the tubes are very thin. The method had some features that made it very user friendly. It was very easy to place the tubes in the right orientation for embedding which saved a lot of time in finding the sample inside the block. And the method had the additional advantage of being free from agar to add to the confusion of the origin of aggregates in the samples.

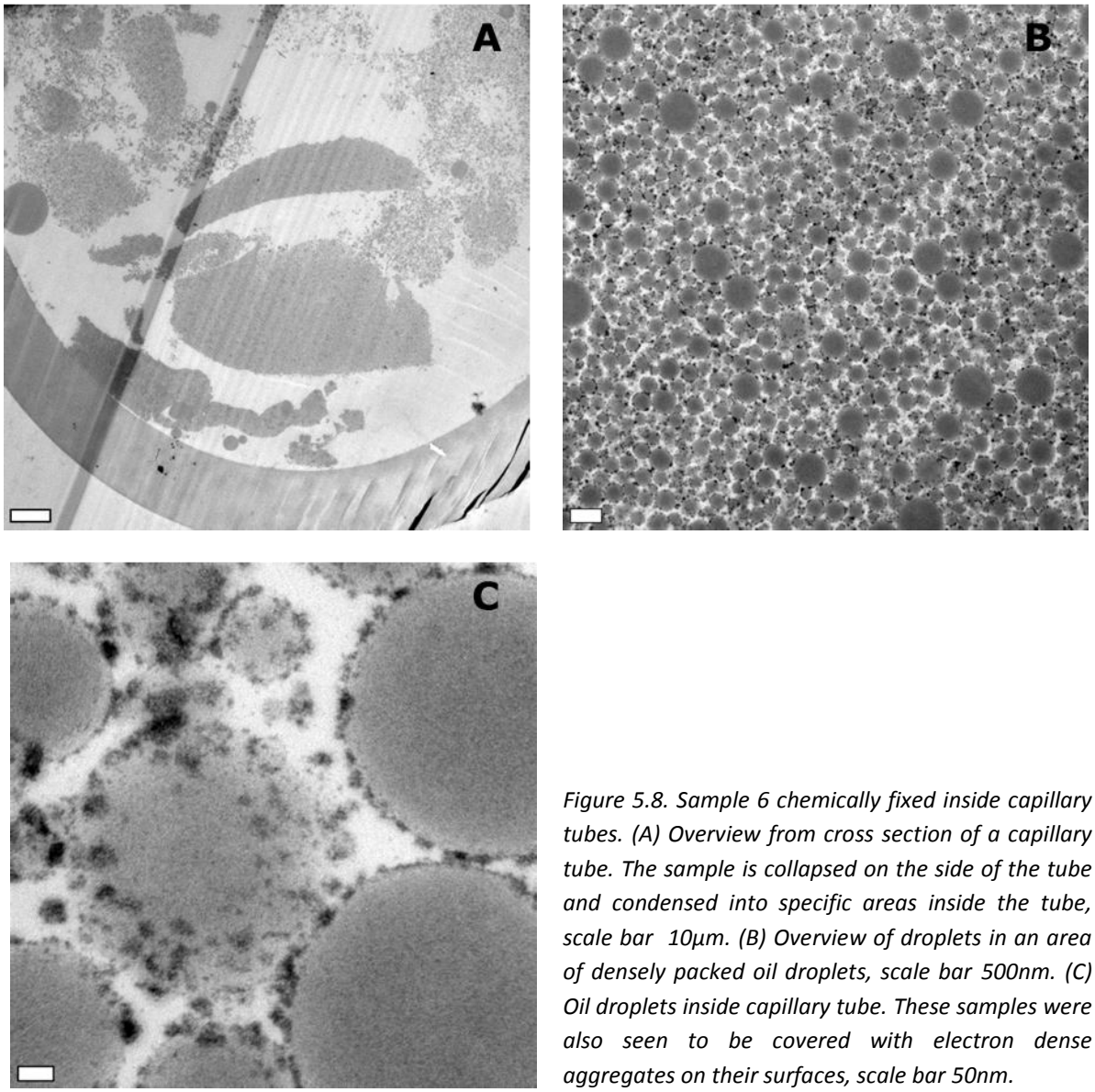

Figure 5.8. Sample 6 chemically fixed inside capillary tubes. (A) Overview from cross section of a capillary tube. The sample is collapsed on the side of the tube and condensed into specific areas inside the tube, scale bar 10µm. (B) Overview of droplets in an area of densely packed oil droplets, scale bar 500nm. (C) Oil droplets inside capillary tube. These samples were also seen to be covered with electron dense aggregates on their surfaces, scale bar 50nm.

The samples in the pockets and capillary tubes were overlapping and therefore it was not possible to do automatic segmentation by thresholding. Measurements done by hand are very time consuming. Time was prioritized to segment the high pressure frozen, freeze substituted samples presented in section 5.2 by hand before the deadline of this thesis.

5.2 Freeze substitution

To avoid some of the artifacts induced by chemical fixations we attempted to do high pressure freezing and freeze substitution of the samples. Initially we attempted to substitute the samples with OsO_4 in methanol. The images are shown in figure 5.9. There were several problems with using this substitution mixture. First of all, the oil droplets seemed distorted in their shape to an extent that they completely lost their normal round appearance (A). We also saw a large extent of lipid extraction as seen from (B). While the first two images in figure 5.9 are from 70% oil emulsions, the last image (C) is from a 10% oil emulsion (sample6). In this case the most predominant artifact is not from the substitution medium but from the freezing. It is obvious that bad freezing has created eutectic lines in the sample and that all the small oil droplets of this sample are pushed into these lines. But there is also visible lipid extraction from the larger oil droplets inside the eutectic ridges. The figure thus exemplify three different artifacts encountered in these samples, (A) unstable membranes, (B) fat extraction and (C) freezing artifacts by formation of coarse eutectic ridges.

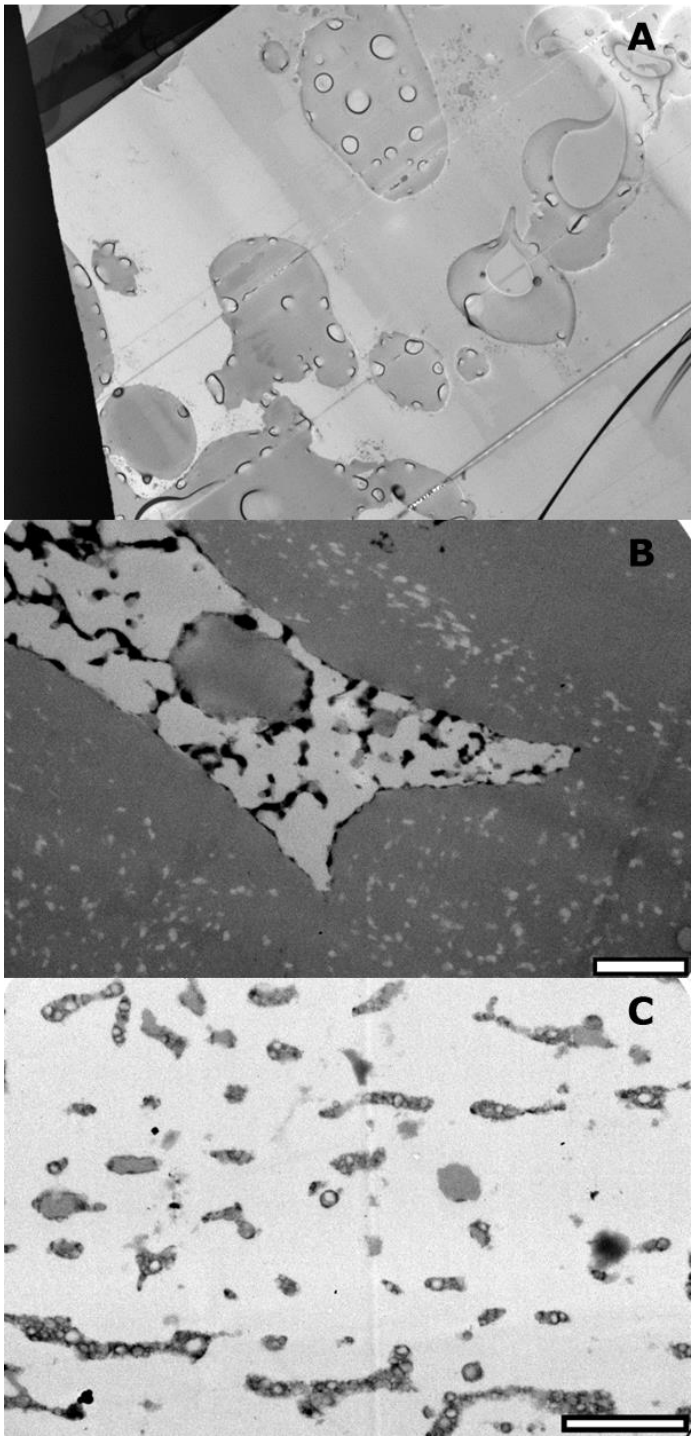

Figure 5.9. (A) Sample 2, The samples were distorted in their shape, scale bar is missing but the image is rather informative, which is why it is used anyway, (B) Sample 4 (MPL20, 70% oil) shows lipid extraction from the samples as shown by the light plaques, scale bar 1µm, (C) Sample6, the largest distortion comes from the artifacts from bad freezing that had apparently taken place in this sample. But it is also apparent that the sample contains some large oil droplets where the lipids appear to have been extracted, scale bar 2µm.

To increase the stability of the emulsions during freeze-substitution we added glutaraldehyde and uranyl acetate to the substitution medium (Müller, Marti et al. 1980).

The addition of glutaraldehyde and uranyl acetate to the substitution medium made a large difference in the appearance of the oil droplets. The results are shown in figure 5.10. The top row shows two images from sample 2. (A) is a close-up on an interface layer and (B) is an area between two oil droplets. For the

70% oil sample there was a dramatic difference compared to the chemically fixed samples. The oil droplets looked more or less the same but the structure of the protein interface was not collapsed. It was possible to see clearly the protein in the water phase. The proteins in the water phase appeared as thread-like structures forming a complex matrix (see discussion below) that seemed to span the entire water phase and in some areas the protein matrix was denser than in others. From the figure it can be seen that the thought of the surface of the oil droplet as an isolated layer of amphiphilic protein molecules in a water phase is probably an oversimplification. Even though there are surface layers and the protein matrix is denser nearer the surface of the droplets the surface layer is not isolated from the protein matrix in the water phase. There are small voids in the protein matrix. Normally, it is a clear sign of artifacts when proteins form a network containing small voids. On the other hand it does look a lot like the structure in the native casein micelle according to the nanocluster model. As described in Chapter 2, it is a complex tubular network with voids that act as water channels in the micelle. α-caseins interact to create the structure and β-caseins lining the water channels. The structure, as obtained from cryo-tomography, i.e. a vitrified hydrated sample imaged in its native state, was shown in figure 2.3. The difference is that in NaCas emulsions, there are no nanoclusters of calcium phosphate which are necessary for the correct assembly of the casein micelle. But it could be speculated that the casein could form similar, but less organized structures throughout the water phase. Whether this is the true structure or the voids are from artifacts can be debated. As described in Chapter 2, pure water devitrifies at -135 °C and in most cells and tissues the devitrification stays below 100 °C (Dubochet 2007). Hence freeze substitution is performed on cubic ice. This is not believed to cause morphological changes in the range of resolution of biological samples (Humbel 2009). But these protein structures are substantially smaller than most biological samples. The devitrification process should not affect biological macromolecules because it probably happens by rotation of the water molecules (Dubochet 2007) and the dimensional change from cubic to hexagonal ice should be only 0.1 nm (Echlin 1992). But again these are estimates and the protein structures are relatively small. We saw the same structures in freeze-fractured samples imaged by cryo-SEM (see section 5.3). The samples imaged by cryo-SEM had also been subjected to -90 °C meaning that they were no longer vitrified and should resemble the samples from the freeze substitution. The holes were slightly bigger, however. See section 5.3 and 6.1.1. But during etching, clumping of smaller protein structures can occur (Bachmann 1987). Yet another reason for the voids could be the action of the fixatives. Even though protein aggregation is decreased by low temperature, it is not because the low temperature counteracts protein denaturation but more likely because the low temperature increases the viscosity of the media (Sjostrand 1990) as mentioned in Chapter 2. Moreover, as pointed out by the comparison of chromatin (among other cell structures) in room temperature embedding, freeze substitution or cryo-microscopy of vitreous sections (Dubochet, Blanc 2001) there is a difference between the slight aggregation in freeze substitution and what is seen in true cryo microscopy of vitrified sections which is referred to by the authors as a thick soup. Third, our samples were not embedded at cryogenic temperature but at room temperature, and even though they were washed at 0 °C, there might have been some further denaturation and thus the small voids could be from slight aggregation/degradation of the proteins. A fourth possibility is the protein degradative action observed from OsO_4 (Bahr 1955). A fifth explanation could be that it is simply not possible to vitrify these liquid samples completely and that the voids are in fact nucleation sites from ice crystals, i.e. not originating from nucleation during the freeze substitution process, but from the freezing process itself. In cells, growing ice crystals are normally connected but stopped at the membranes (Dubochet 2007). In our samples there are no membranes to stop the crystallization and vitrification of

these throughout the entire volume should theoretically be harder. But on the other hand the ice crystals from inefficient freezing are normally large (Dubochet 2007). It can even be a combination of all of these factors. Further investigation would be needed to resolve the issue of whether we are observing the true structure or it is affected by artifacts. This investigation could be performed by cryo-TEM or cryo-negative staining of a fraction where the large oil droplets had been removed for imaging the proteins in the water phase. The most logical step would be to image the samples without removing the oil droplets which would imply sections of vitrified samples imaged in the frozen state, but plans to do so unfortunately had to be given up during the project work.

In the 10% oil emulsion, condensed, darker aggregates were observed. These spherical, dark structures were much less condensed in the freeze substituted samples than in the chemically fixed samples. And it is admittedly hard to see in the micrographs whether they are, in fact, just very small oil droplets. Previous results of both very small casein particles and oil droplets have been reported after the processing of milk in a microfluidizer (Dalgleish, Tosh et al. 1996) Most of the structures looked more like protein aggregates. One small oil droplet is shown in 5.10 (C). 5.10 (D) shows an overview of the sample. The droplets were overlapping and closely associated with each other. There were, however, also voids but they seemed to arise from the absence of material that was not contained in the small aggregates.

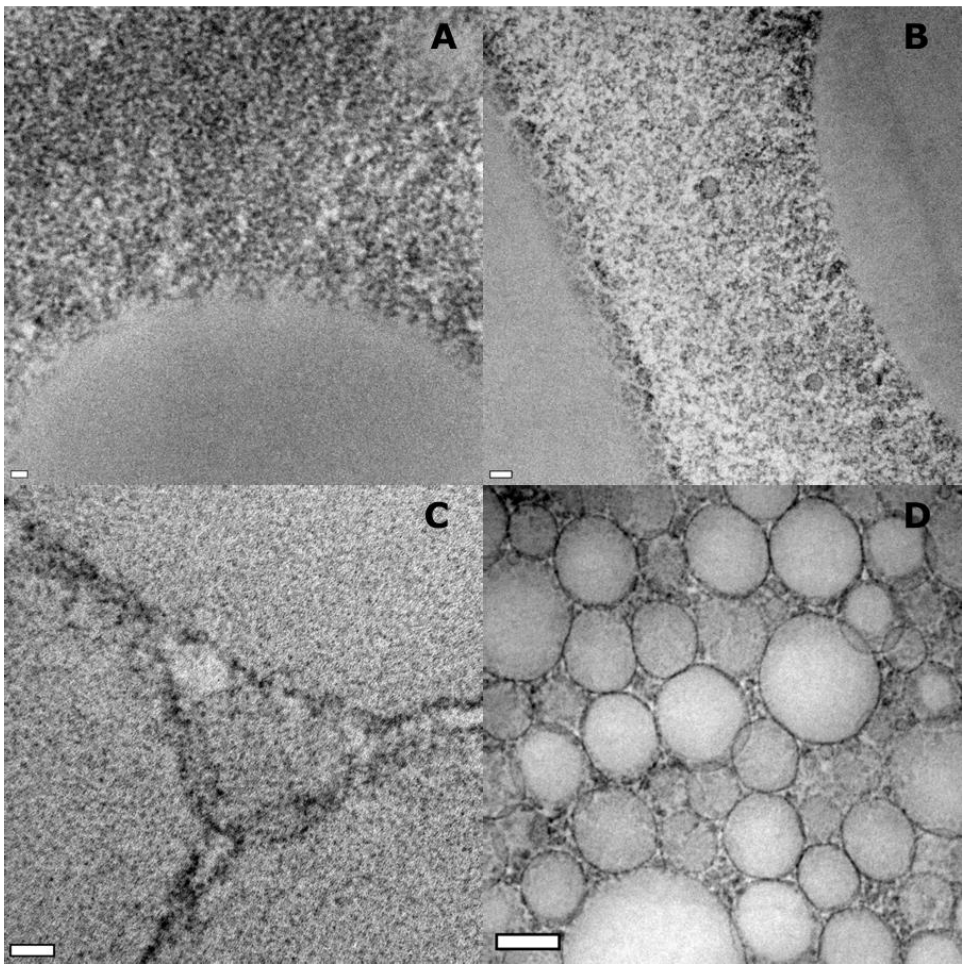

Figure 5.10. Top row: 70% oil emulsion with NaCas, scale bars 50 nm (A) & 100 nm(B). The samples are very well preserved including the protein in the water phase. The excess NaCas has a thread-like structures separated by small

voids. Bottom row 10% oil emulsion with NaCas, Scale bars 20 nm(C) & 200 nm)D). Here there is no visible thread-like structures. Instead there are dark spherical shapes that might be protein, might be small oil droplets.

As can be seen on the image in Figure 5.10 (D) there seems to be a population of droplets that are larger than 100 nm and then a second population of smaller, darker objects that might either be droplets or protein aggregates. The diameters of droplets were measured by hand (n=1498) since the overlapping made it impossible to threshold the image (see Appendix I for an attempt using e-cognition, a program based on object orientated image segmentation instead of the pixel based approach used in ImageJ). Only objects that appeared truly circular and with distinct surfaces were measured. A density diagram of the diameters shows a bimodal curve, indicating indeed what could be assessed also by visual inspection of the micrographs. The data has two populations, one with a median diameter of 210 nm and the other with a median diameter of 33 nm. To compare the data to the chemically fixed oil droplets, we chose to only compare the population with the largest median value. We believe this to be the best option because in the case of the chemically fixed samples we made the choice of leaving out the particles with an area less than 1250 nm^2 to not segment the dark aggregates. Hence the density plot from the chemically fixed sample was unimodal with a possible distinct population of smaller objects left out. We thus applied a cut off value of d=105 nm because of local minimum in the histogram which shows the 2 populations with median diameters of 212 nm and 33 nm, respectively in figure 5.11 (left). The diameter is larger than for the mean diameter of the chemically fixed samples that had median diameter values of 111 nm for 0.05% glutaraldehyde down to 61-60 nm for the 3%-6% glutaraldehyde fixations. A graph of the diameters in the chemical fixations with the addition of the points from the high pressure frozen freeze substituted samples (HPF FS) are displayed in figure 5.11 (right). Additional measurements of droplet sizes for a similar sample to this has been done earlier by cryo-TEM but size measurements of samples in this size range is not effective by cryo-TEM since only droplets that can be contained in the thin vitrified meniscus between the holes on a lacey carbon grid after blotting and quenching are preserved (Almgren, Edwards et al. 2000) and many of the droplets in this sample are simply too large with a median diameter most probably much higher than that thickness. In that particular study which contained the similar sample (images are shown in section 6.4 the Sauter diameter D(3,2) (Sauter 1926) calculated from the microscopy data was 93 nm whereas D(3,2) as measured by laser diffraction it was in fact 126 nm (Horn, Nielsen et al. 2012) thus illustrating this point.

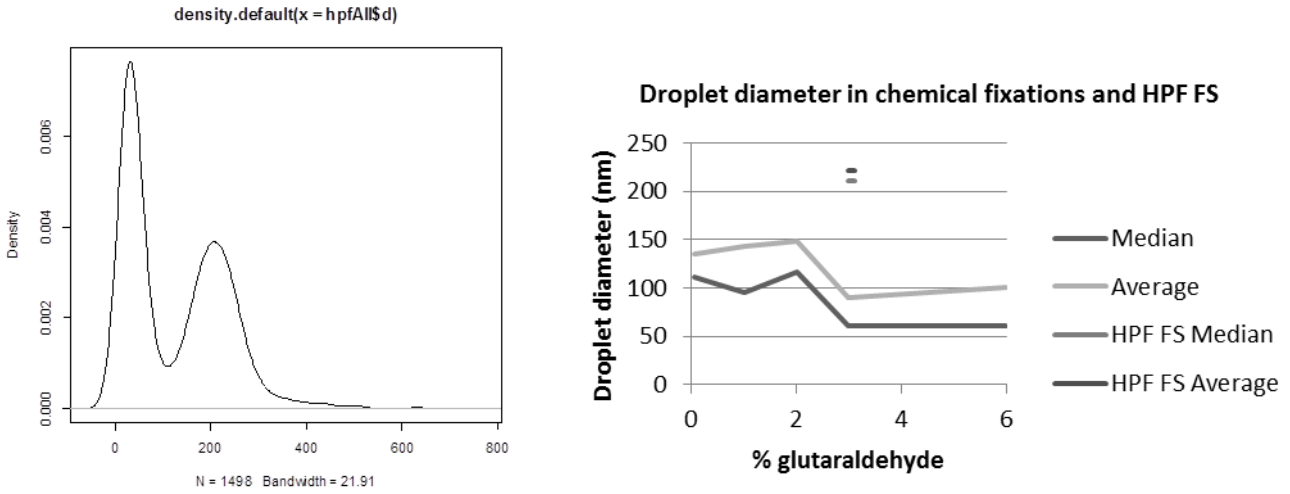

Figure 5.11. Density plot for sample 6 and the mean and average droplet sizes as compared to the chemically fixed samples in agar.

It is very obvious from the micrographs of freeze substituted material that the surface layers are not especially uniform in any of the samples. Any measurement of surface layer thickness would have to consist of several measurements of the same surface and even so, any variation of the droplets' surface is only visible in the plane of the section. Additionally because of the curvature/angle of the sections it is very difficult to really measure the layer thickness. To measure the layer thickness it is necessary to tilt the sample to get the right angle for every single droplet and to tilt it accordingly to the area of that specific surface that needs to be imaged. A true measurement of the droplet surface structure in the 70% oil emulsions would require imaging of a fairly large amount of droplets by a 3D method such as slice and view, followed by segmentation and some statistical modeling. This could be performed on our high pressure frozen, freeze substituted samples. We have the blocks, but time constraints have not allowed us to do so. The good thing with this type of sample preparation is that the samples can always be reexamined later, and we thus still have the possibility to do so. For the smaller droplets in the 10% oil samples a tomogram of a high pressure frozen, freeze substituted sample could be made. We made such a tomogram in STEM bright field and HAADF followed by segmentation. The result is shown in figure 5.12 with dark field (left) and bright field (right). Slices are shown face on and at a 90° angle below. The tomogram confirmed that the droplets are tightly packed with smaller structures in the voids between the larger structures. Also, when comparing the two images, that is from the same tomogram, it is obvious that the slice in bright field is corresponding well to the expected thickness of the section; 70 nm. The dark field image is much thinner indicating that the stains from the post staining did not penetrate fully through the section. According to (Hayat 2000) the penetration of heavy metal stains can be incomplete and non-uniform but this should normally pose serious problems only in thicker sections, i.e. 0.5-2 µm. In our case however, even despite long staining times, the staining seems to be inefficient. Unfortunately we were limited by the time to make new sections from the block and hence we used a thin slice with post staining that was originally prepared for normal bright field imaging in the TEM, not for tomography. For a repetition of this experiment, we would cut a new, thicker section of the block and either refrain from the post staining since it can confuse

the image slightly when it is not uniformly staining the whole section. Alternatively, we could aid the staining process by elevated temperature and ethanol (Hayat 2000).

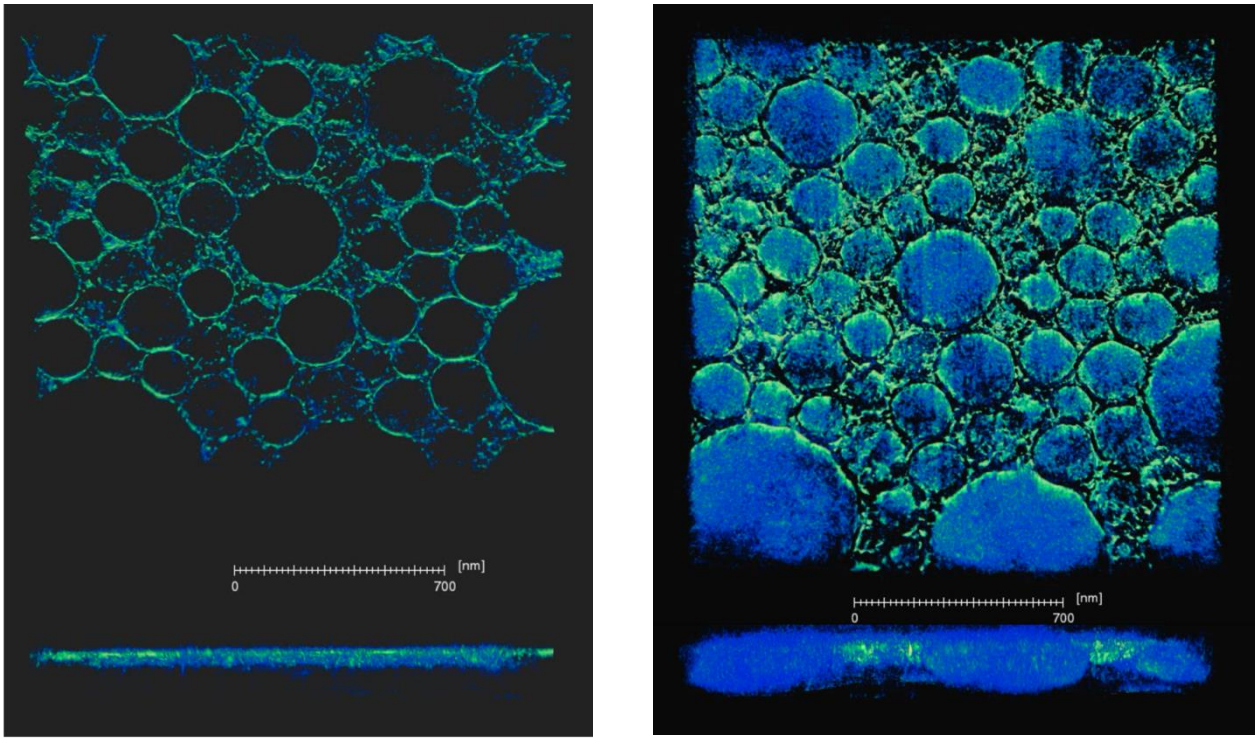

Figure 5.12. Dark field (left) and bright field (right) segmented images taken from the tomogram of sample 6.Top part of images shows the section at 0° and the bottom part of each image shows the sample at 90°. The fact that the bright field slice thickness seems to correspond well to the expected section thickness, whereas the dark field image seems to be thin and only have a uniform surface at one of the sides indicated that the post staining has not penetrated all the way through the section.

5.3 High pressure freezing, freeze fracture and cryo-SEM

Yet another way to image the high pressure frozen samples is by freeze-fracture cryo-SEM. With cryofixation and imaging, the samples should be free from staining and fixation artifacts and the samples can be imaged at their close-to-natural state.

We imaged the high pressure frozen samples after freeze-fracture, sublimation and coating with platinum using a specially built sample holder that is a hybrid between the Baltec sample holders and the Quorum cryo-stage (See Appendix II for specifications). It should be noted that the samples are no longer vitrified after the sublimation step which we performed at -90 °C for 3-5 minutes. It is a slightly harsh etching but it has proven useful for this type of sample. Figure 5.13 shows cryo-SEM micrographs from freeze-fractured samples. The top row shows images from the 70% sample. (A) is an overview of the sample. The large droplets in the image are fractured across, whereas some small droplets are intact. All droplets appear

round and with smooth surfaces. (B) is a closer view of oil the droplets. Some of the droplets have a void around them, which is a drying artifact from prolonged imaging. The structures in the water phase resembles very well the structure in the high pressure frozen, freeze substituted samples with something that looks like a network with small voids in between. This might indicate that these structures are not arising as a consequence of protein shrinkage or degradation, but that the small voids are in fact from the casein structure. Here they were slightly bigger, perhaps indicating clumping after etching. It could also be that the temperature has not been perfectly controlled in the sample preparation (transfer, sublimation and sputter coating steps) and that the structures have been subjected to slight migratory recrystallization as well which can take place at appreciable rates over -90 °C but normally happens at higher temperatures in biological samples (Echlin 1992). For the 10% emulsions, it proved to be difficult to image what was between the droplets since the droplets were positioned so close (C). But that is a feature that corresponds very well to the freeze substitution images as well. (D) Even with drift correction it was difficult to obtain sharp images from the frozen samples in a magnification needed for droplets of this size. It could be that the sample holder was not quite stable enough for this kind of magnification. But also charging can pose huge problems for the imaging. Cryo-SEM of high pressure frozen samples should be a very good method to compare to the high pressure frozen freeze substituted samples as they are not fixed or stained and thus imaged as close to their native state as possible. Any difference in the micrographs between samples imaged in cryo-SEM and samples prepared in alternative ways might point to artifacts from the chemical substances added.

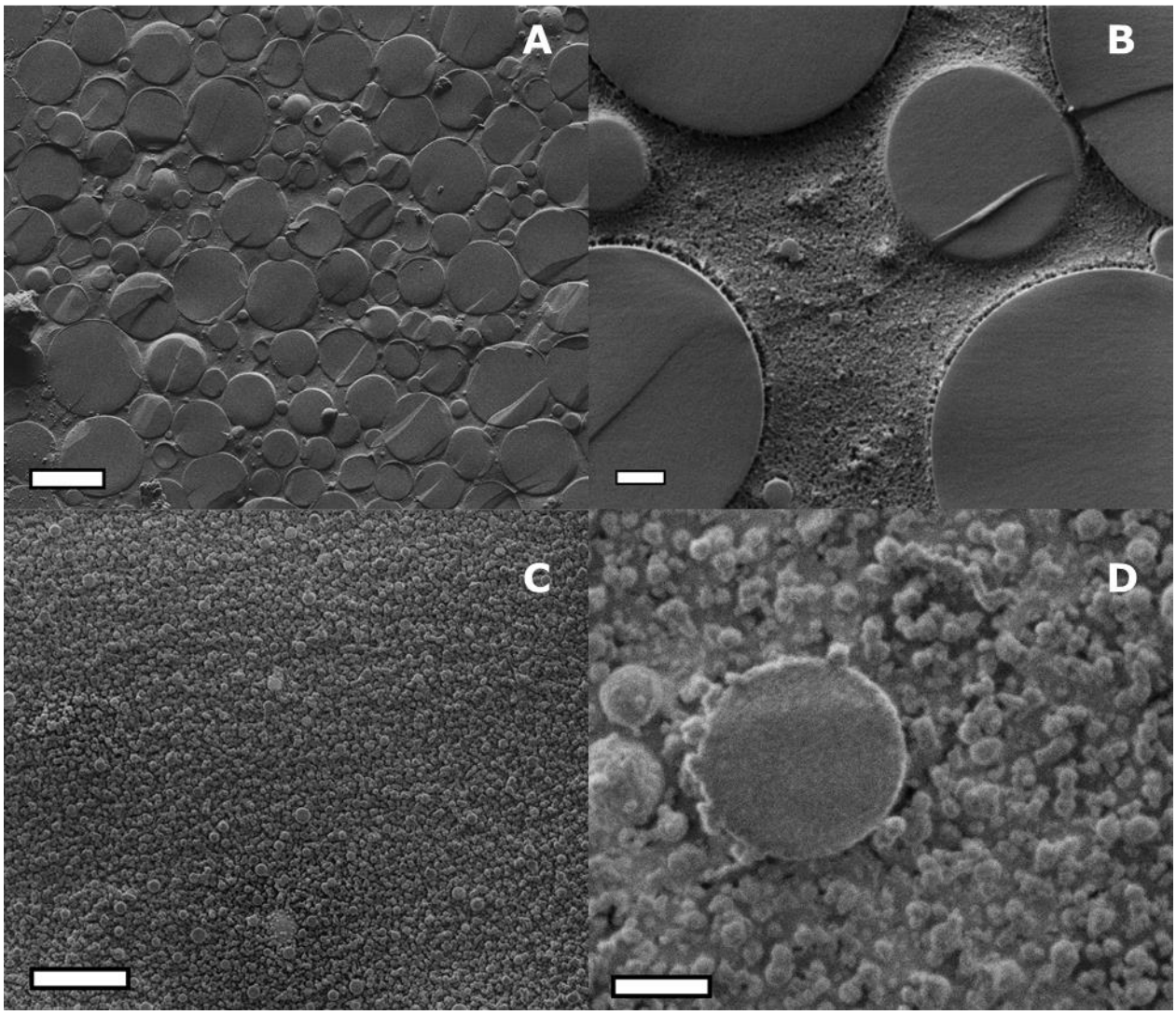

Figure 5.13. High pressure frozen samples, freeze-fractured, freeze-etched and coated with Pt at cryogenic temperatures. (A) Overview of sample 2. Fractured oil droplets with a smooth, round appearance, scale bar 10µm. (B) Oil droplets and protein between the droplets, scale bar 1 µm (C) Sample 6, Overview, scale bar 5 µm (D) Closer view of the small oil droplets in sample 6, scale bar 1 µm. It proved difficult to obtain high magnification images from these frozen samples even with the use of line integration and drift correction.

Ideally the freeze fractured cryo-SEM micrographs could be used to find the relation between the true size of the oil droplets compared to the chemical fixations. However, many of the droplets in the 10% oil emulsions are too small for quantification, see figure 5.14 where an image of freeze-substituted material has been inserted according to scale in the corner of the cryo-SEM micrograph. Smaller droplets are marked in the left image. Also, the contrast in the images from freeze fractured samples makes it very difficult to do segmentation by thresholding and the only possibility is to measure by hand.

A correction method has been suggested for cases where larger particles are covering smaller ones by subtracting the volume that is shadowed by the larger particles, but since the small droplets themselves cannot be segmented and many of them are overlapping, the method cannot be used with the freeze fractured samples (Russ 2004).

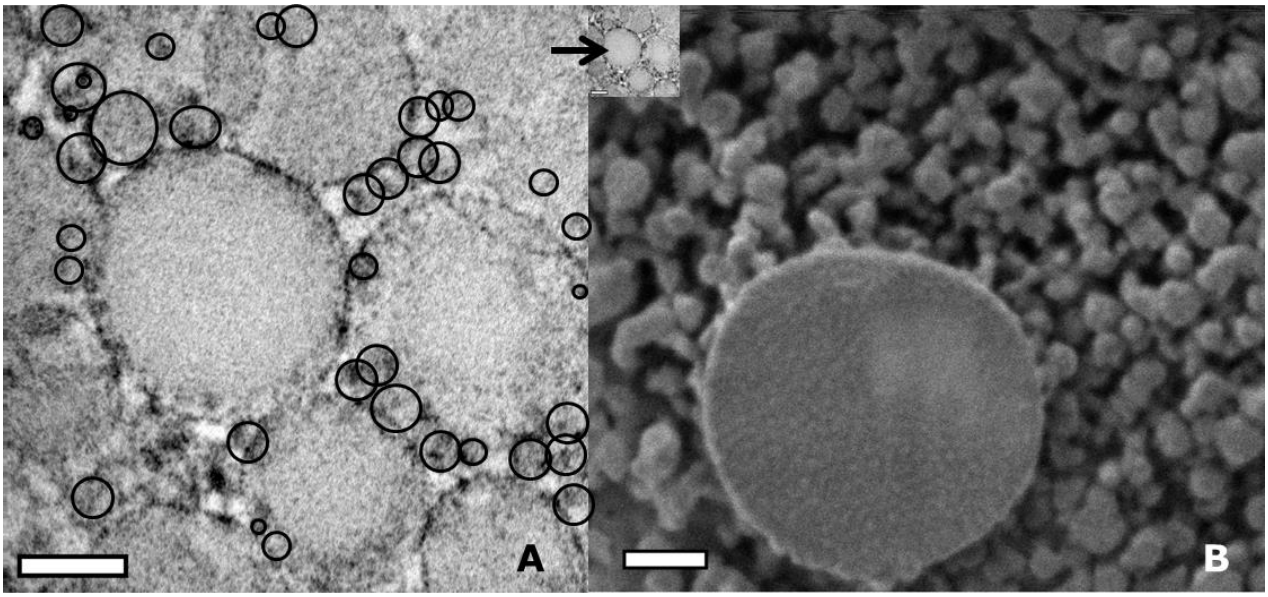

Figure 5.14. (A) Sample 6. High pressure frozen freeze substituted sample, scale bar 100 nm. (B) High pressure frozen sample imaged with cryo-SEM, scale bar 500nm.

Ideally to gain as much knowledge about a sample as possible, it is advantageous to combine several methods. This chapter fully illustrates that there are benefits and shortcomings of all methods. If not in distortion of the sample structure; then perhaps in costs, accessibility or time constraints. In our case, the latter was the case. It can take some time, trial and error to fit a method to a specified sample. Based on the results for the 10% oil and the 70% oil emulsion with NaCas, we chose to use only selected preparation techniques for the rest of the samples.

Chemical fixation in an agar mix is the method we have used that was the easiest to apply. Apart from the mixtures being prepared for fixation within half an hour for one sample, the method requires no specialized equipment like high pressure freezing and can be utilized for both small and large oil droplets. The samples are easy to handle as they contain sample throughout the small cubes and orientation of the sample is thus not an issue. Fixing the emulsions inside an agar mixture does have some drawbacks, though. First of all we are not looking at pure samples but diluted samples. Whether this is a drawback or an advantage actually depends on the scope of the experiment. For easy segmentation and measurement of oil droplet sizes, when comparing the effect of glutaraldehyde fixation, it was an advantage. But the dark aggregates made it difficult to obtain good numerical data on the size distributions and hence the effect of the concentration of glutaraldehyde. The method is well suited for visualization of the morphology of single droplets. But if we need to see the overall structure of the sample or the structure of the interface with proteins that spans the water phase the method cannot be used. The agar pockets should solve that problem but the seemingly partial collapse during dehydration or perhaps during the addition of the second layer of agar, made it difficult to use for the large droplet samples. It was a surprise for us that the method produced the best results with the 10% emulsion. The staining of the agar matrix further complicates the localization of the sample but with a few tweaks to guide localization the sample preparation should be fairly quick. And

based on previously reported results with this method we did quite well. The capillary dialysis tubes presented an even easier way of holding the samples. By simple clamping the sample inside the tubes it was as fast as preparing the agar mixes. A second advantage is that there are no agar lines present in the sample and the tubes should contain pure sample. The protein in the water phase was also contained inside the tubes. The tubes are easy to see in the resin blocks and can be positioned accordingly prior to sectioning. However, the method was only applicable for the 10% oil samples. The drawbacks of this method was that the sample tended to collapse against the tube wall which gave rise to some distorted, oval oil droplets and probably very condensed protein aggregates.

When considering the chemical fixations' effect on the droplets, it makes good sense to compare with cryo-fixed samples. In samples like these with high water content, it is important to avoid the formation of ice crystals. By using high pressure freezing we had samples that were well preserved, though maybe not vitrified, to be imaged either under cryogenic conditions or to be processed further by freeze substitution. Cryo-SEM of freeze fractured samples gave a really good overview of the structure of the samples. The method was primarily limited by the sample holder that we had built. Because of the holder, we lost quite a lot of samples. Furthermore some of the planchettes came loose which made them unstable under the electron beam and thus difficult to image. Also it could be difficult to control the temperature in cases where the planchettes were not fixed properly in the holder. For the 10% oil emulsions with their very small oil droplets, the method could not be used to image the interface or even the smallest of the droplets. Instead this could be achieved by freeze-substitution of the samples, which by far gave the best results when referring to the structure of the interface layers. Also the protein in the water phase was visible here. The method is requiring some equipment that is not so easy accessible by applying high pressure freezing and preferably a freeze substitution machine. And it requires a bit of luck for good cryo-preservation of the samples, especially the samples with high water content.

6. The micro- and nano-structure of fish oil emulsions

This Chapter will outline the effects on the structure of the emulsions made by the type of emulsifier, the concentration of the emulsifier, the type of emulsion, the production method and finally the oxidation of the emulsions.

6.1 The effect of emulsifiers on structure

To compare the effect of the different emulsifiers we have used in this study on the structure of the emulsions, we chose to use fixation in agar, agar pockets, cryo-SEM and freeze substitution. We compared three different emulsifiers, all applied in 70% oil emulsions in a concentration of 2.8%. The emulsifiers were NaCas2.8, the same as were used for the development of the different methods above, whey protein isolate (WPI) and an emulsifier containing 20% phospholipids from milk (MPL20), sample 2, 3 and 4, respectively.

6.1.1 NaCas

The structure in emulsions with NaCas is shown in figure 6.1. (A) Cryo-SEM of a freeze-fractured sample. It gives a good overview and the lack of ice crystal ghosts suggests that the freezing was good. The droplets are round unless they are distorted by close proximity to other droplets and the surfaces seem smooth. (B) shows two oil droplets; one large that spans outside of the image and one smaller that seems to be very close to, but not connected with the large oil droplet. The droplets were fixed in an agar pocket and are surrounded by agar as the visible agar lines suggest. There is a visible contrast at the edge of the two droplets which is approximately 5-8 nm thick. The small droplet edge seems to be much more angled with respect to the section as suggested by the lighter rim of the droplet. (C) shows a chemically fixed sample held in an agar matrix. Apart from the agar lines it is clear that there is a line of contrasted material on the surface of the droplet. It measures to be between 4-8 nm in thickness which corresponds well to the droplets from the agar pocket. (D) is a droplet surface preserved in freeze-substitution. It is imaged at high angle and it can be clearly seen how non-uniform the surface layer is and how it can be necessary to work on tilted samples since the layer projection thickness at its largest is roughly 90 nm while the darkest contrast line (E) is 4-8 nm which corresponds well to the chemically fixed samples. It is clear that there are small spaces between the protein strings in the water phase. The protein strings measure roughly 5-12 nm and the holes in-between are in the range of 5-12 nm for image (E) and 10-20 nm for image (D). These are subtle differences. They could suggest that the samples are affected slightly from the artifacts that could occure (see discussion in previous chapter). Or it could be that the structure of casein is not uniform. (F) depicts a closer look at the freeze-fractured surface. Here we see the same structures with small holes. Only here, the visible holes are between 20 and 80 nm. This is again another size and could suggest either a shift in dimensions from preparation to preparation (different shots in the HPM10) or clumping from the deep-etching process. As mentioned in Chapter 5, it would be useful to image the structure in cryo-TEM, either as a fraction from the sample or in a section of a vitrified sample.

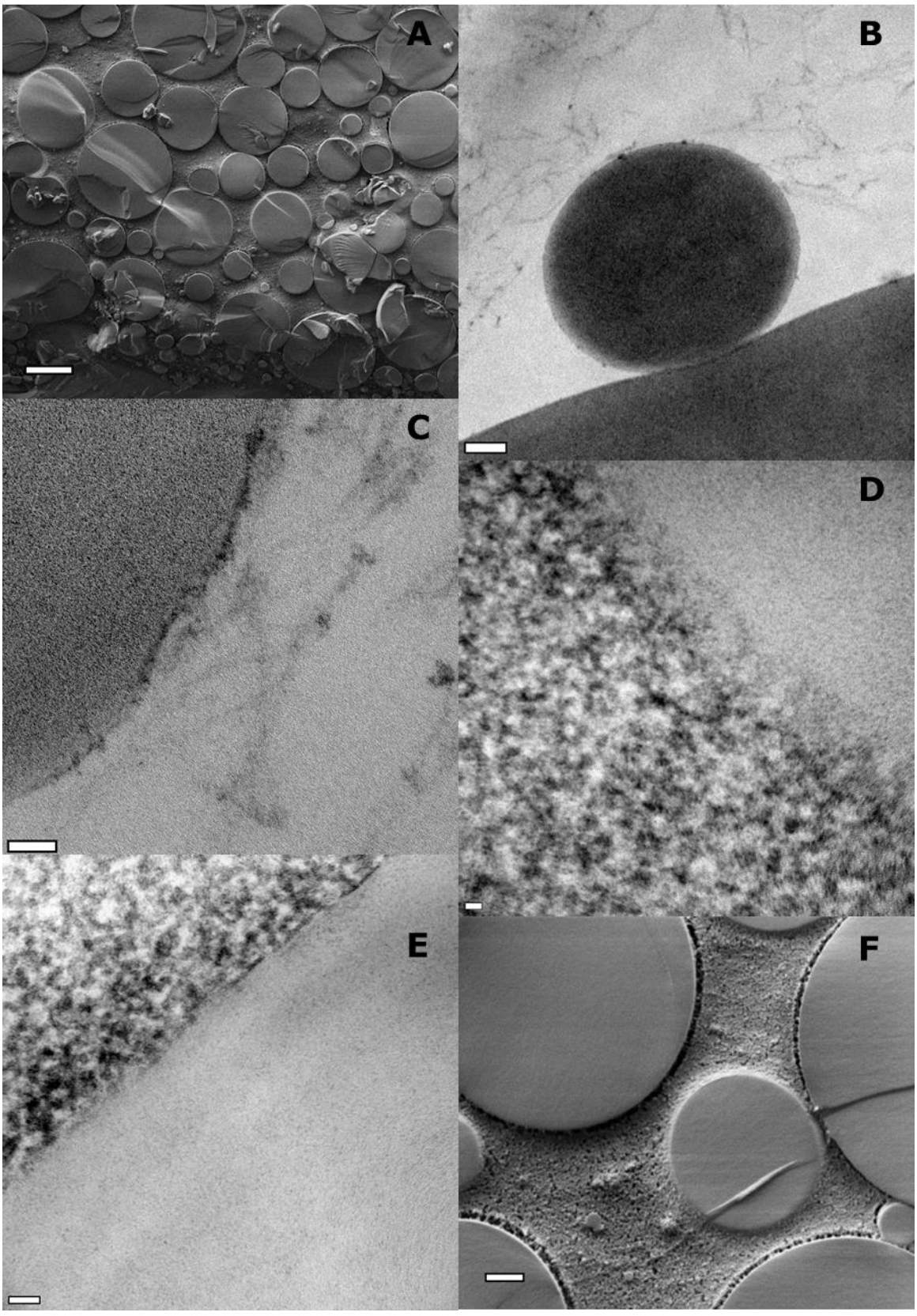

Figure 6.1. The structure of 70% emulsions with 2.8% NaCas. (A) Freeze-fracture cryo-SEM, scale bar 5um, (B) Chemically fixed sample in agar pocket, scale bar 100nm, (C) Chemically fixed sample in agar mix, scale bar 30nm, (D)

Freeze-substituted sample, scale bar 20nm, (E) Freeze substituted sample, scale bar 50nm, (F) Freeze-fracture cryo-SEM, scale bar 1um.

6.1.2 WPI

The structure of the emulsion with WPI is shown in figure 6.2. Due to time constraints we did not succeed in obtaining good micrographs from cryo-SEM for an overall image of the sample. When comparing the chemically fixed samples, the WPI layer was not very visible. Figure 6.2 (A) is an oil droplet mixed into agar which does not seem to have a well-defined, or well stained, interface. The same was the case for closer inspection of interface layers (B) where it looks like the contrast at the surface originates mostly from small dark aggregates but substantially smaller than the ones that were found in the casein samples. The high pressure frozen, freeze-substituted samples showed a stained layer, however, but the layers were of varying thickness and not iniform (C). This layer was around 10-15 nm thick. The protein in the water phase (D) was roughly around 8-12 nm thick strands which contained the same very small dark granules, and the holes between the protein 10-30 nm in diameter.

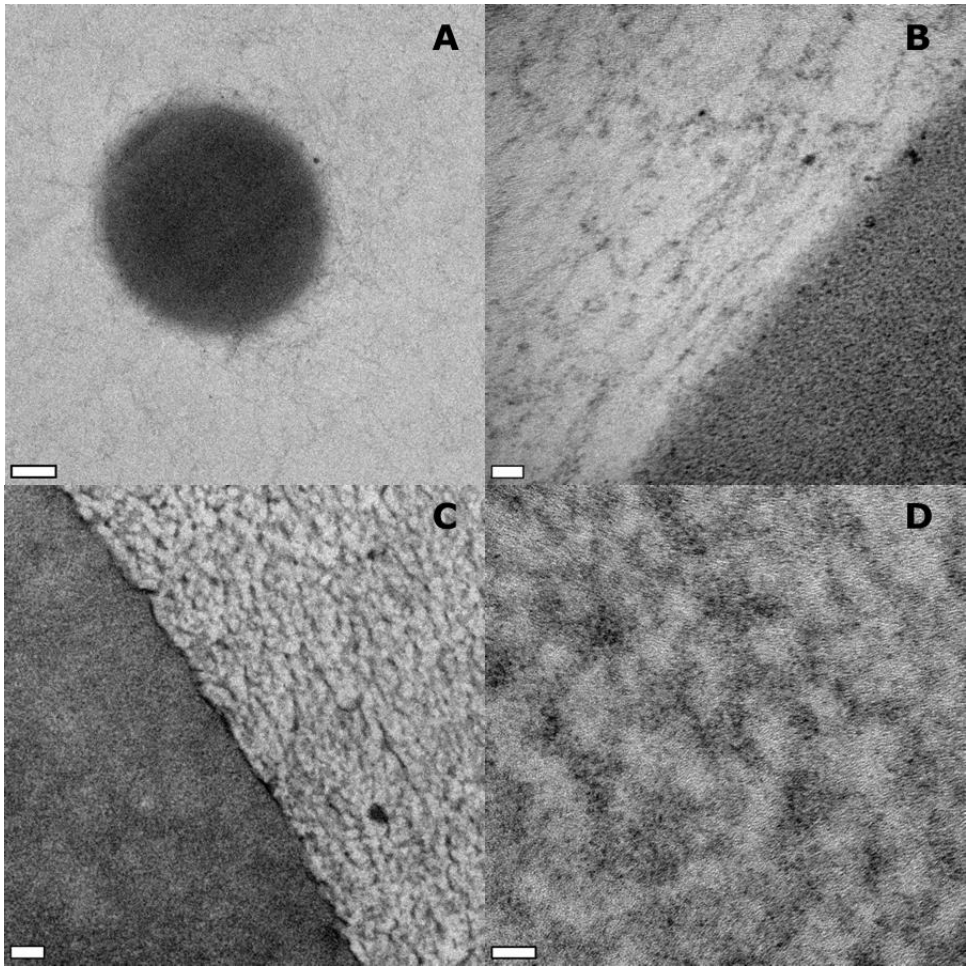

Figure 6.2 (A) Oil droplet fixed in agar mixture, scale bar 200nm, (B) Part of oil droplet (dark) and agar matrix (light with agar lines) and indistinct interface layer, scale bar 20nm, (C) High pressure frozen, freeze substituted sample, scale bar 100nm, (D) high pressure frozen, freeze substitution water phase containing proteins, scale bar 20nm.

6.1.3 MPL20

The emulsifier containing 20% milk phospholipids mixed with protein was expected to display a markedly different surface since it has recently been shown that phospholipids alter the interface and create a large degree of heterogeneity. The structure of this emulsion is shown in figure 6.3 (A) shows a whole droplet that has been chemically fixed in the agar mixture. It does have a very different morphology than the other droplets. It has a less smooth appearance than the other types of oil droplets we have seen so far. It should be noted here that we have seen droplets in all the emulsions that were not completely smooth at the surface and some were even heavily distorted, perhaps due to mechanical shear during the solidification of the agar. But it was always only a very limited number of droplets in the two previous emulsions. In this emulsion, the case was the opposite. None of the droplets appeared smooth. They did not appear distorted from outside forces neither from insufficient fixation. Rather, their surface had a bumpy, almost wavy structure. We saw layers of something that appeared to be protein-lipid mixtures at least if referring to the contrast; see Figure 6.3 (B). The micrograph depicts the edge of two oil droplets and the space between them. On the surface of both of them there seems to be extra material layered on the surface or near the surface 6.3 (C) shows the same tendency in an agar pocket fixed sample. Note the small appendices at the edge of the bumpy surface. In freeze substituted samples we saw this effect too, only here the “extra-material” was not collapsed so much onto the surface. (D) depicts an edge of an oil droplet in a freeze-substituted sample. The material seems to be a mixture of very small oil droplets/micelles and protein. The two micrographs below (E) and (F) show that the structure in high pressure frozen freeze substituted material and high pressure frozen freeze-fractured samples imaged at low temperature is quite similar. The rather unorganized water/emulsifier phase outside the droplets, which contains both small droplets and excess protein, has the same structure in both images. Finally the two images in the lowest panel (G) and (H) are cryo-SEM micrographs from high pressure frozen freeze-fractured samples. In (G) the actual surface of some larger droplets that have been exposed in the fracture are visible and we can clearly see how it is not smooth at all. (H) shows an example of something else we saw in the sections, namely that some oil droplets had smaller oil droplets attached to their surface. In the sections, it was obvious that the droplets were still separated by an emulsifying layer and thus not connected.

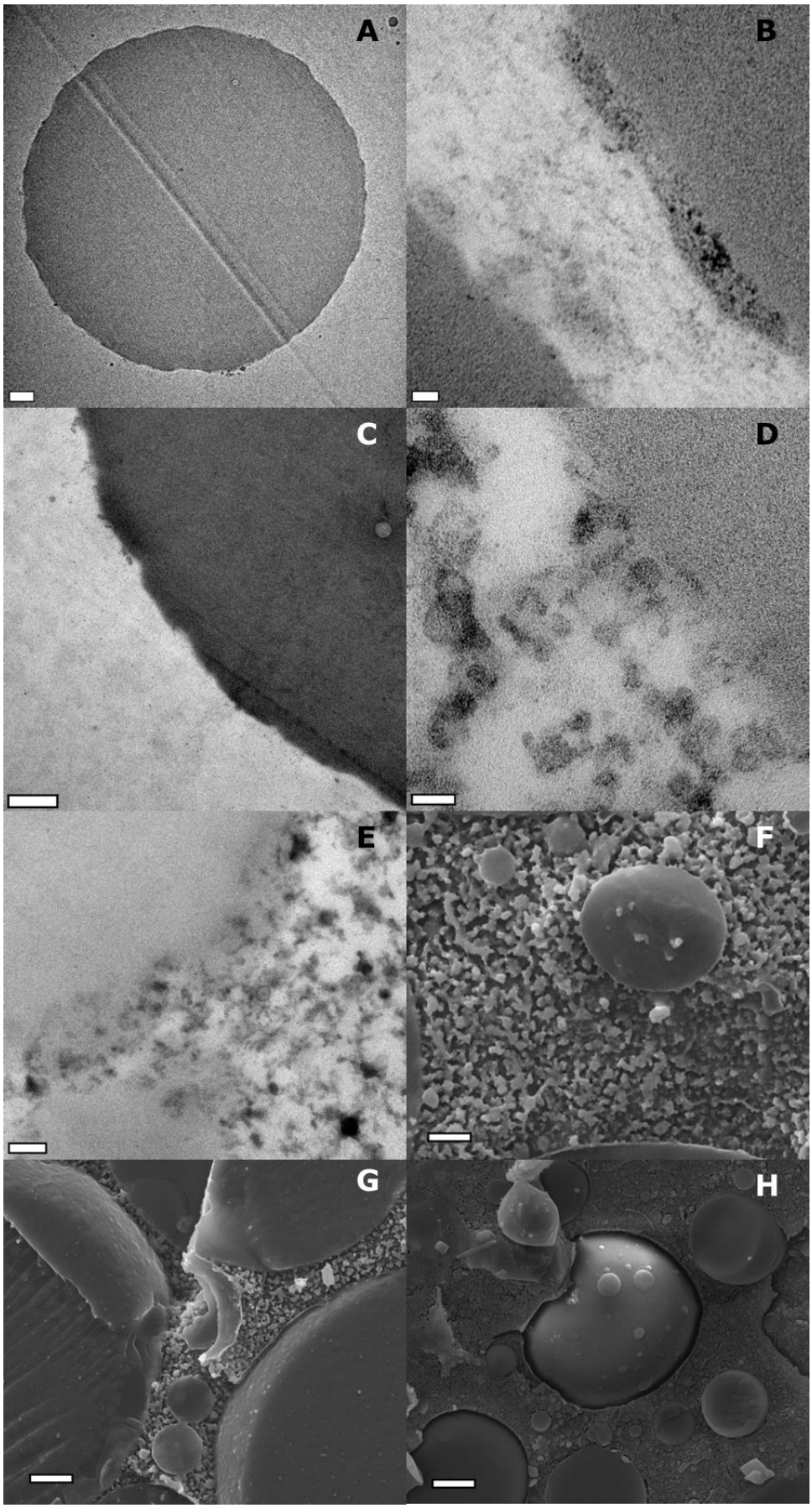

Figure 6.3 (A) Chemically fixed oil droplet in agar mixture, scale bar 500 nm, (B) two edged of chemically fixed oil droplets in agar mixture, scale bar 20 nm, (C) Chemically fixed oil droplet in agar pocket, scale bar 500 nm, (D) Edge and interface layer of high pressure frozen, freeze-substituted oil droplet, scale bar 50 nm, (E) Edges and interface layers of high pressure frozen, freeze-substituted oil droplets, scale bar 200 nm, (F) high pressure frozen, freeze-substituted emulsion, scale bar 500 nm, (G&H) high pressure frozen, freeze-substituted emulsion, scale bar 1 µm. The morphology of the samples emulsified with MPL20 are different than NaCas and Whey with bumpy surfaces and a very heterogenic water phase with many small droplets and extra protein.

It thus seems like MPL20 creates highly unstructured surfaces, perhaps with material packed into domains of tightly packed protein/lipid complexes or flocks of micelles. This was seen before in a 70% oil emulsion prepared with an emulsifier that was similar, but contained 75% milk phospholipids. Figure 6.4 depicts two micrographs of this emulsifier, which was given up early in the project because of poor oxidative stability. 6.4 (A) is a freeze-fractured MPL75 emulsion imaged with cryo-SEM. Here the unstructured effect is highly obvious with fractured surfaces appearing bumpy and with holes. Also multiple layers of material around the droplets are seen (arrows). The holes in the surface layers could be from the same reason as the so-called "etching holes" (Meyer, Richter 2001) which are holes left in the fracture plane in biological lipid bilayers at locations where the fracture passes around robust inter-membrane protein complexes. These will be pulled out of the membrane. It could be speculated that the holes in the MPL75 surfaces could originate from areas of tightly packed, more robust areas as well which have been removed in the freeze-fracture process. 6.4 (B) is a cryo-FIBSEM sample of the same emulsion. It is imaged uncoated and displays a clear SE contrast originating not from topography but from the different phases; water, phospholipid/protein and lipid. The source of this contrast is the different secondary electron emission characteristics, resulting from differences in electron flux density, which are intrinsic to the materials. Known as charge contrast imaging, the effect is normally seen in low-vacuum microscopy and can be tuned by varying the electron flux density. There is no predictive theory for this effect and it is very difficult to obtain in high-vacuum (Thiel, Toth 2005). The effect has previously been demonstrated in environmental scanning electron microscopy of (o/w) emulsions (Stokes, Thiel et al. 2000).

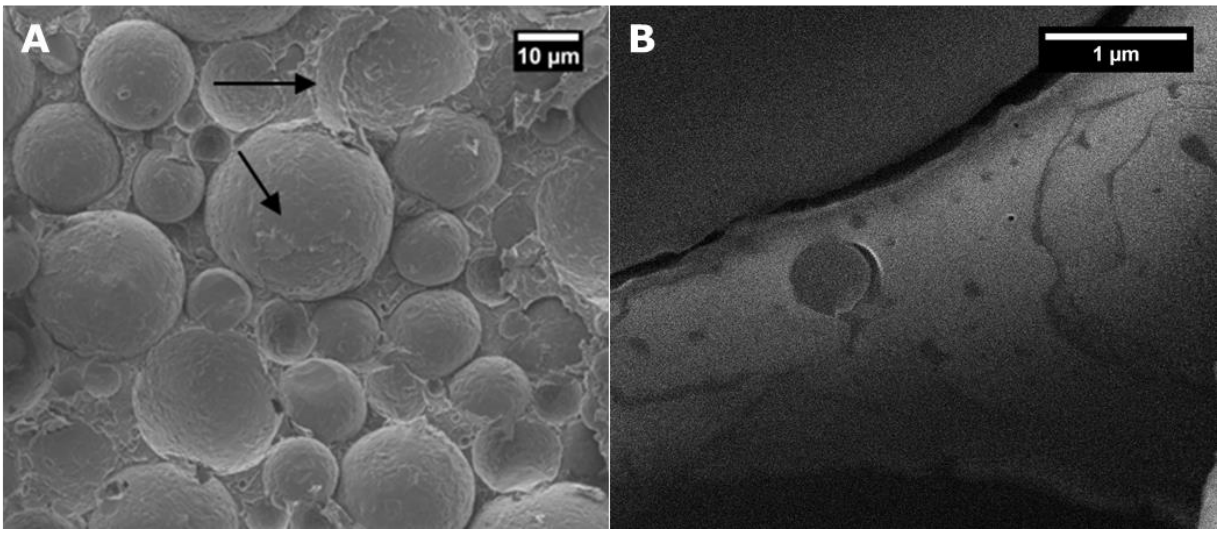

Figure 6.4 For comparison with the MPL20, an MPL75 emulsion is depicted. (A) Freeze-fracture cryo-SEM micrograph showing multiple layers and surfaces with bumps and holes, scale bar 10 µm (Horn, Nielsen et al. 2011). (B) Fresh, uncoated surface prepared by cryo-FIBSEM of the same emulsion. SE contrast enables visualization of the different phases and shows multiple layers and small droplets/micelles, scale bar 1 µm (Jensen, Horn et al. 2011).

Both the samples with protein based emulsifiers showed round droplets in the micron range, and a subpopulation of very small droplets. In some cases the protein interface at the droplets' surface was indistinct because of the angle the droplets were cut but there was a difference between the two in the fact that the surface layer was heavier stained with NaCas than WPI. A surface layer for WPI was visible in the freeze-substituted sample only. The surface layers in NaCas had a thickness of 4-8 nm. The surface layer in the WPI emulsion had a thickness of 10-15 nm, which is slightly thicker. A true value for this would require multiple samples prepared to test for reproducibility. Further, we found large differences between the protein based and the milk phospholipid containing sample. The droplets in the MPL20 had droplets of curvy and bumpy surfaces that were caused by layers of small droplets, micelles and protein other material but they were still round in their overall shape.

6.2 The effect of the amount of added emulsifier on the structure

We prepared two 70% oil emulsions with NaCas that were identical in all respects except that one contained only half of the amount of emulsifier as the emulsions that has been presented until now, namely NaCas1.4. The reason for this is that NaCas is a protein that is able to stretch or fold up according to concentration and one idea of manipulating with the surface layer would be to create a thicker layer of emulsifier. NaCas is also known to sequester prooxidants from the water phase. However, we already knew from laser diffraction that when an emulsion was prepared with less NaCas caused oil droplets to become bigger, thus creating a smaller surface area to cover by the emulsifier. We did not see increased oxidation as an effect of the larger surface area (Horn, Nielsen et al. 2011); quite the contrary, which indicated that other effects than total surface area determined the effect on oxidation. Whether there was any difference in structures at the interface at all would thus be interesting to know. We compared chemically fixed samples, CLSM, cryo-SEM and freeze-substitution to look for any noticeable differences in the surface layers.

Figure 6.5 shows an overview by CLSM stained with fluorescent dyes for protein (green) and lipids (red) together with high pressure frozen, freeze-fractured samples imaged by cryo-SEM. The top panel is NaCas1.4 and the lower panel is NaCas2.8. The difference that first catches the eye in this figure is the already known difference in the droplet sizes in the CLSM images. Concerning the cryo-SEM micrographs, in both in the 1.4% and the 2.8% there are clearly small droplets and protein aggregates/network in the water phase. Despite a factor 2 of difference in the concentration of emulsifier, we did not see any difference in the cryo-SEM micrographs.

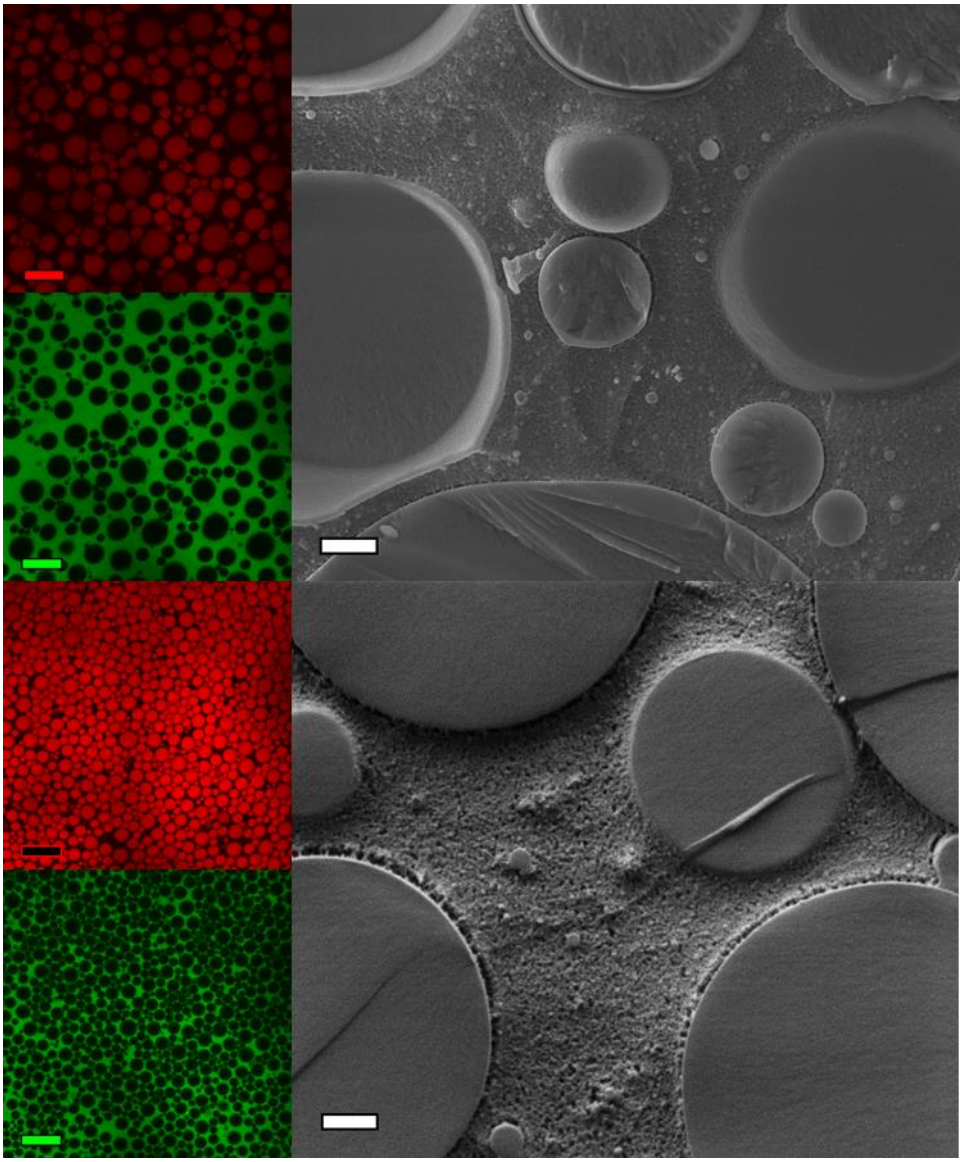

Figure 6.5 Left column; CLSM of stained emulsions, scale bars 30 µm, right column, cryo-SEM of high pressure frozen freeze fractured emulsions, scale bars 1 µm. Top row is NaCas1.4 and bottom row is NaCas2.8. The difference that is obvious between the two samples is the droplet sizes with larger droplet sizes in NaCas1.4 (left panel).

High pressure frozen, freeze substituted samples were compared as well, to look for any difference at the interface layer structure or thickness. Every droplet's surface layer was measured by hand in 10 different positions because the layers are not uniform or they might be angled differently with respect to the section in large oil droplets which gives rise to the layer being imaged from slightly different angles. Therefore we used the median number of these 10 samplings from each droplet. A total of 30 droplets were measured from each sample. Both NaCas1.4 and NaCas2.8 had median values of 7 nm. This leads us to conclude that there are no visible differences in the surface layer thickness between the two samples and that the larger amount of NaCas in NaCas2.8 is merely distributed over the larger surface area that was displayed in the CLSM micrographs in figure 6.4. It is important, however, to note that the 7 nm might not be the true

measure of the surface layer thickness, because the thickness of the surface layers depends heavily on the angle that the layer is imaged at. Layer thicknesses that were much lower than 7 nm have been measured (see below) and it is very likely that the layers are thinner than 7 nm.

One argument for additional enquiries might be the possibility that the surface layer thickness itsef is not affected but the proteins might be arranged differently in the water phase close to the surface. For this reason we inspected tilt series of single droplets to see exactly how the proteins were localized, see figure 6.6. The top panel displays a high pressure frozen, freeze substituted droplet from NaCas1.4 and the bottom panel displays a droplet from NaCas2.8 prepared in the same way. In both cases the thickness of the interface when tilted to the thinnest appearance was between 3-6 nm. There was no noticeable difference between the organization of the protein near the surface in the two samples compared to the surroundings. The slight differences in the organization of protein in the two samples are much more likely to come from minor differences in the freezing and of course the difference in scale bars. Again, the reader can attempt to cross the eyes and focus on the middle micrograph plus one of the adjacent ones to obtain a stereo image of the sample from each side. (Note: Normally the angle between such images should reflect the angle between the eyes at viewing distance, i.e. normally 10°-15°. These images were not meant as stereo micrographs and the angles between them are 40° so it will strain the eyes to see the 3D image).

In both cases the protein network thickness was measured and found to have a median of 13 nm. This did not vary between the samples either.

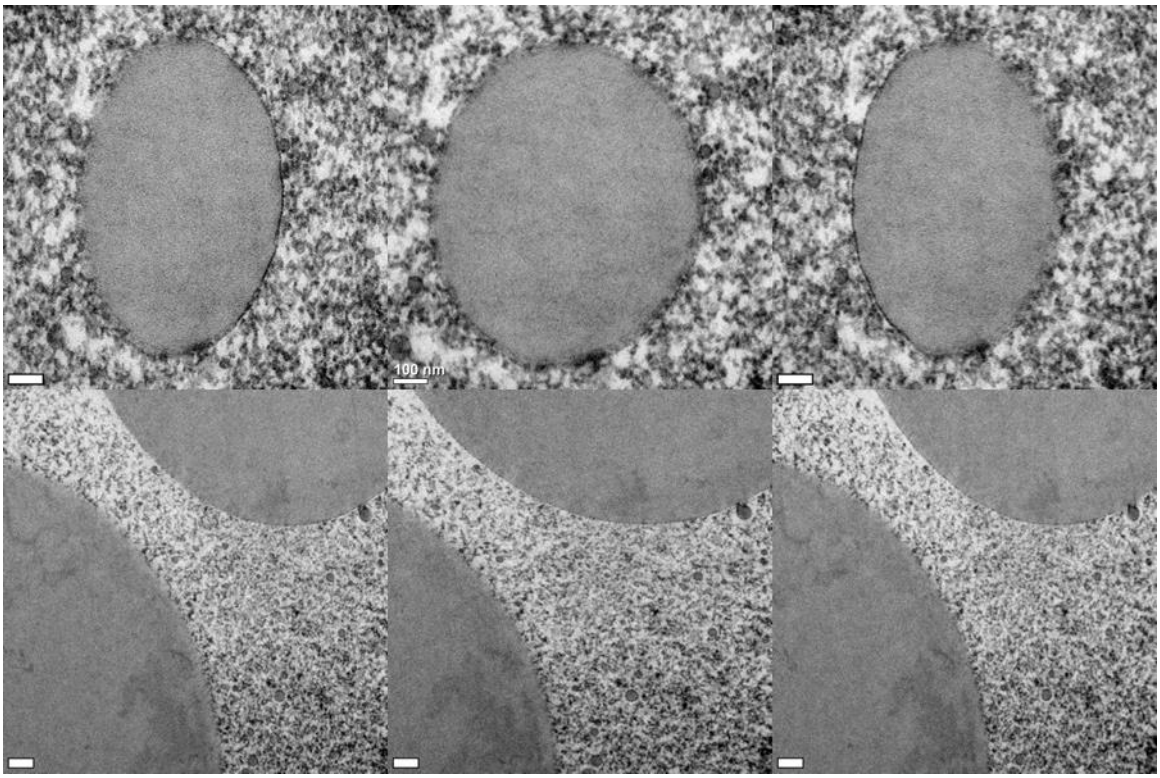

Figure 6.6 Tilting of samples with droplets from either 1.4% or 2.8%. The thickness of the droplets' surfaces at their thinnest are between 3-6 nm. Both panels +40°, 0° and -40°, scale bars 100 nm & 200 nm.

6.3 The effect of emulsion type on structure

We compared two samples containing NaCas. One was the 70% oil emulsion that contained 2.8% NaCas i.e. sample 2 and the other was the 10% oil emulsion that contained NaCas, sample 6. These are the emulsions that were also used to assess the different preparation methods. The emulsions are different in several aspects. First of all, the emulsions have very different oil content, 70% and 10%. Secondly, the emulsions are prepared by different equipment that is suitable to prepare the respective emulsion type. The 70% emulsions were prepared by Stephan mixer and the 10% oil emulsion was prepared by using a microfluidizer. Furthermore, the droplet sizes in the emulsions, measured by DLS were very different; D(3,2)=7.5 µm for sample 2 and D(3.2)=135 nm for sample 6. The difference in oil droplet size and production pressure is therefore dramatic and a comparison serves only to show the behavior of sodium caseinate in two very different emulsions. Figure 6.7 displays the structure of the two types of emulsion. (A) shows parts of three large droplets (sample 2) and some smaller droplets in the space between them. (B) shows a close up on the protein in the water phase (sample 2). Again, these resemble the native casein micelle. (C) shows the overall structure of the 10% oil sample. As has already been mentioned elsewhere, the droplets are overlapping and lying close to each other and smaller droplets are nested in the space between the larger droplets. (D) shows a close-up where the proteins in the water phase are visible. By comparing the excess protein in (B) to the micrograph in (D) it is obvious that there is a difference in the way the extra protein is dispersed in the water phase. In the micrograph (D) it seems that the protein is aggregated loosely into micellar structures of approximately 5-20 nm. This could very well be a structural difference in casein after application of high pressure. High pressure applied to native casein micelles (100-200 nm) have been shown to dissociate them as shown by light scattering and atomic force microscopy (Gebhardt, Doster et al. 2006). In case of pressures below 240 MPa the casein is dissociated into mini micelles of approximately 10-20 nm which relocates into denser 80-120 nm structures containing less calcium after pressure release. And with pressures above 280 MPa the native micelles dissociate into their monomers which relocate to mini micelles of 25 nm devoid of calcium phosphate after pressure release. Calcium phosphate is necessary for the assembly of the native casein micelle and is absent from our emulsifier. So it could very well be that the protein structures we see are such mini micelles that are stable after pressure release in the absence of calcium phosphate. It would be worth to explore further the structural reaction of casein to pressure.

The interface thickness was measured in the 10% oil emulsions the same way as in the 70% emulsions, the median of 10 samplings per interface, and a total of 30 droplets were measured. The median thickness of the interface was measured to 4-5 nm which is only slightly smaller than the 70% oil emulsions with their 7 nm which could be smaller. It is difficult to really assume that the surface layers are smaller in the 10% emulsion, both because of uncertainty in the measuring method and because a lot of the droplets that were measured in the 70% emulsions were actually in the lower size range in these emulsions. This as a consequence of the data available where the large droplets often had a large angle in the sections and it would have needed tilting of each droplet to find the good angle and hence sufficient contrast. Hence, a lot of the droplets that were measured in the 70% emulsion were actually quite small so they could be

contained in the image. To really test the hypothesis whether the droplet size is dependent on the droplet size, a larger dataset with data for large, tilted droplets is needed.

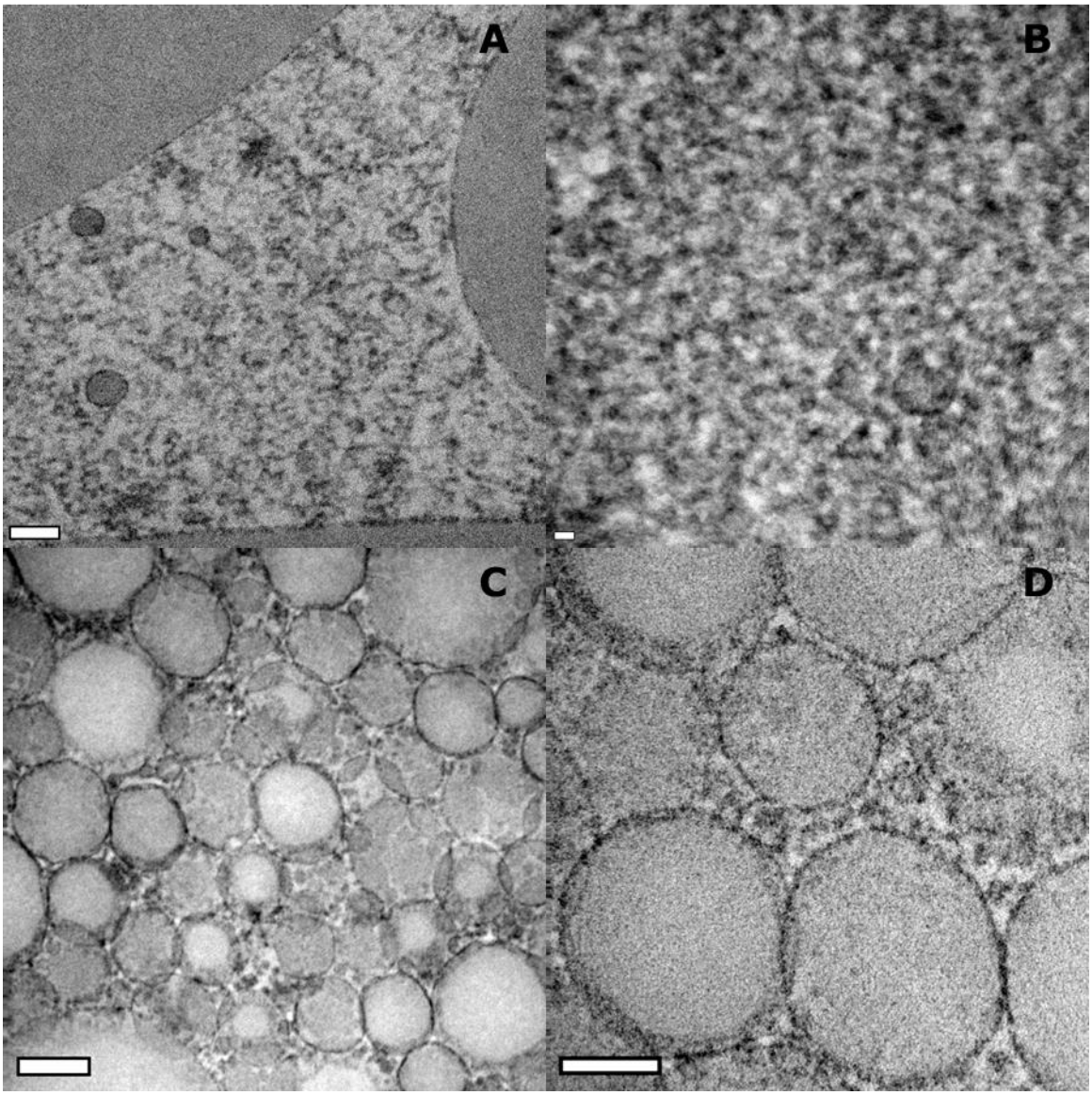

Figure 6.7 (A) High pressure frozen, freeze substituted 70% emulsion oil droplets, scale bar 100 nm, (B) High pressure frozen, freeze substituted protein in the water phase of an 70% emulsion, scale bar 20 nm, (C) High pressure frozen, freeze substituted 10% oil emulsion, scale bar 200 nm, (D) high pressure frozen, freeze substituted oil droplets and protein aggregates, scale bar 100 nm.

6.4 The effect of production method on structure

In a study about differences between emulsions containing two different emulsifiers (NaCas and WPI) and each processed with two different equipment types; a microfluidizer and a two-valve high-pressure homogenizer (Horn, Nielsen et al. 2012) we tested whether there was any morphological differences in the

structures. Studies have previously reported different organization and localization of milk proteins as a consequence of the equipment type (Dalgleish, Tosh et al. 1996).

Cryo-TEM was applied to visualize these emulsions with their small oil droplets. The images are shown in figure 6.8. Samples given in parenthesis is from the paper (Horn, Nielsen et al. 2012). The top row are NaCas emulsions prepared with either microfluidizer (sample 6 (NaCas_M), left) and with the two-valve high-pressure homogenizer (sample 8 (NaCas_H), right) and the bottom row are whey protein emulsions (sample 7 (WPI_M) and sample 9 (WPI_H), respectively). The oil droplets appear as well-defined round dark objects on a lighter background which is the amorphous water phase. The thick dark bands in the micrographs are the lacey carbon film. It can be seen that the oil droplets are perfectly round shaped, and positioned in the vitrified film that spans the holes of the lacey carbon according to size with the largest oil droplets closest to the lacey carbon and the smallest droplets closest to the center. The distribution of the oil droplets according to size is a consequence of the constraints caused by the geometry of the vitrified liquid film which is a meniscus with the thickest part at the edge of the carbon film. The dark grey areas in the middle of the film are probably lipids forming diffuse droplets on the surface of the liquid film after blotting. Droplet sizes were similar in all four emulsions. The oil droplets were non-aggregated and especially for oil droplets emulsified with NaCas the droplets all seemed to be evenly distributed in the film. Distances to nearest neighbors were measured by hand. This included an evaluation of each oil droplet to identify which oil droplets could be described as neighboring. NaCas droplets had mean distances of 28 ± 13 and 24 ± 12 nm for sample 6 (NaCas_M) and sample 8 (NaCas_H) emulsions (A and B). On the contrary, in WPI emulsions the droplets were located in a less ordered way with relatively more varying distances between the oil droplets. Mean distances were 19 ± 19 and 21 ± 17 nm for sample 7 (WPI_M) and sample 9 (WPI_H) (C and D). Differences in the distances were found to be statistically significant between emulsions with different emulsifiers ($p = 2E\text{-}12$ between sample 8 (NaCas_H) and sample 9 (WPI_H); and $p = 2E\text{-}15$ between sample 6 (NaCas_M) and sample 7 (WPI_M) and the distances were significantly smaller for WPI emulsions. We found no statistically significant difference between production method in NaCas emulsions ($p = 0.3$). There was, however a significant difference between sample 9 (WPI_H) and sample7 (WPI_M) ($p = 9E\text{-}4$). (Horn, Nielsen et al. 2012). This result correlated with the findings that the oxidative stability was different between the emulsifiers and between the two emulsions with WPI, but not between the two emulsions with NaCas. Visual inspection of micrographs gave no indication as to an explanation for the phenomenon but casein should be negatively charged at pH7 which might explain this behavior. Cryo-TEM was a good technique to visualize the oil droplets in their close-to-native state. We did not, however, obtain information about the structure of the interface layer or the protein in the water phase. The difference in mass between lipid and proteins was apparently not large enough to allow for contrast between the two in bright field TEM.

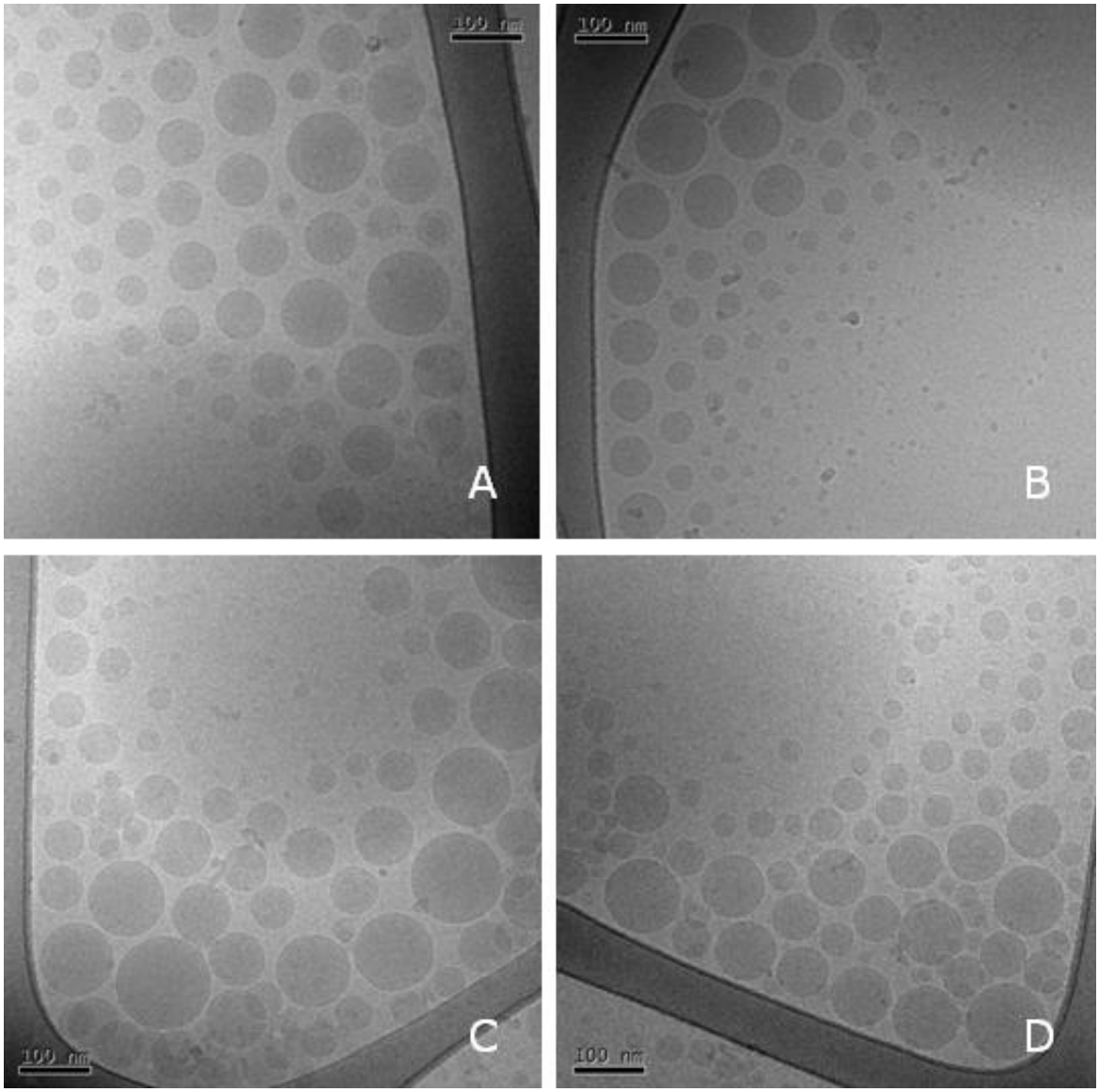

Fig. 6.8 Cryo-TEM images: (A) sample 6 (NaCas_M), (B) sample 8 (NaCas_H), (C) sample 7 (WPI_M) and (D) sample 9 (WPI_H). Scale bars=100nm. In the emulsions that contained NaCas, the oil droplets were seen to localize with a distance between them that seemed to be the same throughout the vitrified film suggesting some sort of mutual repelling; whereas the droplets in the WPI emulsions were located with varying distances including closely located and overlapping droplets.

We also fixed the emulsions in capillary tubes. Sample 9 (WPI_H) was for some reason difficult to fix chemically. When fixed in agar-mixes, the cubes failed to solidify and fell apart and the sample seemed to be missing from the other matrices when the samples were prepared. The only images that we managed to acquire were from a freeze substitution of the sample and it looked distorted and disintegrated. We do not know whether it is due to the sample proteins being difficult to fix or if it is just a coincidence that all attempts to image this sample failed. In the cryo-TEM images we did see a significant difference in the distances between this sample and the WPI emulsion that was prepared in the microfluidizer and there was

a difference in the oxidative stability (Horn, Nielsen et al. 2012). Hence it would be interesting to obtain images from this sample.

Figure 6.9 displays the other three emulsions (A+B) sample 6 (NaCas_M), (C+D) sample8 (NaCas_H), (E+F) sample 7 (WPI_M). In sample 6 (NaCas_M) the droplets had the same structure that we have seen throughout the result section, with condensed black particles on the surface. The same particles were seen in sample 8 (NaCas_H), but here they seemed to form chains and thus interact with each other instead of being attached to the surface of the oil droplets only. The same effect was seen in agar mixed samples. Preferably, we would like to confirm the existence of such chains by other methods such as freeze substitution. It has previously been shown that emulsification process with a two-valve homogenizer is gentler than that of the microfluidizer (Dalgleish, Tosh et al. 1996) and it could be that the chains are a result of a slightly less disrupting emulsification compared to the totally disrupted small structures in sample 6 (NaCas_M). The emulsion with WPI sample 7 (WPI_M) was slightly different in the structure. There seemed to be a population of larger oil droplets and they seemed to be associated with smaller oil droplets on the surface. The droplets in both NaCas and WPI emulsions were measured by dynamic laser diffraction to be similar but as mentioned earlier there is an underestimation of small populations of larger sizes by such methods (Benita, Levy 1993) and this might give a wrong interpretation of the distributions overall which is why microscopy is needed as a supplementary technique (Preetz, Hauser et al. 2010).

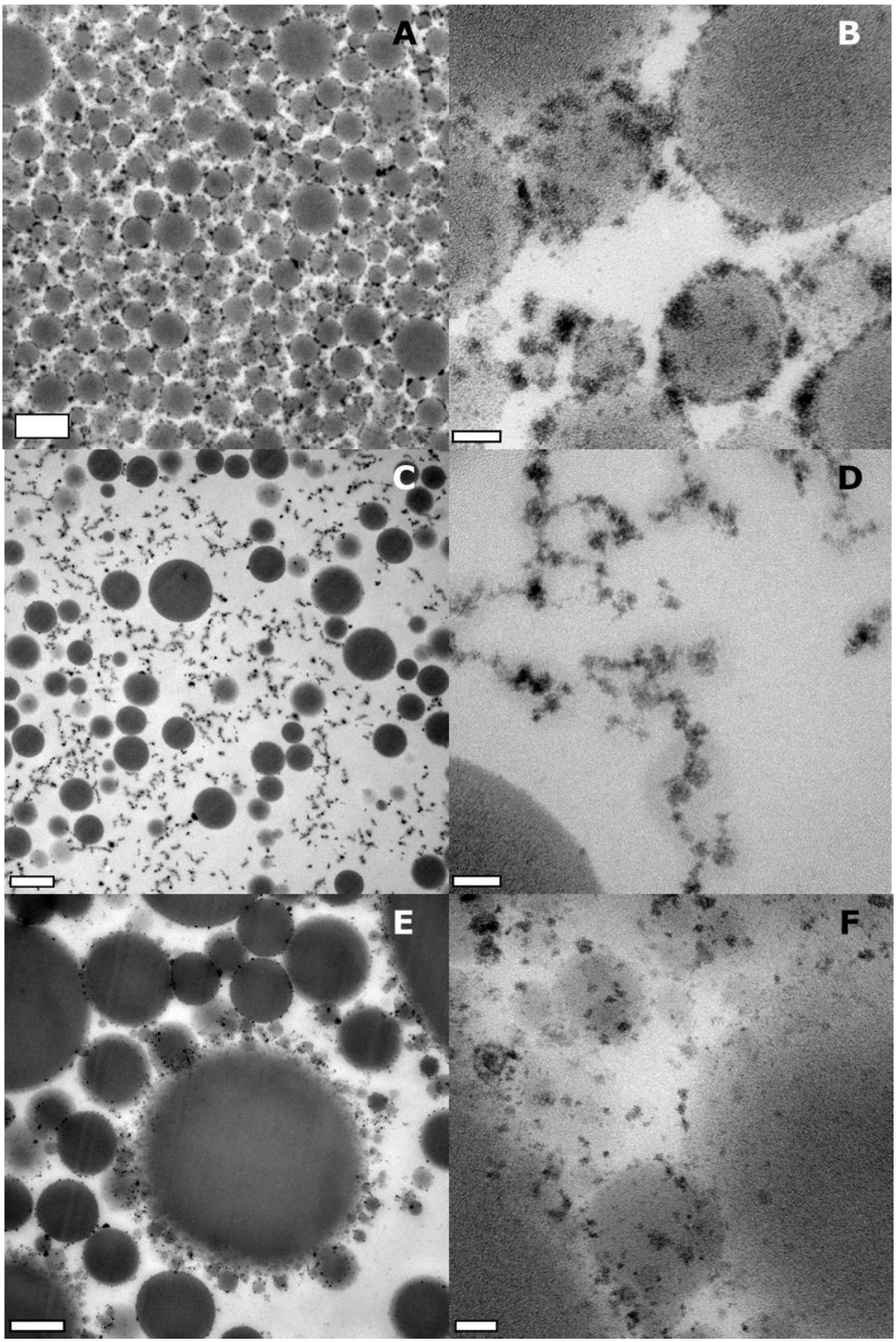

Figure 6.9. (A)+(B) sample 6 (NaCas_M), scale bar 500 nm and 50 nm, (C)+(D) sample 8 (NaCas_H), scale bar 500 nm and 50 nm, (E) sample 7 (WPI_M), scale bar 500 nm and 50 nm.

6.5 The effect of oxidation on structure

The samples were stored at 4 °C for 40-42 days and prepared for electron microscopy to be compared to micrographs of the fresh samples. This was done to assess whether there was any notable differences in the morphology of oxidized samples. We chose to fix the samples chemically in agar mixes for an assessment of their appearance. The oxidized samples did show some morphological differences to the fresh samples. Where the fresh samples (apart from MPL20 which had some extra surface material of varying thickness) in most cases had smooth, round droplets, the oxidized samples had wavy and bumpy surfaces. As mentioned above, the fresh emulsions did contain a few droplets with wavy and bumpy surface, but only in a few cases. The opposite counted for the oxidized samples where the majority of the droplets that were imaged had wavy and bumpy surfaces, while only a few maintained the smooth surface.

Chemical fixed 70% emulsions mixed with agar are shown in figure 6.10 below. (A) NaCas1.4, (B) NaCas 2.8, (C) WPI and (D) MPL20.

MPL20 displayed a similar morphology to that of the fresh sample except that the surface was even more distorted than in the fresh samples.

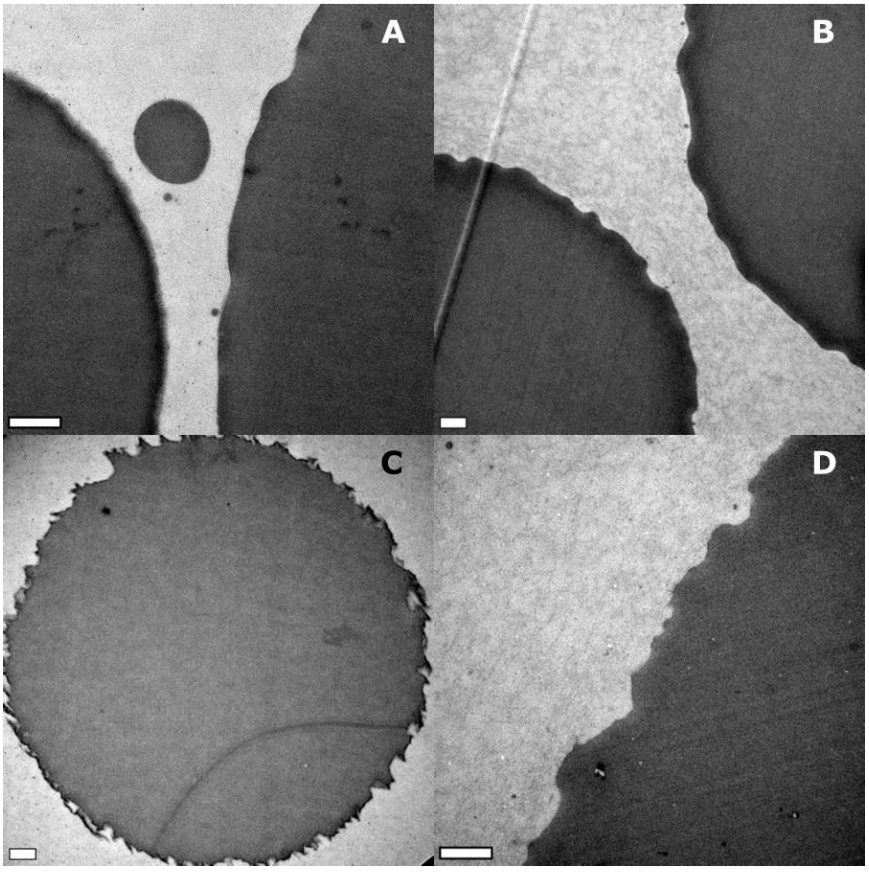

Figure 6.10 (A) Chemical fixed sample from 70% emulsion with NaCas1.4 (B) Chemical fixed sample from 70% emulsion with NaCas2.8 (C) Chemical fixed sample from 70% emulsion with whey protein (D) Chemical fixed 70% emulsion with MPL20. All scale bars 500 nm.

For the 10% oil emulsion it could be speculated that the close proximity of the droplets or the different protein dispersion in the water phase would lead to a different appearance, but at least in the chemically fixed samples, the result was the same as for the high fat emulsions. Figure 6.11 shows a chemical fixed sample from the 10% NaCas emulsion. The droplets have the same wavy and bumped surfaces and the effect of oxidation is even more clear in this sample since we did not see any droplets with morphology like these in the fresh samples.

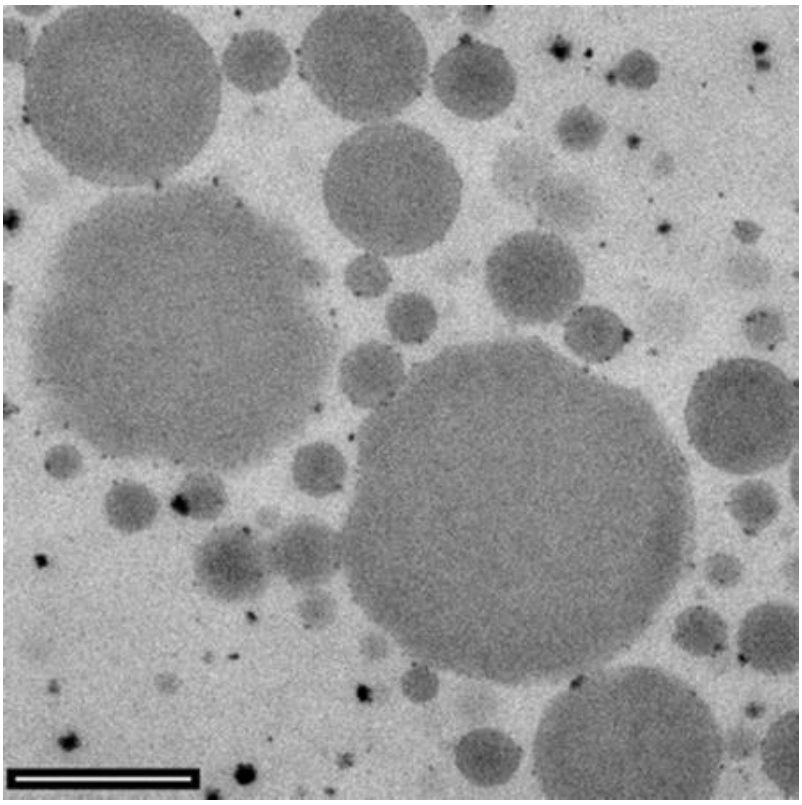

Figure 6.11. Chemical fixed oxidized sample 6, 10% emulsion with NaCas, scale bar 500 nm.

What exactly is causing this distortion of the surfaces is unknown. It has been shown that the proteins at the interface layers are degraded during oxidation and that this is initiated even prior to lipid oxidation (Berton, Ropers et al. 2012). Hence it could be that the distorted appearance of the oxidized droplets is because of a degraded surface layer. As was shown in Chapter 5, section 5.1.1, it is necessary with sufficient glutaraldehyde fixation of the protein layers for a well-preserved sample. This could be interpreted as a need for a minimum of fixed surface protein for preservation of the oil droplets in the chemical fixations and indicate that this layer is no longer sufficient when the protein layer has been degraded by oxidation. It could also be that the modified proteins at the interface react differently with the fixatives. OsO_4 can distort lipid bilayers by undulation and introduction of sharp angles in freeze substitutions (Matsko, Mueller 2005) and perhaps the distribution of lipids and proteins at the surface are changed in oxidized samples, leading to an altered reaction with OsO_4. High pressure freezing followed by freeze substitution and comparing protocols with and without OsO_4 would be helpful in solving this question. We subjected the

oxidized sample 2 to elemental analysis with STEM EDX to see if we could detect any difference in the components at the surface. But a line scan showed exactly the same results as for the fresh oil droplets from the same sample (section 5.1.2). Results are shown below.

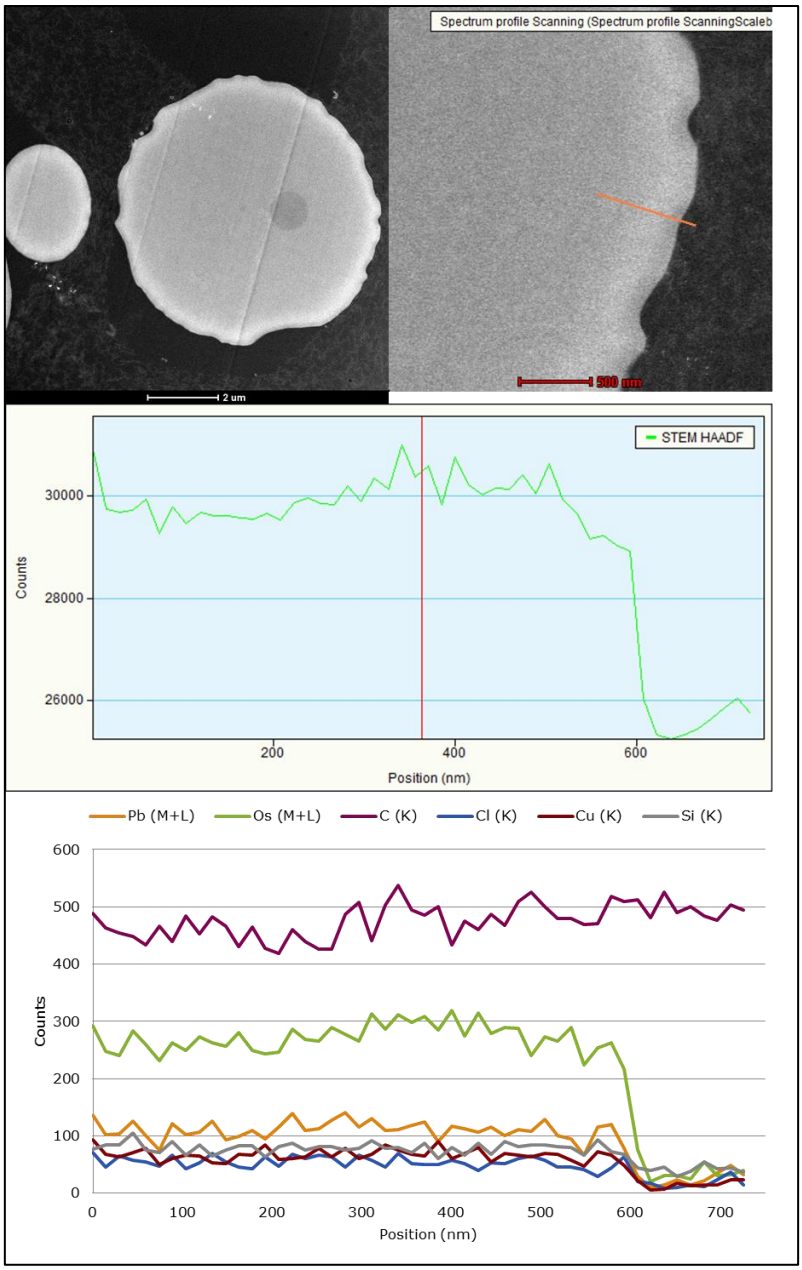

Figure 6.12. Line scan EDX analysis in an oxidized sample. Again, the edge of the droplet is slightly denser, mostly ascribed to osmium.

7. Conclusion and outlook

The present chapter outlines the most important findings in this thesis work in section 7.1. There were, however, a number of open questions and hence an array of further experiments that time and equipment restrictions did not allow us to perform. These are outlined in section 7.2 together with a general outlook.

7.1 Conclusions

We have compared a number of methods which can be applied to the structural characterization of (o/w) emulsions. A number of different matrices were evaluated for holding the liquid samples during chemical fixations. Agar mixtures were easy to work with and were well suited for morphological assessment of large oil droplets. The method also proved to be very useful for automatic and high throughput segmentation in image processing for statistical analysis of small droplets sizes. The images of the surface layers were slightly confusing due to interaction with lines from the agar matrix, which was shown to be of similar thickness in all fixation concentrations. Both methods for retaining the sample in a fixative-permeable container during fixation, i.e. agar pockets and capillary dialysis tubes resulted in slight segmentation of the sample. This was expected from the literature but the samples were not greatly distorted. With the emulsions being liquid at the time of fixation, the lipid droplets had still maintained their shape. When accounting for the aggregation, the methods gave good results with 10% oil droplets. The pocket method must be developed further for 70% samples.

Importantly, it was shown that emulsion oil droplets shrink as a consequence of chemical fixation with glutaraldehyde and that this process is related to the concentration of glutaraldehyde. There was a large shift between 2% and 3 % glutaraldehyde in these experiments, both in shrinkage of small droplets and in preservation of the protein interface layer for large droplets. And compared to freeze substitutions of the same sample, the droplets were considerably smaller in all concentrations of glutaraldehyde fixations.

Dark aggregates which were identified in the chemically fixed samples and were assumed to be aggregated protein, were composed of small, ~0.5 nm granules stained by osmium and lead which assembled into larger aggregates.

Furthermore, it was shown that the staining of emulsion droplets with heavy metals follows a similar pattern for osmium and lead, exemplified by the fact that when there is an enhanced contrast from lead close to the droplet surface, the same is true for osmium, which was expected to stain mostly the unsaturated lipids.

A tomogram created in HAADF STEM of a 10% emulsion sample prepared by high pressure freezing and freeze substitution confirmed that in the nanoemulsions, the droplets are tightly packed with smaller particles nested between the larger droplets. Furthermore, the tomogram indicated that even after long post staining times (see Chapter 8) the stains did not penetrate all the way through the sections, indicating that for future staining of these samples it might be necessary to aid the staining process with elevated temperature and ethanol.

Freeze substitution of high pressure frozen samples was shown to give insufficient results when the media consisted of OsO_4 in methanol only. However, addition of glutaraldehyde and uranyl acetate (Müller, Marti et al. 1980) preserved emulsion samples of both 10% and 70% oil satisfactorily to a degree that made it possible to preserve even the liquid suspensions of proteins in the water phase and provided information about the structure of the proteins at the interface and in the water phase.

The characterization of the structure of casein in emulsions has been attempted in a wealth of studies, often using indirect methods such as laser scattering in combination with latex particles or enzyme digestion. Here we show directly the structure of sodium caseinate and its behavior in emulsions as a consequence of the processing. In emulsions that were prepared by a blade mixer, the structure resembled that of the native casein micelle except that the caseins were not assembled into the native casein micelles as they are in the presence of calciumphosphate. Rather they formed a continuous and probably dynamical structure throughout the water phase. That this could be the potential structure and not mere artifacts from the freezing and freeze substitution is supported by a recent cryo-tomography study of the native casein micelle (Trejo, Dokland et al. 2011). Additional experiments must be carried out to support this conclusion. In emulsions that were subjected to high pressures in a microfluidizer, the caseins seemed to form mini micelles of ~30 nm, as suggested by the high pressure frozen, freeze substituted samples. It could thus very well be, that sodium caseinate, without the calcium phosphate that is necessary for the formation of the casein micelle, is affected to form mini micelles at lower pressures than was shown to cause these structures in milk (Gebhardt, Doster et al. 2006).

Furthermore it was shown that the amount of casein does not change the surface structure to any observable degree at the nano-scale. Rather, all the extra protein seems to be located in the water phase when comparing two emulsions with a factor 2 in difference between emulsifier concentrations; this can explain the higher oxidative stability of NasCas2.8 to NaCas 1.4 despite the smaller oil droplets, and hence larger surface area in NaCas2.8. Median values of 7 nm thickness were measured but thicknesses as low as 3 nm were observed. The content of metal chelating NaCas in the water phase thus seems to be the explanation for the high resistance of this emulsion to oxidation, which was even shown to exceed that of neat oil (Horn, Nielsen et al. 2011). And finally it was shown for casein that emulsion droplets in thin liquid films tend to separate over the largest possible area with very similar distances to nearest neighbors as observed by cryo-SEM, clearly indicating repulsion between the droplets. At pH7 the droplets should be negatively charged, which could possibly explain the behavior as electrostatic repulsion.

WPI emulsions were seen to form slightly thicker layers at the surface than caseins, perhaps containing small clusters.

Also, emulsifiers containing milk phospholipids were shown to form a wide variety of structures both on the surface of the droplets and in the water phase. The structures consisted of mini droplets, micelles and layers and patches of what seemed to be densely packed protein and phospholipids. In the case of high content of phospholipid, i.e. 75% of the total emulsifier content, multiple layers surrounding the oil droplets were seen, as demonstrated by unique fracture profiles in freeze fracture cryo-SEM and charge contrast imaging in high vacuum after cryo-FIB milling.

Finally it was demonstrated that oil droplets in oxidized samples display highly distorted surfaces after chemical fixation. Whether this is their true structure, the effect of degradation of the protein layer during

oxidation and thus altered fixation, or perhaps other reactions with the fixatives, is not known at the present time.

7.2 Outlook and future experiments

It is obvious from the comparison of the different methods applied in this work that the result of a microscopy structure analysis depends very much on the method. And that the better the structure of interest is preserved during preparation, the closer to reality the result will be. Recently, near-atomic resolution of low symmetry protein complexes, i.e. without the need for alignment and classification of huge datasets of symmetric particles and fitting of atomic models that is normally applied in single particle EM, has been achieved (Li, Mooney et al. 2013) and high resolution cryo TEM imaging of native, hydrated molecules is predicted to open a whole new array of microscopy studies. There are still applications for other methods, though. In particular, it remains essential to have methods that cover a range of scales larger than near-atomic resolution. Even though classical preparation techniques induce artifacts, as long as they are recognized and interpreted correctly, the micrographs of such samples provide already much information. It could be argued that if a clear relation between the appearance of samples prepared by different methods could be developed, e.g. by multivariate data analysis and modeling, then classic preparation techniques could effectively be related to the outcome of advanced and sophisticated techniques either as a bridge between different microscopy types or in cases where advanced equipment was not available. Developing and publishing such models could even democratize the accessibility to advanced methods. This could for example be applied to predict the reaction of different sample types to e.g. chemical fixation numerically; a known degree of shrinkage could then be built into the analysis of specimens that were prepared by standard preparation techniques. Obstacles for creating universal models about the effect of sample preparation are the complexity of biological systems and the difficulties relating to quantifying microscopy data. In general, chemometrics could be useful for directly relating of numerical datasets obtained from image analysis of microscopy data to other and very different data types. There are examples of this, e.g. the relation between principle component analysis of the multitude of different consumer preferences concerning apple cultivars, and apple microstructures established by SEM (Allan-Wojtas, Sanford et al. 2003).

There are a number of experiments that we could be performed to clarify some of the open questions of this thesis work.

It was unclear whether the casein structures in the water phase was affected to a large degree by artifacts from freeze-substitution or if the caseins in the 70% emulsions' water phase really form structures that are reminiscent of the native casein micelle. Cryo-TEM could be performed for protein fractions of the 70% samples to confirm that the structure is, in fact, like that of the native casein micelle. Analysis of diffraction patterns during the approach of the T_g could reveal at which temperature these samples devitrify. Microscopy analysis, before and after devitrification, could provide an estimate of the potential rearrangement of the suspended emulsifiers that occurs as a consequence of devitrification.

Cryo-TEM of the protein fraction of sample 6 would also be interesting to reveal more about the structure of the casein mini micelles, perhaps in combination with cryo-negative staining.

Segmentation by hand should be performed both for the agar mixed samples (for comparison with the mechanical segmentation by ImageJ) and for the samples that were fixed in capillary tubes and agar pockets. This would further strengthen the analysis of droplet sizes. Furthermore, it could be very interesting to subject several emulsions, with chemically different emulsifiers, to fixation with glutaraldehyde and thereby explore if they would react differently to the chemical fixation. If possible, the aim would be to relate this to the chemical features of the emulsifiers.

Slice and view could be applied for obtaining the 3D structure of the 70% oil emulsion droplets and the 3D organization of the caseins in the water phase. We already have the blocks, and a 3D reconstruction will provide a further understanding as to the structural variations that might exist both at the surface layers and in the water phase.

For a verification of the seemingly distorted surfaces of the oxidized samples it would be useful to obtain cryo-SEM images of high pressure frozen, freeze fractured 70% emulsions in which the surface of the droplets could be imaged. Freeze-substitution should be performed on the oxidized samples as well for structural analysis of these layers. Freeze-fracture cryo-TEM could possibly reveal altered surface structures in the small oil droplets (Belkoura, Stubenrauch et al. 2004).

Unfortunately we have been limited by time since the relevant equipment had not yet become accessible in Denmark at the time of the work in this thesis. Hence, many preparation steps involving cryo-techniques had to be done primarily during my research stay at the EMF UNIL or during short visits to other microscopy facilities. For this reason there were limitations to further explore some of the results. The impending introduction of a large collection of sophisticated cryo preparation equipment in Denmark will hopefully enable easier method development for projects like this in the future including the possibility to carefully plan projects over a longer time scale. To cite a recent cryo-EM review paper (Hurbain, Sachse 2011):

The future is cold!

8. Materials and methods

8.1 Chemicals, consumables, equipment and microscopes

8.1.1 Chemicals

	Application	Stock	Manufacturer
Methanol	Freeze substitution	99.9%	Sigma-Aldrich
Ethanol	Dehydration	99.9%	Sigma-Aldrich
Acetone	Washing after freeze substitution	100%	Merck
Sorensen buffer: Disodium phosphate Sodium dihydrogen phosphate	Chemical fixation	Solid	Merck
Uranyl acetate; 4% in H_2O	Post staining	solid	Merck
Uranyl acetat; 0.5% in methanol	Freeze substitution	Solid	Merck
Lead citrate; 0.4% in H_2O: Sodium citrate Lead nitrate	Post staining		Sigma-Aldrich Merck
OsO_4; 2% in H_2O	Post fixation	Solid	EMS
OsO_4; 2% in methanol	Freeze substitution	Solid	EMS
Glutaraldehyde; 0.05%, 1%, 2%, 3%, 6% in Sorensen buffer	Chemical fixation	25% in H_2O	
Glutaraldehyde	Freeze substitution	10% in methanol	EMS
Paraformaldehyde; 2.5% in Sorensen buffer	Chemical fixation	32% in H_2O	EMS

Low melting agar 4%	Encapsulation	Agar type VII low gelling temperature	Sigma-Aldrich
Epon+ DMP30	Embedding + Epoxy accelerator		kit from FULKA
Nile Red in acetone	Fluorescent lipid stain		Sigma-Aldrich
FITC in ethanol	Fluorescent protein stain		Sigma-Aldrich

8.1.2 Consumables

	Details	Manufacturer
Capillary dialysis tubes	LH 01843 VN; 200 µm inner diameter cellulose capillary tubes, cut off 5000 Dalton	BAL-TEC
TEM Grids	Various formvar carbon coated Cu EM grids	EMS
3 mm aluminum specimen carriers for high pressure freezing and spacer grid	type A LZ 02135 VN used on 100 µm side and type B LZ 02136 VN used as lid with flat side 50 mesh copper grid G209	BAL-TEC

8.1.3 Equipment

	Function	Manufacturer
Balzers HPM010	High pressure freezing machine	Abra-Fluid, AG, Switzerland At EMF, UNIL, Lausanne, Switzerland and EMEZ, ETH, Zürich, Switzerland
Leica EM AFS	Freeze substitution machine	Leica Microsystems. Vienna, Austria At EMF, UNIL, Lausanne, Switzerland
EM TP	Tissue processor	Leica Microsystems. Vienna, Austria At EMF, UNIL, Lausanne, Switzerland
Microtome Ultracut S and Reichert-Jung Ultracut E	Ultra microtomes	Leica Microsystems. Vienna, Austria At EMF, UNIL, Lausanne, Switzerland
Selection of various diamond knives	Sectioning and trimming	Diatome. Hatfield, UK At EMF, UNIL, Lausanne, Switzerland
Quorum PP3000T automated cryo preparation system with Prepdeck®	Freeze fracture, Pt sputter coating and cryo-stage	Quorum Technologies Ltd. West Sussex, UK At EMF, UNIL, Lausanne, Switzerland
Quorum PT2000T cryo preparation system	Freeze fracture, Pt sputter coating and cryo-stage	Quorum Technologies Ltd. West Sussex, UK At CFIM, KU, Copenhagen, Denmark
Quorum PP2000 preparation system	Freeze fracture, Pt sputter coating and cryo-stage	Quorum Technologies Ltd. West Sussex, UK At DTU CEN, Kgs. Lyngby, Denmark

Leica EM VCT100	Vacuum cryo transfer system	Leica Microsystems. Vienna, Austria At EMEZ, ETH, Zürich, Switzerland
Mastersizer 2000	Droplet size measurements by dynamic light scattering	Malvern Instruments Ltd. Worcestershire, UK At DTU FOOD, Kgs. Lyngby, Denmark
BAF 060	Freeze etching and shadow coating	BAL-TEC, Balzers, Liechtenstein At Biocentrum, Martin Luther Universität Halle-Wittenberg, Halle, Germany And EMEZ, ETH, Zürich, Switzerland
JFD 030	Propane jet freezer	BAL-TEC, Balzers, Liechtenstein At At Biocentrum, Martin Luther Universität Halle-Wittenberg, Halle, Germany
Home-made plunge freezing device	Cryo-TEM preparation	At Kemicentrum, Lunds Universitetet, Sweden

8.1.4 Microscopes

	Technique + extra equipment used	Manufacturer
Tecnai T20 G2	TEM	FEI Company, Eindhoven, The Netherlands At DTU CEN, Kgs. Lyngby, Denmark
Titan	STEM Aberation corrected, HAADF detector, EDS Oxford Instruments INCAx-sight	FEI Company, Eindhoven, The Netherlands At DTU CEN, Kgs. Lyngby, Denmark
CM100	TEM	Philips Electron Optics At EMF, UNIL, Lausanne, Switzerland
CM120 BioTWIN Cryo	Cryo-TEM	Philips Electron Optics
Quanta 250 FEG	Cryo-SEM Drift corrected frame integration software	FEI Company, Eindhoven, The Netherlands At EMF, UNIL, Lausanne, Switzerland
Quanta 200 FEG	Cryo-SEM	FEI Company, Eindhoven, The Netherlands At DTU CEN, Kgs. Lyngby, Denmark
Leo Gemini 1530 FEG	Cryo-SEM, SE in-lens detector	Carl Zeiss, Oberkochen, Germany At EMEZ, ETH, Zürich, Switzerland
Quanta FEG 3D	Cryo-FIBSEM	
Leica TCS SP II	Confocal laser scanning microscope. Inverted vertically. 100x oil immersion objective	Leica Microsystems, Heidelberg, Germany At Arla Strategic Innovation Centre, Brabrand, Denmark

8.2 Preparation of emulsions

The emulsions were prepared by the Lipid and Oxidation Group at the National Food Institute, Technical University of Denmark, Kgs. Lyngby, Denmark.

The fish oil used for the emulsions was commercially available cod liver oil without added antioxidants from Maritex A/S, subsidiary of TINE BA, Sortland, Norway. It was stored at -40 °C until use.

The continuous phase was 10 mM sodium acetate imidazole buffer.

The emulsifiers were all from Arla Foods Ingredients amba, Viby J, Denmark and are listed below.

Abbreviation	Emulsifier	Trade name
NaCas	sodium caseinate	Miprodan ® 30
WPI	whey protein isolate	Lacprodan ® DI-9224
MPL20	milk phospholipid containing approximately 20% phospholipids	Lacprodan ® PL-20

Emulsions were produced either at 70% oil concentration or 10% oil concentration. 70% emulsions were prepared at rpm 450, 450 sec by a single blade mixer, Stephan Universal mixer (Stephan, UMC5, 1995, Hameln, Germany) equipped with a vacuum system for reducing pressure and a double sided bowl for cooling with circulation water at 0 °C.

10% emulsions were prepared by primary homogenization at 16000 rpm (Ystral mixer, Ballrechten-Dottingen, Germany) and secondary homogenization either by a microfluidizer (M110L Microfluidics, Newton, USA) equipped with a ceramic chamber (CIXC, F20Y, 75 µm) or by a two-valve high-pressure homogenizer (Panda 2K, GEA Niro Soavi, Parma, Italy).

Emulsions were prepared fresh and transported under cooling. They were prepared for electron microscopy within one week of production; a timespan within which there should be no physical or chemical changes of the emulsions. The batch of emulsions, that were imaged while oxidized was subsequently stored for 42-45 days at 4 °C in Falcon tubes in the dark and prepared for electron microscopy again. The work in this thesis comprises at least 6 different batches of emulsions prepared through 2010-2012. These emulsions are similar, prepared with the same equipment, ingredients and personnel and as assessed by droplet sized and stability.

8.3 Protocols

8.3.1 Room temperature fixation and embedding in agar mix

1. Samples were mixed 1:1 with lukewarm low-melting agar (4%) and incubated 15 minutes at 37 °C in a heat cupboard. The samples were cooled on ice and cut into 1 mm^3 cubes after solidification.
2. The cubes were fixed with 0.05%, 1%, 2%, 3% or 6% glutaraldehyde, all with 2.5% paraformaldehyde in 0.1M Sorensen buffer at 4 °C for one week. After fixation the samples were washed 3 x 5 minutes in Sorensen buffer and poststained in 2% OsO_4 in H_2O for 1.2 hours. The cubes were rinsed and loaded into the Tissue processor.
3. Dehydration and infiltration was performed at 4 °C in the following steps (‘=minutes; h=hour)

Ethanol	Epon (in acetone)	Time
30%		30’
50%		30’
70%		1 h
80%		30’
85%		30’
100%		3 x 1 h
	10%	1 h
	30%	1 h
	50%	1 h
	70%	1 h
	100%	3 x 1 h
	100%	12 h

The cubes were placed in moulds with fresh resin with DMP30 and polymerization was done at 60 °C for at 72 hours.

8.3.2 Fixation in capillary tubes

Samples were sucked into the capillary tubes by capillary force and the tubes were cut into smaller pieces by a blunt scalpel to ensure simultaneous clamping of the ends of the tubes. The filled tubes were surrounded by hexadecane at the ends to avoid dehydration during clamping. After clamping, the tubes were transferred to fixative and treated as from step 2 in the agar mix protocol, except that only two concentrations of glutaraldehyde (3% and 6%) were applied.

8.3.3 Imaging in the confocal laser scanning microscope

Drops of fluorescent stains were applied to a microscope slide sequentially. The solvent was allowed to volatize and a drop of emulsion was subsequently applied on top of the stains and the stains were allowed time to penetrate into the emulsion droplets prior to imaging. The slides were imaged in a vertically inverted confocal laser scanning microscope using a 100x oil immersion objective.

8.3.4 Fixation in agar pockets

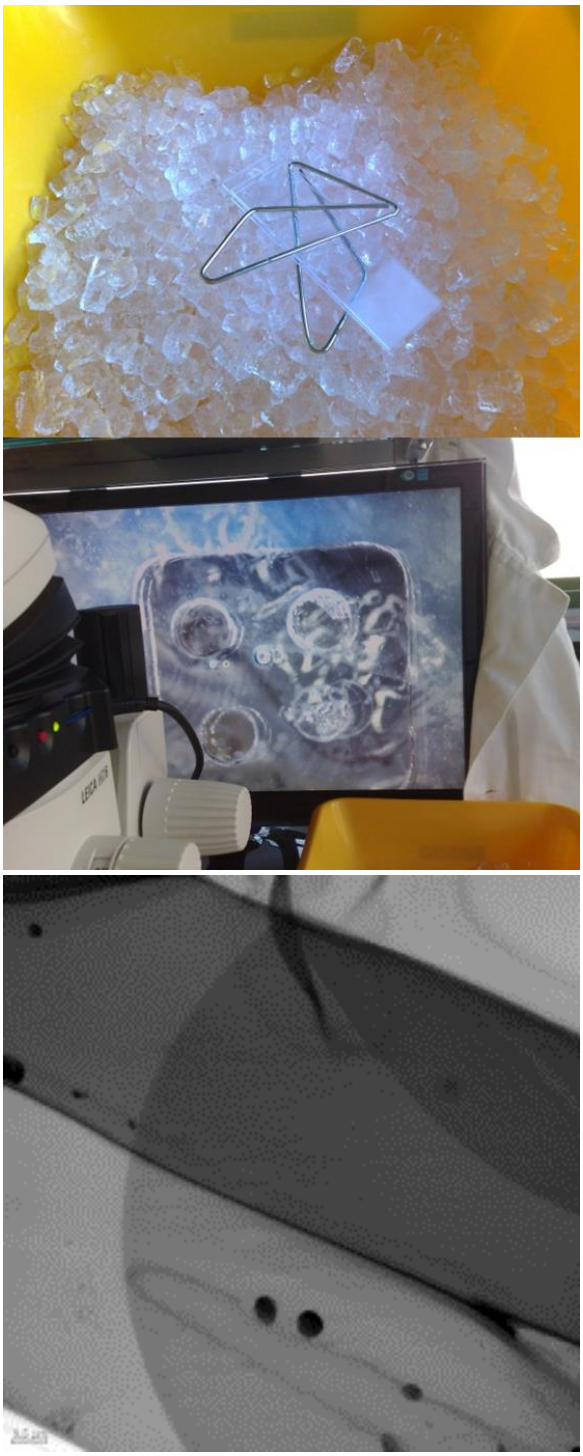

All operations were performed on ice and under a stereo microscope. Agar pockets were made by casting agar in small silicon molds between two microscope glass slides, thickness approximately 2-3 mm. Small holes were punched in the agar with a biopsy tool. Very small amounts of agar was placed to seal the bottom of the holes and sample was filled in the holes. Finally the holes were sealed with agar in which we had mixed some micron sized agarose beads to identify which side had been exposed to molten agar.

After solidification, the small sample-pockets were excised and trimmed to promote entry of fixatives and post fixative. After the trimming, the samples were treated as above from step 2, except that only two concentrations of glutaraldehyde (3% and 6%) were applied.

Figure 8.1. Casting agar pockets. The bottom image depicts a cross-section of one of the agarose beads that were used to avoid imaging the part of the sample that had been in contact with the molten agar-lid (section is folded).

8.3.5 Freeze substitution

Freeze substitution was done in the Leica AFS machine with the substitution media and the temperature program as specified below:

Substitution media as in (Müller, Marti et al. 1980) except for 2% OsO_4 instead of 1%.

Methanol 2% OsO_4	or	Methanol 2% OsO_4 0.5% uranyl acetat 3.3% glutaraldehyde

Temperature	Holding time (h) or ramp (Δ°C/h)
-90 °C	~30 h
-90 °C -> -30 °C	5 °C/h
-30 °C	3 h
-30 °C -> 0 °C	5 °C/h
0 °C	~8-16 h

The substitution medium was replaced by pure anhydrous acetone for 10 minutes at 0 °C, in 1/3 epon + 2/3 acetone for 1 h at 0 °C and the metal block from the AFS machine was subsequently brought to the fume hood to heat up for 1 h, after which the medium was changed to 2/3 epon in 1/3 acetone for 3 h. Finally the samples were left in pure epon overnight and finally polymerized at 60 °C for 72 h.

8.3.6 Sectioning and post staining

All polymerized sections were sectioned in an ultramicrotome to a thickness of approximately 70 nm (silver) and post stained with uranyl acetate (4% in H_2O) for 20 minutes in the dark and lead citrate (0.4% in H_2O) for 5 minutes. Grids were rinsed with milliQ water and blotted between staining steps.

9. References

ABRA-FLUID AG, 2007-last update, High Pressure Freezing Machine HPM 010. Available: http://www.high-pressure-freezing-machine-hpm-010.com/high-pressure-freezing-machine-hpm-010.pdf [05/11, 2013].

ADRIAN, M., DUBOCHET, J., FULLER, S. and HARRIS, J., 1998. Cryo-negative staining. *Micron,* **29**(2-3), pp. 145-160.

ADRIAN, M., DUBOCHET, J., LEPAULT, J. and MCDOWALL, A., 1984. Cryo-Electron Microscopy of Viruses. *Nature,* **308**(5954), pp. 32-36.

ALLAN-WOJTAS, P., SANFORD, K., MCRAE, K. and CARBYN, S., 2003. An integrated microstructural and sensory approach to describe apple texture. *Journal of the American Society for Horticultural Science,* **128**(3), pp. 381-390.

ALMGREN, M., EDWARDS, K. and KARLSSON, G., 2000. Cryo transmission electron microscopy of liposomes and related structures. *Colloids and Surfaces A-Physicochemical and Engineering Aspects,* **174**(1-2), pp. 3-21.

APPEL, L.J., MILLERI, E.R.I., SEIDLER, A.J. and WHELTON, P.K., 1993. Does supplementation of diet with "fish oil" reduce blood pressure? A meta-analysis of controlled clinical trials. *Archives of Internal Medicine,* **153**(12), pp. 1429-1438.

BACHMANN, L., 1987. *Freeze-Etching of Dispersions Emulsions and Macromolecular Solutions of Biological Interest.*

BACHMANN, L. and MAYER, E., 1987. *Physics of Water and Ice Implications for Cryofixation.*

BAHR, G., 1955. Continued Studies about the Fixation with Osmium Tetroxide - Electron Stains .4. *Experimental cell research,* **9**(2), pp. 277-285.

BELKOURA, L., STUBENRAUCH, C. and STREY, R., 2004. Freeze fracture direct imaging: A new freeze fracture method for specimen preparation in cryo-transmission electron microscopy. *Langmuir,* **20**(11), pp. 4391-4399.

BELLARE, J., DAVIS, H., SCRIVEN, L. and TALMON, Y., 1988. Controlled Environment Vitrification System - an Improved Sample Preparation Technique. *Journal of electron microscopy technique,* **10**(1), pp. 87-111.

BENITA, S. and LEVY, M., 1993. Submicron Emulsions as Colloidal Drug Carriers for Intravenous Administration - Comprehensive Physicochemical Characterization. *Journal of pharmaceutical sciences,* **82**(11), pp. 1069-1079.

BERTON, C., ROPERS, M., GUIBERT, D., SOLE, V. and GENOT, C., 2012. Modifications of Interfacial Proteins in Oil-in-Water Emulsions Prior to and During Lipid Oxidation. *Journal of Agricultural and Food Chemistry,* **60**(35), pp. 8659-8671.

BERTON, C., ROPERS, M., VIAU, M. and GENOT, C., 2011. Contribution of the Interfacial Layer to the Protection of Emulsified Lipids against Oxidation. *Journal of Agricultural and Food Chemistry,* **59**(9), pp. 5052-5061.

BERTON-CARABIN, C., GENOT, C., GAILLARD, C., GUIBERT, D. and ROPERS, M.H., 2013. Design of interfacial films to control lipid oxidation in oil-in-water emulsions. *Food Hydrocolloids,* **33**(1), pp. 99-105.

BIBETTE, J., CALDERON, F. and POULIN, P., 1999. Emulsions: basic principles. *Reports on Progress in Physics,* **62**(6), pp. 969-1033.

BLASCHKE, T., 2010. Object based image analysis for remote sensing. *ISPRS Journal of Photogrammetry and Remote Sensing,* **65**, pp. 2.

BOZZOLA, J.J., 2007. Conventional Specimen Preparation Techniques for Transmission Electron Microscopy of Cultured Cells. In: J. KUO, ed, *Electron Microscopy Methods and Protocols.* 2nd edition edn. Totowa, New Jersey, USA: Humana Press Inc., pp. 1.

BRENNA, J.T., SALEM, N., Jr., SINCLAIR, A.J., CUNNANE, S.C. and ISSFAL, 2009. alpha-Linolenic acid supplementation and conversion to n-3 long-chain polyunsaturated fatty acids in humans. *Prostaglandins Leukotrienes and Essential Fatty Acids,* **80**(2-3), pp. 85-91.

BRENNER, S. and HORNE, R., 1959. A Negative Staining Method for High Resolution Electron Microscopy of Viruses. *Biochimica et biophysica acta,* **34**(1), pp. 103-110.

BROOKER, B. and WELLS, K., 1984. Preparation of Dairy-Products for Scanning Electron-Microscopy - Etching of Epoxy Resin-Embedded Material. *Journal of Dairy Research,* **51**(4), pp. 605-613.

BRUGGELLER, P. and MAYER, E., 1980. Complete Vitrification in Pure Liquid Water and Dilute Aqueous-Solutions. *Nature,* **288**(5791), pp. 569-571.

BURTON, E.F. and OLIVER, W.F., 1935. The crystal structure of ice at low temperatures. *Proc. R. Soc. Lond. A,* **153**, pp. 166.

BUSER, C. and WALTHER, P., 2008. The structure and behavior of liquid water. *Journal of Microscopy-Oxford,* **230**(2), pp. 268-277.

CHAPLIN, M., 2013-last update, Water Structure and Science. Available: http://www.lsbu.ac.uk/water/ [05/01, 2013].

DALGLEISH, D.G., 1998. Casein micelles as colloids: Surface structures and stabilities. *Journal of dairy science,* **81**(11), pp. 3013-3018.

DALGLEISH, D.G., TOSH, S.M. and WEST, S., 1996. Beyond homogenization: The formation of very small emulsion droplets during the processing of milk by a Microfluidizer. *Netherlands Milk and Dairy Journal,* **50**(2), pp. 135-148.

DALGLEISH, D., 1996. Conformations and structures of milk proteins adsorbed to oil-water interfaces. *Food Research International,* **29**(5-6), pp. 541-547.

DALGLEISH, D., SRINIVASAN, M. and SINGH, H., 1995. Surface-Properties of Oil-In-Water Emulsion Droplets Containing Casein and Tween-60. *Journal of Agricultural and Food Chemistry,* **43**(9), pp. 2351-2355.

DALGLEISH, D.G. and CORREDIG, M., 2012. The Structure of the Casein Micelle of Milk and Its Changes During Processing. *Annual Review of Food Science and Technology, Vol 3,* **3**, pp. 449-467.

DE CARLO, S., 2009. Plunge-freezing (holey carbon method). In: A. CAVALIER, D. SPEHNER and B.M. HUMBEL, eds, *Handbook of Cryo-Preparation Methods for Electron Microscopy.* Boca Raton, FL, USA.: CRC Press, Francis and Taylor Group, pp. 49.

DE KRUIF, C.G., HUPPERTZ, T., URBAN, V.S. and PETUKHOV, A.V., 2012. Casein micelles and their internal structure. *Advances in Colloid and Interface Science,* **171**, pp. 36-52.

DE LEIRIS, J., DE LORGERIL, M. and BOUCHER, F., 2009. Fish Oil and Heart Health. *Journal of cardiovascular pharmacology,* **54**(5), pp. 378-384.

DOBOCHET, J. and MCDOWALL, A., 1981. Vitrification of Pure Water for Electron-Microscopy. *Journal of Microscopy-Oxford,* **124**(DEC), pp. RP3-RP4.

DONELLY, W., MCNEILL, G., BUCHHEIM, W. and MCGANN, T., 1984. A Comprehensive Study of the Relationship between Size and Protein-Composition in Natural Bovine Casein Micelles. *Biochimica et biophysica acta,* **789**(2), pp. 136-143.

DU PLESSIS, J., TIEDT, L.R., VAN WYK, C.J. and ACKERMANN, C., 1986. A New Transmission Electron Microscope Method for the Determination of Particle Size in Parenteral Fat Emulsions. *International Journal of Pharmaceutics (Kidlington),* **34**(1-2), pp. 173-174.

DUBOCHET, J., 2009. Vitreous Water. In: A. CAVALIER, D. SPEHNER and B.M. HUMBEL, eds, *Handbook of Cryo-Preparation Methods for Electron Microscopy.* Boca Raton, FL, USA.: CRC Press, Francis and Taylor Group, pp. 1.

DUBOCHET, J., ADRIAN, M., CHANG, J., HOMO, J., LEPAULT, J., MCDOWALL, A. and SCHULTZ, P., 1988. Cryo-Electron Microscopy of Vitrified Specimens. *Quarterly reviews of biophysics,* **21**(2), pp. 129-228.

DUBOCHET, J. and BLANC, N., 2001. The cell in absence of aggregation artifacts. *Micron,* **32**(1), pp. 91-99.

DUBOCHET, J., 2007. The physics of rapid cooling and its implications for cryoimmobilization of cells. *Cellular Electron Microscopy,* **79**, pp. 7-21.

ECHLIN, P., 1992. *Low-Temperature Microscopy and Analusis.* New York: Plenum Press.

ELIAS, R., MCCLEMENTS, D. and DECKER, E., 2005. Antioxidant activity of cysteine, tryptophan, and methionine residues in continuous phase beta-lactoglobulin in oil-in-water emulsions. *Journal of Agricultural and Food Chemistry,* **53**(26), pp. 10248-10253.

ELLIS, E.A., 2007. Poststaining grids for transmission electron microscopy: conventional and alternative protocols. *Methods in molecular biology (Clifton, N.J.),* **369**, pp. 97-106.

EUSTON, S., 2004. Computer simulation of proteins: adsorption, gelation and self-association. *Current Opinion in Colloid & Interface Science,* **9**(5), pp. 321-327.

EVERHART, T. and THORNLEY, R., 1960. Wide-Band Detector for Micro-Microampere Low-Energy Electron Currents. *Journal of scientific instruments,* **37**(7), pp. 246-248.

FANG, Y. and DALGLEISH, D., 1997. Conformation of beta-lactoglobulin studied by FTIR: Effect of pH, temperature, and adsorption to the oil-water interface. *Journal of colloid and interface science,* **196**(2), pp. 292-298.

FANG, Y. and DALGLEISH, D., 1993. Dimensions of the Adsorbed Layers in Oil-In-Water Emulsions Stabilized by Caseins. *Journal of colloid and interface science,* **156**(2), pp. 329-334.

FANG, Y. and DALGLEISH, D.G., 1993. Casein adsorption on the surfaces of oil-in-water emulsions modified by lecithin. *Colloids and Surfaces B: Biointerfaces,* **1**(6), pp. 357-364.

FARAJI, H., MCCLEMENTS, D. and DECKER, E., 2004. Role of continuous phase protein on the oxidative stability of fish oil-in-water emulsions. *Journal of Agricultural and Food Chemistry,* **52**(14), pp. 4558-4564.

FARAJI, H., MCCLEMENTS, D. and DECKER, E., 2004. Role of continuous phase protein on the oxidative stability of fish oil-in-water emulsions. *Journal of Agricultural and Food Chemistry,* **52**(14), pp. 4558-4564.

FARRELL, H., JIMENEZ-FLORES, R., BLECK, G., BROWN, E., BUTLER, J., CREAMER, L., HICKS, C., HOLLAR, C., NG-KWAI-HANG, K. and SWAISGOOD, H., 2004. Nomenclature of the proteins of cows' milk - Sixth revision. *Journal of dairy science,* **87**(6), pp. 1641-1674.

FRANKEL, E., 1991. Recent Advances in Lipid Oxidation. *Journal of the science of food and agriculture,* **54**(4), pp. 495-511.

FRANKEL, E., SATUE-GRACIA, T., MEYER, A. and GERMAN, J., 2002. Oxidative stability of fish and algae oils containing long-chain polyunsaturated fatty acids in bulk and in oil-in-water emulsions. *Journal of Agricultural and Food Chemistry,* **50**(7), pp. 2094-2099.

FRAUENFELDER, H., CHEN, G., BERENDZEN, J., FENIMORE, P.W., JANSSON, H., MCMAHON, B.H., STROE, I.R., SWENSON, J. and YOUNG, R.D., 2009. A unified model of protein dynamics. *Proceedings of the National Academy of Sciences of the United States of America,* **106**(13), pp. 5129-5134.

FREDERIK, P.M., DE HAAS, F. and STORMS, M.M.H., 2009. Controlled vitrification. In: A. CAVALIER, D. SPEHNER and B.M. HUMBEL, eds, *Handbook of Cryo-Preparation Methods for Electron Microscopy.* Boca Raton, FL, USA.: CRC Press, Francis and Taylor Group, pp. 69.

GASPAR, A.M., APPAVOU, M.-., BUSCH, S., UNRUH, T. and DOSTER, W., 2008. Dynamics of well-folded and natively disordered proteins in solution: a time-of-flight neutron scattering study. *European Biophysics Journal with Biophysics Letters,* **37**(5), pp. 573-582.

GEBHARDT, R., DOSTER, W., FRIEDRICH, J. and KULOZIK, U., 2006. Size distribution of pressure-decomposed casein micelles studied by dynamic light scattering and AFM. *European Biophysics Journal with Biophysics Letters,* **35**(6), pp. 503-509.

GIGG, R. and PAYNE, S., 1969. The reaction of glutaraldehyde with tissue lipids. *Chemistry and physics of lipids,* **3**(3), pp. 292-295.

GOLDSTEIN, J.I., NEWBURY, D.E., ECHLIN, P., JOY, D.C., LYMAN, C.E., LIFSHIN, E., SAWYER, L. and MICHAEL, J.R., 2003. *Scanning Electron Microscopy and X-Ray Microanalysis.* Third edition edn. New York, USA.: Springer.

GRAMM, F., MÜLLER, E., HEIGHT, M. and WEPF, R., 2010. *Re-Viewing of Stereoscopic imaging: a real alternative to EM tomography techniques?* .

HALLE, B., 2004. Protein hydration dynamics in solution: a critical survey. *Philosophical Transactions of the Royal Society of London Series B-Biological Sciences,* **359**(1448), pp. 1207-1223.

HARRIS, J.R., 2008. Negative staining across holes: Application to fibril and tubular structures. *Micron,* **39**(2), pp. 168-176.

HATZIANTONIOU, S., DELI, G., NIKAS, Y., DEMETZOS, C. and PAPAIOANNOU, G.T., 2007. Scanning electron microscopy study on nanoemulsions and solid lipid nanoparticles containing high amounts of ceramides. *Micron,* **38**(8), pp. 819-823.

HAYAT, M.A., 2000. *Principles and Techniques of Electron Microscopy. Biological Applications.* 4th edition edn. Cambridge, UK: Cambridge University Press.

HAYAT, M., 1986. Glutaraldehyde - Role in Electron-Microscopy. *Micron and Microscopica Acta,* **17**(2), pp. 115-135.

HEIDE, H.G. and ZEITLER, E., 1985. The Physical Behavior of Solid Water at Low-Temperatures and the Embedding of Electron Microscopical Specimens. *Ultramicroscopy,* **16**(2), pp. 151-160.

HEIDE, H., 1984. Observations on Ice Layers. *Ultramicroscopy,* **14**(3), pp. 271-278.

HEUSER, J.E., 2011. The origins and evolution of freeze-etch electron microscopy. *Journal of electron microscopy,* **60**, pp. S3-S29.

HIGGINS, M.J., POLCIK, M., FUKUMA, T., SADER, J.E., NAKAYAMA, Y. and JARVIS, S.P., 2006. Structured Water Layers Adjacent to Biological Membranes. *Biophysical journal,* **91**(7), pp. 2532-2542.

HOHENBERG, H., MANNWEILER, K. and MULLER, M., 1994. High-Pressure Freezing of Cell-Suspensions in Cellulose Capillary Tubes. *Journal of microscopy,* **175**, pp. 34-43.

HOLM, S., 1979. A Simple Sequentially Rejective Multiple Test Procedure. *Scandinavian Journal of Statistics,* **6**(2), pp. 65-70.

HOLT, C. and SAWYER, L., 1993. Caseins as Rheomorphic Proteins - Interpretation of Primary and Secondary Structures of the Alpha-S1-Caseins, Beta-Caseins and Kappa-Caseins. *Journal of the Chemical Society-Faraday Transactions,* **89**(15), pp. 2683-2692.

HORN, A.F., NIELSEN, N.S., ANDERSEN, U., SOGAARD, L.H., HORSEWELL, A. and JACOBSEN, C., 2011. Oxidative stability of 70% fish oil-in-water emulsions: Impact of emulsifiers and pH. *European Journal of Lipid Science and Technology,* **113**(10), pp. 1243-1257.

HORN, A.F., NIELSEN, N.S., ANDERSEN, U., SØGAARD, L.H., HORSEWELL, A. and JACOBSEN, C., 2011. Oxidative stability of 70% fish oil-in-water emulsions: Impact of emulsifiers and pH. *European Journal of Lipid Science and Technology,* **113**(10), pp. 1243-1257.

HORN, A.F., NIELSEN, N.S., JENSEN, L.S., HORSEWELL, A. and JACOBSEN, C., 2012. The choice of homogenisation equipment affects lipid oxidation in emulsions. *Food Chemistry,* **134**(2), pp. 803-810.

HOVONGTON, P., DROUIN, D., HORNY, P., DEMERS, H., COUTURE, A.R. and GAUVIN, R., . Available: http://www.gel.usherbrooke.ca/casino/What.html [January, 2013].

HUMBEL, B.M., 2009. Freeze-Substitution. In: A. CAVALIER, D. SPEHNER and B.M. HUMBEL, eds, *Handbook of Cryo-Preparation Methods for Electron Microscopy.* Boca Raton, FL, USA.: CRC Press, Francis and Taylor Group, pp. 322.

HUMBEL, B.M., MARTI, T. and MÜLLER, M., 1983. Improved structural preservation by combining freeze substitution and low temperature embedding. *Beitr. elektronenmikroskop. Direktabb. Oberfl.,* **16**, pp. 585.

HUMBEL, B. and MUELLER, M., 1986. Freeze Substitution and Low Temperature Embedding, M. MUELLER and E. AL, eds. In: *The Science of Biological Specimen Preparation for Microscopy and Microanalysis 1985; 4th Pfefferkorn Conference*, Mar. 25-30, 1985 1986, Scanning Electron Microscopy, Inc., pp. 175-184.

HUNT, J. and DALGLEISH, D., 1994. Adsorption Behavior of Whey-Protein Isolate and Caseinate in Soya Oil-In-Water Emulsions. *Food Hydrocolloids,* **8**(2), pp. 175-187.

HURBAIN, I. and SACHSE, M., 2011. The future is cold: cryo-preparation methods for transmission electron microscopy of cells. *Biology of the Cell,* **103**(9), pp. 405-420.

IKEDA, K., INOUE, K., KANEMATSU, S., HORIUCHI, Y. and PARK, P., 2011. Enhanced Effects of Nonisotopic Hafnium Chloride in Methanol as a Substitute for Uranyl Acetate in TEM Contrast of Ultrastructure of Fungal and Plant Cells. *Microscopy research and technique,* **74**(9), pp. 825-830.

JACOBSEN, C. and NIELSEN, N., 2007. Optimization of oxidative stability of omega-3 enriched foods. In: H. BREIVIK, ed, *Long-chain omega-3 specialty oils.* The Oily Press (now Woodhead Publishing Ltd, Cambridge, UK)., pp. 197.

JACOBSEN, C., 1999. Sensory impact of lipid oxidation in complex food systems. *Fett-Lipid,* **101**(12), pp. 484-492.

JACOBSEN, C., HARTVIGSEN, K., LUND, P., THOMSEN, M., SKIBSTED, L., ADLER-NISSEN, J., HOLMER, G. and MEYER, A., 2000. Oxidation in fish oil-enriched mayonnaise 3. Assessment of the influence of the emulsion structure on oxidation by discriminant partial least squares regression analysis. *European Food Research and Technology,* **211**(2), pp. 86-98.

JAFFE, J. and GLAESER, R., 1984. Preparation of Frozen-Hydrated Specimens for High-Resolution Electron-Microscopy. *Ultramicroscopy,* **13**(4), pp. 373-377.

JAHN, A., LUCAS, F., WEPF, R.A. and DITTRICH, P.S., 2013. Freezing Continuous-Flow Self-Assembly in a Microfluidic Device: Toward Imaging of Liposome Formation. *Langmuir,* **29**(5), pp. 1717-1723.

JENSEN, L., HORN, A., JACOBSEN, C., NIELSEN, N. and HORSEWELL, A., 2011. Cryo-FIB SEM for Characterization of the Structure of Fish Oil Emulsions, 2011, DGE – German Society for Electron Microscopy.

JEPPSSON, R. and SCHOEFL, G., 1974. Ultrastructure of Lipid Particles in Emulsions Prepared with various Emulsifiers. *Australian Journal of Experimental Biology and Medical Science,* **52**(AUG), pp. 697-702.

KAECH, A., 2012. Center for Microscopy and Image Analysis, University of Zürich, Zürich, Switzerland.

KAECH, A., 2009. Bal-Tec HPM010 High Pressure Freezing Machine. In: A. CAVALIER, D. SPEHNER and B.M. HUMBEL, eds, *Handbook of Cryo-Preparation Methods for Electron Microscopy.* Boca Raton, FL, USA.: CRC Press, Francis and Taylor Group, pp. 101.

KALAB, M. and LAROCQUE, G., 1996. Suitability of agar gel encapsulation of milk and cream for electron microscopy. *Food Science and Technology-Lebensmittel-Wissenschaft & Technologie,* **29**(4), pp. 368-371.

KANNO, H., MIYATA, K., TOMIZAWA, K. and TANAKA, H., 2004. Additivity rule holds in supercooling of aqueous solutions. *Journal of Physical Chemistry a,* **108**(28), pp. 6079-6082.

KANNO, H., SPEEDY, R. and ANGELL, C., 1975. Supercooling of Water to -92 degrees C Under Pressure. *Science,* **189**(4206), pp. 880-881.

KELLENBERGER, E., 1987. *The Response of Biological Macromolecules and Supramolecular Structures to the Physics of Specimen Cryopreparation.*

KELLERBY, S.S., GU, Y.S., MCCLEMENTS, D.J. and DECKER, E.A., 2006. Lipid oxidation in a menhaden oil-in-water emulsion stabilized by sodium caseinate cross-linked with transglutaminase. *Journal of Agricultural and Food Chemistry,* **54**(26), pp. 10222-10227.

KELLERBY, S.S., MCCLEMENTS, D.J. and DECKER, E.A., 2006. Role of proteins in oil-in-water emulsions on the stability of lipid hydroperoxides. *Journal of Agricultural and Food Chemistry,* **54**(20), pp. 7879-7884.

KONTOPIDIS, G., HOLT, C. and SAWYER, L., 2004. Invited Review: beta-lactoglobulin: Binding properties, structure, and function. *Journal of dairy science,* **87**(4), pp. 785-796.

KRALOVA, I. and SJOBLOM, J., 2009. Surfactants Used in Food Industry: A Review. *Journal of Dispersion Science and Technology,* **30**(9), pp. 1363-1383.

KRIS-ETHERTON, P., HARRIS, W., APPEL, L. and NUTRITION COMM, 2002. Fish consumption, fish oil, omega-3 fatty acids, and cardiovascular disease. *Circulation,* **106**(21), pp. 2747-2757.

LANA LAI, Y., PETRONE, A., PANKOW, J., ARNETT, D., NORTH, K., ELLISON, R., HUNT, S. and DJOUSSÉ, L., 2013. Association of dietary omega-3 fatty acids with prevalence of metabolic syndrome: The National Heart, Lung, and Blood Institute Family Heart Study. *Clinical nutrition,* **In press**.

LEA, P., HOLLENBERG, M., TEMKIN, R. and KHAN, P., 1992. Chemical-Extraction of the Cytosol using Osmium-Tetroxide for High-Resolution Scanning Electron-Microscopy. *Microscopy research and technique,* **22**(2), pp. 185-193.

LEFORESTIER, A., RICHTER, K., LIVOLANT, F. and DUBOCHET, J., 1996. Comparison of slam-freezing and high-pressure freezing effects on the DNA cholesteric liquid crystalline structure. *Journal of microscopy,* **184**, pp. 4-13.

LEICA MICROSYSTEMS, 2013-last update, Self Pressurized Freezer Leica EM SPF. Available: http://www.leica-microsystems.com/products/em-sample-prep/biological-specimens/low-temperature-techniques/fixation/details/product/leica-em-spf/ [05/11, 2013].

LENARD, J. and SINGER, S., 1968. Alteration of Conformation of Proteins in Red Blood Cell Membranes and in Solution by Fixatives used in Electron Microscopy. *Journal of Cell Biology,* **37**(1), pp. 117-&.

LENORMAND, G., MILLET, E., PARK, C.Y., HARDIN, C.C., BUTLER, J.P., MOLDOVAN, N.I. and FREDBERG, J.J., 2011. Dynamics of the cytoskeleton: How much does water matter? *Physical Review E,* **83**(6), pp. 061918.

LET, M.B., JACOBSEN, C. and MEYER, A.S., 2007. Lipid oxidation in milk, yoghurt, and salad dressing enriched with neat fish oil or pre-ernulsified fish oil. *Journal of Agricultural and Food Chemistry,* **55**(19), pp. 7802-7809.

LET, M.B., JACOBSEN, C., SORENSEN, A.M. and MEYER, A.S., 2007. Homogenization conditions affect the oxidative stability of fish oil enriched milk emulsions: Lipid oxidation. *Journal of Agricultural and Food Chemistry,* **55**(5), pp. 1773-1780.

LETHUAUT, L., METRO, F. and GENOT, C., 2002. Effect of droplet size on lipid oxidation rates of oil-in-water emulsions stabilized by protein. *Journal of the American Oil Chemists Society,* **79**(5), pp. 425-430.

LEUNISSEN, J.L.M. and YI, H., 2009. Self-pressurized rapid freezing (SPRF): a novel cryofixation method for specimen preparation in electron microscopy. *Journal of Microscopy-Oxford,* **235**(1), pp. 25-35.

LI, X., MOONEY, P., ZHENG, S., BOOTH, C., BRAUNFELD, M., GUBBENS, S., AGARD, D. and CHENG, Y., 2013. Electron counting and beam-induced motion correction enable near-atomic-resolution single-particle cryo-EM. *Nature Methods,* .

LIU, J., 2005. Scanning transmission electron microscopy and its application to the study of nanoparticles and nanoparticle systems. *Journal of electron microscopy,* **54**(3), pp. 251-278.

LOERTING, T., WINKEL, K., SEIDL, M., BAUER, M., MITTERDORFER, C., HANDLE, P.H., SALZMANN, C.G., MAYER, E., FINNEY, J.L. and BOWRON, D.T., 2011. How many amorphous ices are there? *Physical Chemistry Chemical Physics,* **13**(19), pp. 8783-8794.

LU, F.S.H., NIELSEN, N.S., BARON, C.P., JENSEN, L.H.S. and JACOBSEN, C., 2012. Physico-chemical Properties of Marine Phospholipid Emulsions. *Journal of the American Oil Chemists Society,* **89**(11), pp. 2011-2024.

MA, T., LIASET, B., HAO, Q., PETERSEN, R.K., FJAERE, E., HA THI NGO, LILLEFOSSE, H.H., RINGHOLM, S., SONNE, S.B., TREEBAK, J.T., PILEGAARD, H., FROYLAND, L., KRISTIANSEN, K. and MADSEN, L., 2011. Sucrose Counteracts the Anti-Inflammatory Effect of Fish Oil in Adipose Tissue and Increases Obesity Development in Mice. *Plos One,* **6**(6), pp. e21647.

MARION, G.M. and JAKUBOWSKI, S.D., 2004. The compressibility of ice to 2.0 kbar. *Cold Regions Science and Technology,* **38**(2-3), pp. 211-218.

MASON, T.G., WILKING, J.N., MELESON, K., CHANG, C.B. and GRAVES, S.M., 2006. Nanoemulsions: formation, structure, and physical properties. *Journal of Physics-Condensed Matter,* **18**(41), pp. R635-R666.

MATSKO, N. and MUELLER, M., 2005. Epoxy resin as fixative during freeze-substitution. *Journal of structural biology,* **152**(2), pp. 92-103.

MCCLEMENTS, D. and DECKER, E., 2000. Lipid oxidation in oil-in-water emulsions: Impact of molecular environment on chemical reactions in heterogeneous food systems. *Journal of Food Science,* **65**(8), pp. 1270-1282.

MCDONALD, K.L. and WEBB, R.I., 2011. Freeze substitution in 3 hours or less. *Journal of microscopy,* **243**(3), pp. 227-233.

MCMAHON, D.J. and OOMMEN, B.S., 2008. Supramolecular structure of the casein micelle. *Journal of dairy science,* **91**(5), pp. 1709-1721.

MCNAUGHT, A. and WILKINSON, A., 1997. *IUPAC. Compendium of chemical terminology.* 2nd edn. Oxford: Blackwell Scientific Publications.

MEYER, H. and RICHTER, W., 2001. Freeze-fracture studies on lipids and membranes. *Micron,* **32**(6), pp. 615-644.

MILITZER, B. and WILSON, H.F., 2010. New Phases of Water Ice Predicted at Megabar Pressures. *Physical Review Letters,* **105**(19), pp. 195701.

MOOR, H., KISTLER, J. and MULLER, M., 1976. Freezing in a Propane Jet. *Experientia,* **32**(6), pp. 805-805.

MOORE, E.B. and MOLINERO, V., 2011. Structural transformation in supercooled water controls the crystallization rate of ice. *Nature,* **479**(7374), pp. 506-U226.

MÜLLER, M., MARTI, T. and KRIZ, S., 1980. Improved structural preservation by freeze substitution. *Brederoo P, de Priester W (eds) Electron microscopy, Proc 7th Eur Congr Electron Microsc, Leiden,* **II**, pp. 721.

MURRAY, B.J., KNOPF, D.A. and BERTRAM, A.K., 2005. The formation of cubic ice under conditions relevant to Earth's atmosphere. *Nature,* **434**(7030), pp. 202-205.

NAKAKOSHI, M., NISHIOKA, H. and KATAYAMA, E., 2011. New versatile staining reagents for biological transmission electron microscopy that substitute for uranyl acetate. *Journal of electron microscopy,* **60**(6), pp. 401-407.

NIELSEN, N.S. and JACOBSEN, C., 2009. Methods for reducing lipid oxidation in fish-oil-enriched energy bars. *International Journal of Food Science and Technology,* **44**(8), pp. 1536-1546.

NUCHI, C., MCCLEMENTS, D. and DECKER, E., 2001. Impact of tween 20 hydroperoxides and iron on the oxidation of methyl linoleate and salmon oil dispersions. *Journal of Agricultural and Food Chemistry,* **49**(10), pp. 4912-4916.

POUDYAL, H. and BROWN, L., 2013. The Role of n-3 Polyunsaturated Fatty Acids in Human Heart Failure. *Endocrine Metabolic & Immune Disorders-Drug Targets,* **13**(1), pp. 105-117.

PREETZ, C., HAUSER, A., HAUSE, G., KRAMER, A. and MAEDER, K., 2010. Application of atomic force microscopy and ultrasonic resonator technology on nanoscale: Distinction of

nanoemulsions from nanocapsules. *European Journal of Pharmaceutical Sciences,* **39**(1-3), pp. 141-151.

R DEVELOPMENT CORE TEAM, 2011. *R: A language and environment for statistical computing. R Foundation for Statistical Computing, Vienna, Austria. ISBN 3-900051-07-0, URL http://www.R-project.org/.* .

RASBAND, W.S., 1997-2012-last update, ImageJ, U. S. National Institutes of Health, Bethesda, Maryland, USA. Available: http://imagej.nih.gov/ij/.

RASMUSSE, D. and MACKENZI, A., 1973. Clustering in Supercooled Water. *Journal of Chemical Physics,* **59**(9), pp. 5003-5013.

REYNOLDS, E., 1963. Use of Lead Citrate at High Ph as an Electron-Opaque Stain in Electron Microscopy. *Journal of Cell Biology,* **17**(1), pp. 208-&.

RICHTER, K., 1994. High-Density Morphologies of Ice in High-Pressure Frozen Biological Specimens. *Ultramicroscopy,* **53**(3), pp. 237-249.

RIES, D., YE, A., HAISMAN, D. and SINGH, H., 2010. Antioxidant properties of caseins and whey proteins in model oil-in-water emulsions. *International Dairy Journal,* **20**(2), pp. 72-78.

RONCAGLIONI, M., TOMBESI, M., AVANZINI, F., BARLERA, S., CAIMI, V., LONGONI, P., MARZONA, I., MILANI, V., SILLETTA, M., TOGNONI, G. and MARCHIOLI, R., 2013. n–3 Fatty Acids in Patients with Multiple Cardiovascular Risk Factors. *N Engl J Med,* **368**(19), pp. 1800-1808.

RUIZ-LOPEZ, N., SAYANOVA, O., NAPIER, J.A. and HASLAM, R.P., 2012. Metabolic engineering of the omega-3 long chain polyunsaturated fatty acid biosynthetic pathway into transgenic plants. *Journal of experimental botany,* **63**(7), pp. 2397-2410.

RUSS, J.C., 2004. *Image Analysis of Food Microstructure.* CRC Press.

SAGALOWICZ, L. and LESER, M.E., 2010. Delivery systems for liquid food products. *Current Opinion in Colloid & Interface Science,* **15**(1-2), pp. 61-72.

SALZMANN, C., RADAELLI, P., HALLBRUCKER, A., MAYER, E. and FINNEY, J., 2006. The preparation and structures of hydrogen ordered phases of ice. *Science,* **311**(5768), pp. 1758-1761.

SATO, S., ADACHI, A., SASAKI, Y. and GHAZIZADEH, M., 2008. Oolong tea extract as a substitute for uranyl acetate in staining of ultrathin sections. *Journal of Microscopy-Oxford,* **229**(1), pp. 17-20.

SAUTER, J., 1926. Die Größenbestimmung der im Gemischnebel von Verbrennungskraftmaschinen vorhandenen Brennstoffteilchen. *VDI-Forschungsheft Nr. 279
*. VDI-Verl, .

SCHULTZ, S., WAGNER, G., URBAN, K. and ULRICH, J., 2004. High-pressure homogenization as a process for emulsion formation. *Chemical Engineering & Technology,* **27**(4), pp. 361-368.

SITTE, H., EDELMANN, L. and NEUMANN, K., 1987. *Cryofixation without Pretreatment at Ambient Pressure.*

SJOSTRAND, F., 1990. Common-Sense in Electron-Microscopy - about Cryofixation, Freeze-Substitution, Low-Temperature Embedding, and Low Denaturation Embedding. *Journal of structural biology,* **103**(2), pp. 135-139.

SJOSTRAND, F., 1989. Common-Sense in Electron-Microscopy - about Osmium Fixation. *Journal of ultrastructure and molecular structure research,* **102**(1), pp. 1-8.

SMITH, A., GOFF, H. and SUN, B., 2004. Freeze-substitution and low-temperature embedding of dairy products for transmission electron microscopy. *Journal of Microscopy-Oxford,* **213**, pp. 63-69.

SONIA GONZALEZ, J.M., HUERTA, S.F., PATTERSON, A.M. and LASHERAS, C., 2010. The relationship between dietary lipids and cognitive performance in an elderly population. *International journal of food sciences and nutrition,* **61**(2), pp. 217-225.

SORENSEN, A.M., BARON, C.P., LET, M.B., BRUEGGEMANN, D.A., PEDERSEN, L.R.L. and JACOBSEN, C., 2007. Homogenization conditions affect the oxidative stability of fish oil enriched milk emulsions: Oxidation linked to changes in protein composition at the oil-water interface. *Journal of Agricultural and Food Chemistry,* **55**(5), pp. 1781-1789.

STEINBRECHT, R.A. and MUELLER, M., 1987. *Freeze-Substitution and Freeze-Drying.*

STILLWELL, W., SHAIKH, S., ZEROUGA, M., SIDDIQUI, R. and WASSALL, S., 2005. Docosahexaenoic acid affects cell signaling by altering lipid rafts. *Reproduction Nutrition Development,* **45**(5), pp. 559-579.

STOKES, D.J., 2008. *Principles and Practice of Variable Pressure/Environmental Scanning Electron Microscopy (VP-ESEM).* West Sussex, United Kingdom: John Wiley & Sons Ltd.

STOKES, D., MUGNIER, J. and CLARKE, C., 2004. Static and dynamic experiments in cryo-electron microscopy: comparative observations using high-vacuum, low-voltage and low-vacuum SEM. *Journal of Microscopy-Oxford,* **213**, pp. 198-204.

STOKES, D., THIEL, B. and DONALD, A., 2000. Dynamic secondary electron contrast effects in liquid systems studied by environmental scanning electron microscopy. *Scanning,* **22**(6), pp. 357-365.

STRYER, L., 1999. *Biochemistry.* 4th edn. New York: W.H. Freeman and Company.

STUDER, D., MICHEL, M., WOHLWEND, M., HUNZIKER, E. and BUSCHMANN, M., 1995. Vitrification of Articular-Cartilage by High-Pressure Freezing. *Journal of microscopy,* **179**, pp. 321-332.

SUGIARTO, M., YE, A. and SINGH, H., 2009. Characterisation of binding of iron to sodium caseinate and whey protein isolate. *Food Chemistry,* **114**(3), pp. 1007-1013.

THIBERGE, S., NECHUSHTAN, A., SPRINZAK, D., GILEADI, O., BEHAR, V., ZIK, O., CHOWERS, Y., MICHAELI, S., SCHLESSINGER, J. and MOSES, E., 2004. Scanning electron microscopy of cells and tissues under fully hydrated conditions. *Proceedings of the National Academy of Sciences of the United States of America,* **101**(10), pp. 3346-3351.

THIEL, B. and TOTH, M., 2005. Secondary electron contrast in low-vacuum/environmental scanning electron microscopy of dielectrics. *Journal of Applied Physics,* **97**(5), pp. 051101.

THOMPSON REUTERS, 2013-last update, Web of Knowledge. Available: www.webofknowledge.com [04/24, 2013].

TIEDE, D. and HOFMANN, P., *eCognition Architect.*

TIEDE, K., BOXALL, A.B.A., TIEDE, D., TEAR, S.P., DAVID, H. and LEWIS, J., 2009. A robust size-characterisation methodology for studying nanoparticle behaviour in 'real' environmental samples, using hydrodynamic chromatography coupled to ICP-MS. *Journal of Analytical Atomic Spectrometry,* **24**(7), pp. 964-972.

TOMASCHUNAS, M., HINRICHS, J., KOEHN, E. and BUSCH-STOCKFISCH, M., 2012. Effects of casein-to-whey protein ratio, fat and protein content on sensory properties of stirred yoghurt. *International Dairy Journal,* **26**(1), pp. 31-35.

TONG, L., SASAKI, S., MCCLEMENTS, D. and DECKER, E., 2000. Mechanisms of the antioxidant activity of a high molecular weight fraction of whey. *Journal of Agricultural and Food Chemistry,* **48**(5), pp. 1473-1478.

TREJO, R., DOKLAND, T., JURAT-FUENTES, J. and HARTE, F., 2011. Cryo-transmission electron tomography of native casein micelles from bovine milk. *Journal of dairy science,* **94**(12), pp. 5770-5775.

UMRATH, W., 1977. Principles of Cryo-Preparation Method - Freeze-Drying and Freeze-Etching. *Mikroskopie,* **33**(1-2), pp. 11-29.

VAN BRUGGEN, E.F.J., WIEBENGA, E.H. and GRUBER, M., 1960. Negative-staining electron microscopy of proteins at pH values below their isoelectric points. Its application to hemocyanin. *Biochimica et biophysica acta,* **42**(0), pp. 171-172.

VANHARREVELD, A. and CROWELL, J., 1964. Extracellular Space in Central Nervous Tissue. *Federation proceedings,* **23**(2P1), pp. 304-&.

VANHARREWELD, A. and CROWELL, J., 1964. Electron Microscopy After Rapid Freezing on Metal Surface + Substitution Fixation. *Anatomical Record,* **149**(3), pp. 381-&.

VANHECKE, D., GRABER, W. and STUDER, D., 2008. Close-to-Native Ultrastructural Preservation by High Pressure Freezing. In: T. ALLEN, ed, *Introduction to Electron Microscopy for Biologists.* 1st edn. Elsevier Inc. San Diego, USA, pp. 151.

VARELA, P., CHEN, J., FISZMAN, S. and POVEY, M.J.W., 2006. Crispness assessment of roasted almonds by an integrated approach to texture description: texture, acoustics, sensory and structure. *Journal of Chemometrics,* **20**(6-7), pp. 311-320.

VILLIERE, A., VIAU, M., BRONNEC, I., MOREAU, N. and GENOT, C., 2005. Oxidative stability of bovine serum albumin- and sodium caseinate-stabilized emulsions depends on metal availability. *Journal of Agricultural and Food Chemistry,* **53**(5), pp. 1514-1520.

VINSON, P.K., BELLARE, J.R., DAVIS, H.T., MILLER, W.G. and SCRIVEN, L.E., 1991. Direct Imaging of Surfactant Micelles, Vesicles, Disks, and Ripple Phase Structures by Cryo-Transmission Electron-Microscopy. *Journal of colloid and interface science,* **142**(1), pp. 74-91.

WALTHER, P. and ZIEGLER, A., 2002. Freeze substitution of high-pressure frozen samples: the visibility of biological membranes is improved when the substitution medium contains water. *Journal of microscopy,* **208**, pp. 3-10.

WARAHO, T., MCCLEMENTS, D.J. and DECKER, E.A., 2011. Mechanisms of lipid oxidation in food dispersions. *Trends in Food Science & Technology,* **22**(1), pp. 3-13.

WATSON, M., 1958. Staining of Tissue Sections for Electron Microscopy with Heavy Metals. *Journal of Biophysical and Biochemical Cytology,* **4**(4), pp. 475-&.

WEIBULL, C., VILLIGER, W. and CARLEMALM, E., 1984. Extraction of Lipids during Freeze-Substitution of Acholeplasma-Laidlawii-Cells for Electron-Microscopy. *Journal of Microscopy-Oxford,* **134**(MAY), pp. 213-216.

WEPF, R.A., 2010. *EMEZ, ETH, Zürich, Switzerland.*

WHITE, D., ANDREWS, S., FALLER, J. and BARRNETT, R., 1976. Chemical Nature of Osmium Tetroxide Fixation and Staining of Membranes by X-Ray Photoelectron-Spectroscopy. *Biochimica et biophysica acta,* **436**(3), pp. 577-592.

WILD, P., SCHRANER, E., ADLER, H. and HUMBEL, B., 2001. Enhanced resolution of membranes in cultured cells by cryoimmobilization and freeze-substitution. *Microscopy research and technique,* **53**(4), pp. 313-321.

WOOD, J., 1973. Effects of Glutaraldehyde and Osmium on Proteins and Lipids of Myelin and Mitochondria. *Biochimica et biophysica acta,* **329**(1), pp. 118-127.

WOOD, J. and KLOMPARENS, K., 1993. Characterization of Agarose as an Encapsulation Medium for Particulate Specimens for Transmission Electron-Microscopy. *Microscopy research and technique,* **25**(4), pp. 267-275.

WU, M., HARVEY, K., RUZMETOV, N., WELCH, Z., SECH, L., JACKSON, K., STILLWELL, W., ZALOGA, G. and SIDDIQUI, R., 2005. Omega-3 polyunsaturated fatty acids attenuate breast cancer growth through activation of a neutral sphingomyelinase-mediated pathway. *International Journal of Cancer*, **117**(3), pp. 340-348.

ZACHARIASSEN, K. and KRISTIANSEN, E., 2000. Ice nucleation and antinucleation in nature. *Cryobiology*, **41**(4), pp. 257-279.

ZHAO, F. and CRAIG, R., 2003. Capturing time-resolved changes in molecular structure by negative staining. *Journal of structural biology*, **141**(1), pp. 43-52.

A. Appendix I

In some cases the segmentation was done by thresholding in ImageJ (Rasband 1997-2012) but for some cases e.g. the freeze substituted sample the contrasts are complicated i.e. light in dark and dark on light and the droplets are overlapping. Techniques such as skeletonization and watershed algorithms did not help the process further (data discarded and not shown).

An attempt was made using the software e-cognition(Tiede, Hofmann , Blaschke 2010) which is a software based on object orientated image segmentation (versus the pixel orientated segmentation in ImageJ) that has proven useful for measuring nanoparticles in TEM (Tiede, Boxall et al. 2009). Unfortunately as the figure below shows, the results are far from reality and leaves out a big part of the droplets, so even though the results might be more reproducible by using automated approaches, they might not be very accurate and segmentation was thus done by hand.

Thanks for the e-cognition segmentation to Agnieszka Dudekiewski, Food and Environment Research Agency, Sand Hutton, York, YO41 1 LZ and University of York, Heslington, York, YO10 5DD, UK.

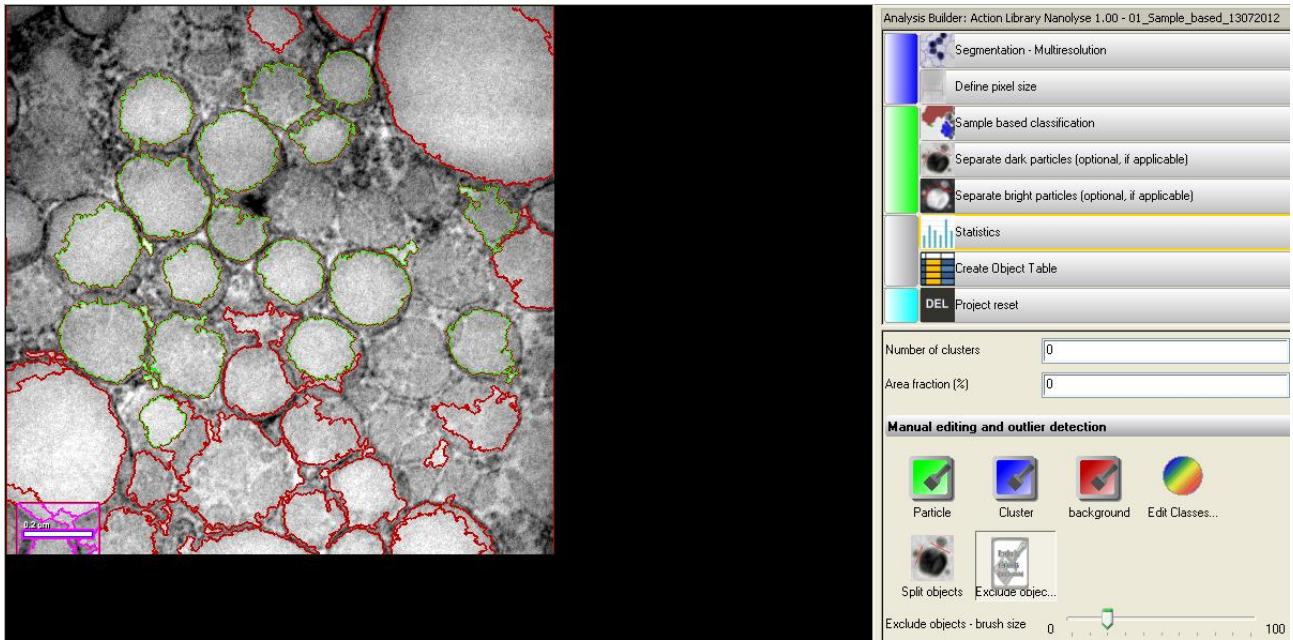

Figure AI. Screen shot from segmentation with e-cognition.

B. Appendix II

Cryo-SEM holder for freeze fracture, hybrid system. Base is modeled after the standard holder from Quorum Technologies Ltd. Top part is modeled after a BAL-TEC freeze fracture holder. The holder fits two standard 3 mm carriers for high pressure freezing which can be loaded under liquid nitrogen as sandwiches to be fractured once inside the vacuum preparation chamber in the Quorum system. The holder clamps the carriers by tightening of the screws which lift the flexible end of the holder. The cryo holder is shown with carriers. The holder was machined from brass. Dimensions are approximately: height: 8 mm; with: 17.5 mm (base) and 13 mm (top); length 22 mm. Built after idea from (Wepf 2010), personal communication.

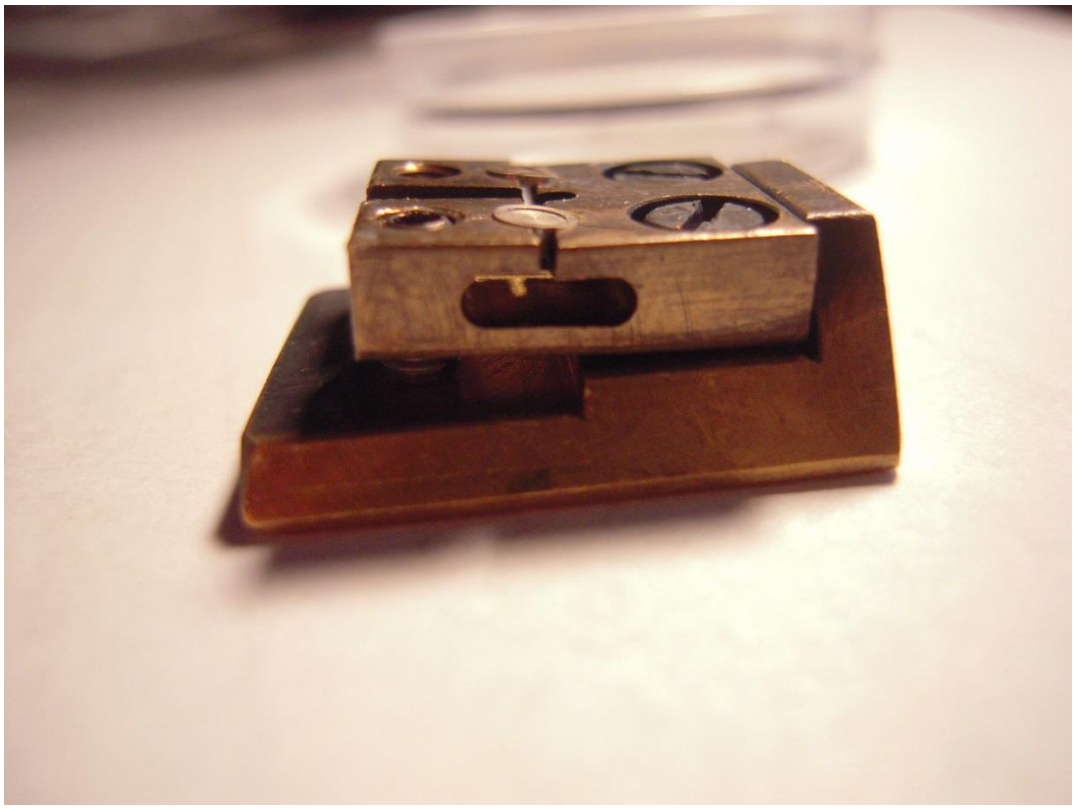

Figure AII.1. Cryo-SEM holder for freeze fracture, hybrid system.

The design worked well, but it was impossible to keep both fracture planes (both planchettes) due to the nature of the clamping system and the sample was often lost during the fracture step or mainly attached to the planchette that was broken off, not the one in the holder. With advice (Kaech 2012) personal communication, we started to freeze the samples using a grid as spacer inside the planchette-sandwiches and this effectively helped. The grid effectively ensured that some sample was left in the carrier after fracture. See figure AII.2 below. No matter if the spacer grid was still present after fracture or not, and if the lid type carrier (type B) or the hollow carrier (type A) was imaged, we very frequently obtained good fracture planes after freeze-fracture.

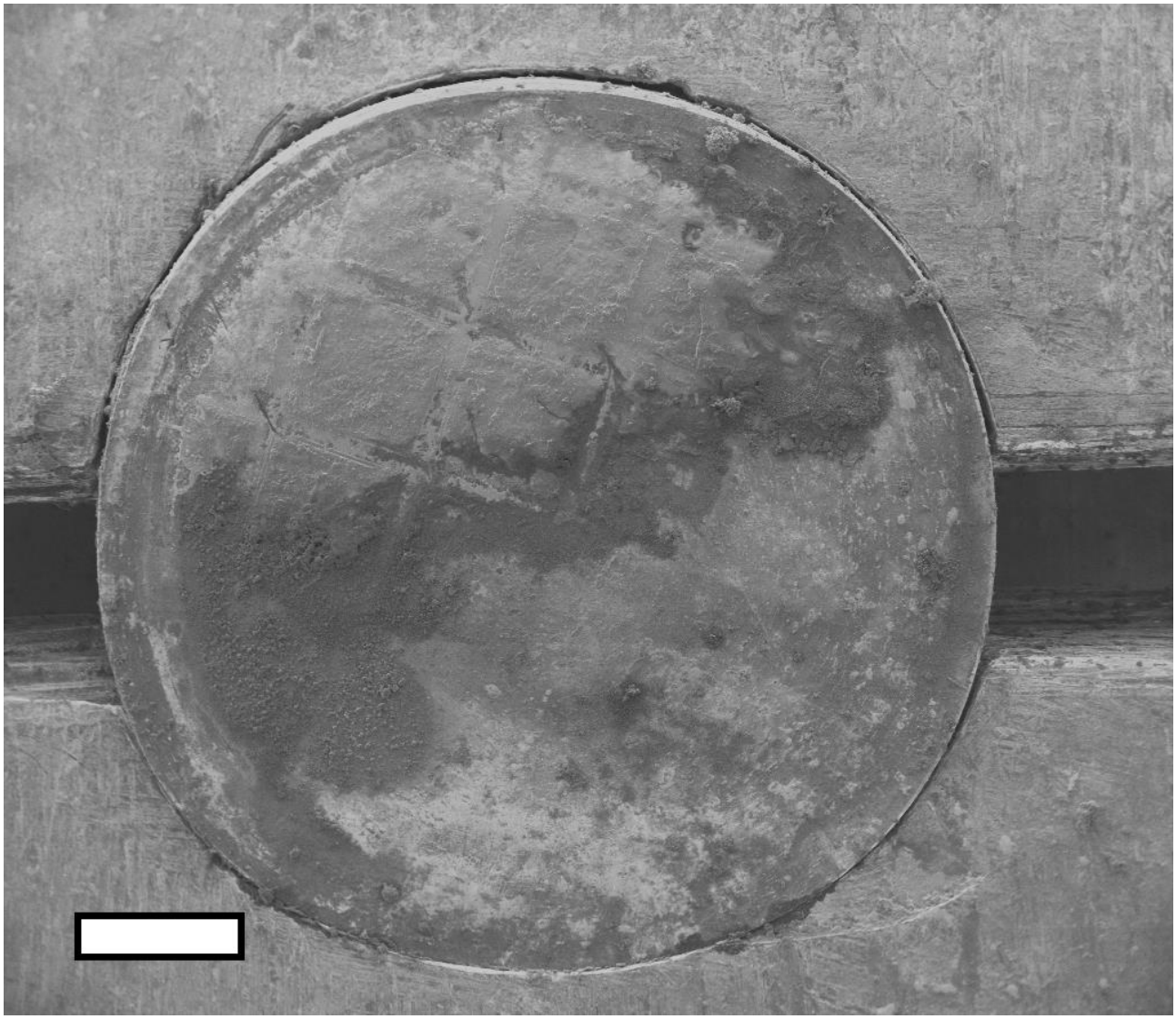

Figure AII.2. Specimen carrier after fracture without grid spacer displaying empty area (lower right corner), fracture plane (middle section) and unfractured surface (upper left corner). Scalebar 500 µm.